UNIVERSITY OF CALIFORNIA, SAN DIEGO

# The Structure–Function Relationship in Knee Menisci: A Multiscale Study of Aging, Degeneration and Osteoarthritis

A dissertation submitted in partial satisfaction of the
requirements for the degree
Doctor of Philosophy

in

Materials Science and Engineering

by

Jeanie Kwok Meckes

Committee in charge:

Professor Ratnesh Lal, Chair
Professor Renkun Chen
Professor Darryl D'Lima
Professor Jiang Du
Professor Koichi Masuda
Professor Samuel Ward

2015

The dissertation of Jeanie Kwok Meckes is approved, and it is acceptable in quality and form for publication on microfilm and electronically:

_____

_____

_____

_____

_____

Chair

University of California, San Diego

2015

DEDICATION

To Brian and my family

# EPIGRAPH

*How incessant and great are the ills with which a prolonged old age is replete.*

—C.S. Lewis

TABLE OF CONTENTS

LIST OF FIGURES

LIST OF TABLES

ACKNOWLEDGEMENTS

First and foremost, I would like to thank my family. I am most thankful for my husband, Brian, who has been there for me through it all, whether it was just his love and support or his sound scientific advice. My parents deserve much thanks for their love, encouragement, and support as well as their patience. They always ask me when I am going to graduate. I am happy to tell them: "at last." I would also like to thank my older, Annie, for being that friendly competition all my life. I am sure I would not have made it this far without her. My younger siblings, Kelvin, Spring, and Aaron, are the sweetest, and I thank them for providing me entertainment along the way. Then there is my Meckes family, whom have welcomed me with open arms and an overwhelming outpour of love and support. From the bottom of my heart, I thank them all.

Next, I would like to thank Professor Ratnesh Lal, my advisor. His distinguished contributions to research in multiscale imaging and biomechanics with atomic force microscopy (AFM) have been a great inspiration to this dissertation. His mentorship has helped foster my growth and development as a researcher and scientist. Professor Darryl D'Lima, my co-advisor, at the Shiley Center for Orthopaedic Research and Education (SCORE) at Scripps Clinic has also helped spruce my development and training as a biologist, especially in orthopaedic research, cartilage and meniscus biology and biomechanics, and molecular biology and medicine. Coming from a background in mechanical engineering and materials science, his mentorship and training was essential for my development and future success as a biologist and engineer. I am grateful for his guidance and support in the making of this dissertation.

I would also like to thank all of the professors on my dissertation committee: Professors Renkun Chen, Jiang Du, Koichi Masuda, Samuel Ward. These professors have provided valuable insight to this dissertation, particularly Professor Jiang Du from the Department of Radiology at UCSD who is one of my collaborators. Our collaboration explores magnetic resonance imaging (MRI) sequences for early detection of meniscus degeneration. I have learned a great deal from him about MRI, from the basic principles, operations, and applications. I would also like

to thank my other collaborator, Professor Martin Lotz at The Scripps Research Institute (TSRI), who is a key expert in the field of cartilage biology. It has been an honor to work alongside him and his group.

In addition, I would like to thank all contributing members of the Nano-bio-imaging and Devices Laboratory, SCORE, the Lotz lab, and Professor Du's research group. From the Nano-bio-imaging and Devices Laboratory, Drs. Fernando Arce and Srinivasan Ramachandran have been great mentors and trained me in atomic force microscopy (AFM) and molecular biology techniques, respectively. To my lab mates: Dr. Brian Meckes, Dr. Alan Gillman, Dr. Alexander Mo, and Joon Lee, I would like to thank them for sharing in this Ph. D. journey with me. From SCORE, I must thank Dr. Shawn Grogan, who has been instrumental in helping me develop this dissertation. He has helped me with, what seems to be, everything from experimental design and execution to manuscript editing and revisions. I would also like to thank Nicholas Glembotski and Judy Blake for their technical assistance in sample preparation and manuscript preparation and copy-editing, respectively. From the Lotz lab, I would like to thank Merissa Olmer and Lilo Creighton for their technical assistance in the mice studies. From Professor Du's research group, I would like to thank Dr. Graeme Bydder, Hongda Shao, Dr. Soorena Azam Zanganeh, and Qun He for their contributions to the MRI studies.

Chapter 2 in part is a reprint of the material *Kwok J, Grogan S, Meckes B, Arce F.T., Lal R, D'Lima D. Atomic force microscopy reveals age-dependent changes in nanomechanical properties of the extracellular matrix of native human menisci: implications for joint degeneration and osteoarthritis. Nanomedicine: Nanotechnology, Biology, and Medicine. 2014; 10(8): 1777-1785.* The dissertation author was the primary author.

Chapter 3 in part is a reprint of the material *Kwok J, Onuma H, Olmer M, Lotz M, Grogan S P, D'Lima D D. Histopathological analyses of murine menisci: implications for joint aging and osteoarthritis. Osteoarthritis and Cartilage. 2015; Accepted.* The dissertation author was the primary author.

Chapter 4 is a publication in preparation. *Kwok J, Carames B, Olmer*

*M, Kiosses W, Grogan S, Lotz M, D'Lima D. Compromised autophagy precedes meniscus degeneration and cartilage damage.* The dissertation author is the primary author.

Chapter 5 is a publication in preparation. *Kwok J, Shao H, D'Lima D D, Du J. Qualitative and quantitative UTE MRI for morphological and functional assessment of regional variations in meniscus during joint aging, degeneration, and osteoarthritis.* The dissertation author is a primary author.

## VITA

| | |
|---|---|
| 2009 | B. S. in Mechanical Engineering, University of California, San Diego |
| 2011 | M. S. in Materials Science and Engineering, University of California, San Diego |
| 2015 | Ph. D. in Materials Science and Engineering, University of California, San Diego |

## PUBLICATIONS

**Kwok J**, Grogan S, Meckes B, Teran Arce F, Lal R, D'Lima D. Atomic force microscopy reveals age-dependent changes in nanomechanical properties of the extracellular matrix of native human menisci. Nanomedicine: Nanotechnology, Biology, and Medicine. 2014; 10(8): 1777-85.

Fior R, **Kwok J**, Malfatti F, Sbaizero O, Lal R. Biocompatible optically transparent MEMS for simultaneous micromechanical stimulation living cells. Annals of Biomedical Engineering. 2014; 43(8): 1841-50.

**Kwok J**, Onuma H, Olmer M, Lotz M, Grogan S, D'Lima D. Histopathological analyses of murine menisci: implications for joint aging and osteoarthritis. Osteoarthritis and Cartilage. 2015; (Accepted)

**Kwok J**, Carames B, Olmer M, Kiosses W, Grogan S, Lotz M, D'Lima D. Compromised autophagy precedes meniscus degeneration and cartilage damage. (In preparation)

ABSTRACT OF THE DISSERTATION

**The Structure–Function Relationship in Knee Menisci: A Multiscale Study of Aging, Degeneration and Osteoarthritis**

by

Jeanie Kwok Meckes

Doctor of Philosophy in Materials Science and Engineering

University of California, San Diego, 2015

Professor Ratnesh Lal, Chair

Osteoarthritis (OA) is the most prevalent joint disorder with risk factors that include aging and joint injury. OA is characterized as the degeneration of articular cartilage, but invariably affects other joint tissues, including subchondral bone, menisci, synovium, ligaments, tendons, and muscles. Of these tissues, the meniscus, in particular, plays a critical role in the knee joint, providing load bearing and transmission, shock absorption, smooth articulation, and joint stability. These biomechanical functions are dependent upon the hierarchical structure and composition of the meniscus at the tissue level, as well as homeostatic mechanisms maintained at the cell and molecular level. The importance of the meniscus is emphasized by the fact that meniscal degeneration and injuries as well

as partial/total meniscectomy contribute to the development and/or progression of OA. However, the precise relationship between meniscus degeneration and aging, injury, and OA is poorly understood. Previous studies have examined the macroscopic and microscopic meniscus structure, composition, and biomechanical properties independently, but do not provide a global understanding of meniscus degeneration. This dissertation investigates the structure-function relationship of the meniscus in humans and mice during aging, injury, and OA using multidisciplinary biological and engineering tools and techniques across multiple scales, from tissue to molecular level. Age-dependent changes in the nanobiomechanical properties of the extracellular matrix of human meniscus were characterized by atomic force microscopy (AFM), which revealed distinct nanobiomechanical profiles of healthy, aged, degenerated, and OA tissue. A semi-quantitative histopathological grading system was developed to assess degenerative changes in the structure and composition of menisci from mice models of normal aging, injury, and OA. This histopathological grading system was applied to understand changes in and the function of autophagy in mice menisci during aging and injury. Lastly, qualitative and quantitative ultrashort echotime (UTE) magnetic resonance imaging (MRI) was used to assess morphological and functional properties in menisci as well as determine the potential for identifying early biomarkers of meniscus degeneration and progression. This multiscale study of the structure–function relationship in the meniscus provides insight into diagnostics and treatment of meniscus injuries and degeneration for the prevention or slowing of the progression of OA.

# Introduction

The musculoskeletal system is multifunctional and dynamic, giving form, support, stability, and mobility to the human body. It consists of the bones, joints, ligaments, muscles, tendons, and other connective tissue that support other tissues and organs, including the central nervous and hematopoietic systems. Therefore, diseases and disorders of the musculoskeletal system invariably affects the overall health, well-being, and function of the human body. A primary musculoskeletal disorder is osteoarthritis (OA), which is characterized as the degradation of articular cartilage in the knee joint. OA is the leading cause of disability in the United States and affects more than 27 million Americans, and is a debilitating condition that causes pain, stiffness, swelling, and reduced mobility that dramatically reduces ones' quality of life [1]. In addition to physical pain and disability, OA is associated with large societal and economic burdens, costing over $186 billion in healthcare alone [2]. Presently, there are no disease-modifying drugs to cure OA, as the disease itself is poorly understood. Current treatments alleviate the symptoms of the disease, such as pain and swelling, but do not target the underlying root cause of the disease for healing and regeneration.

Ultimately, OA is a whole-joint disorder that invariably affects articular cartilage, subchondral bone, meniscus, synovium, ligaments, and muscles. Of these tissues, articular cartilage is the most susceptible to structural damage, and displays the most profound age-related changes [3]. The meniscus also plays a critical role in the complex biomechanics of the knee joint, emphasized by the fact that damage or degeneration of the meniscus, due to aging or injury, as well as partial/total meniscectomy all contribute to the development or progression of OA [4]. More than 50% of patients with OA, one-third in middle to advanced ages,

concomitantly suffer from meniscal lesions or degeneration. In patients with a meniscus injury, the most common type being meniscal tears, or that have undergone partial/total meniscectomy are at high risk of developing post-traumatic OA within 10–20 years [5, 6]. Despite the high incidence of meniscus-related pathophysiologies, the mechanisms of meniscus degeneration during aging, injury, and OA are poorly understood.

The meniscus is composed of multiple levels of structural organization from the tissue to the cells and at the molecular level. Previous studies have focused on macroscopic and microscopic biomechanical and chemical changes independently, but do not provide a global understanding of the degenerative changes in the meniscus during joint aging, injury, and OA. To better understand meniscus physiology and pathophysiology, a comprehensive look at the structure and composition of the meniscus at the tissue, cell, and molecular level is required. Furthermore, the use of both biochemical and biomechanical characterization techniques will provide greater understanding of the multifunctional properties of the meniscus. These studies will contribute to the research and development of diagnostic and therapeutic treatment of meniscus injuries and degeneration.

This dissertation investigates the mechanisms of meniscal degeneration in both human and mice at the multiscale, from the tissue to molecular level. While the study of human tissue is more clinically relevant, the use of mouse models in this study provides more controlled study designs. Multidisciplinary biological and engineering techniques and tools were applied to characterize the structure, composition, biomechanical properties, and cellular homeostasis of healthy, degenerated, and diseased meniscus tissue. Finally, high resolution magnetic resonance imaging (MRI) sequences were assessed for potential of clinically relevant imaging of early meniscus degeneration and progression.

The objectives of this dissertation were to identify degenerative changes in the structure, composition, and biomechanical properties during joint aging, injury, and OA. Chapter 1 provides background information on the meniscus, describing its structure and anatomy at the multiscale, from tissue, cell, to molecular level, and its pathophysiology during aging, injury, and OA. Current diagnosis

and therapeutics for meniscal degeneration and injuries are also described. Chapter 2 evaluates age-related changes in biomechanical properties of human meniscal tissue measured by atomic force microscopy (AFM). Chapter 3 reports the development of a semi-quantitative histopathological grading system for meniscal degeneration in mouse models for aging, injury, and OA. This system was used to assess meniscal degeneration in relationship to changes in and function of autophagy in meniscus as well as articular cartilage, which is described in Chapter 4. Chapter 5 assesses degenerative changes in human menisci using quantitative ultrashort echo time (UTE) 3.0 T MRI. The morphological changes including collagen fibers and vasculature were assessed with high resolution 11.7 T MRI.

# Chapter 1

# Background

## 1.1 Knee Meniscus

The knee joint contains a medial meniscus and a lateral meniscus located between the articular surfaces of the femoral condyle and tibial plateau, which play an important role in joint loading and kinematics. The menisci provide load bearing and transmission [7, 8], shock absorption, smooth articulation, and joint stability within the knee joint [9, 10]. These biomechanical functions are carried out through the structure and composition of the meniscus at the tissue, cell, and molecular level. Damage or degeneration at any scale inversely affects the structure–function relationship of the tissue and ultimately the entire joint, leading to an increased risk for joint injury and disease, most commonly osteoarthritis (OA) [4].

## 1.2 Structure and Anatomy

Both the medial and lateral meniscus have a unique crescent shape with a wedge-shaped cross-section. The lateral meniscus is more circular in shape and slightly smaller in size compared to the medial meniscus. In humans, the medial meniscus measures approximately 40.5–45.5 mm in length and 27 mm in width, while the lateral meniscus is 32.4–35.7 mm in length and 26.6–29.3 mm in width [11, 12]. The meniscus surfaces appear white and glossy, and lie congruent to the

curved articular surfaces in the knee joint to permit smooth articulation during joint movement.

To maintain tissue stability during motion, each menisci is attached to the tibial plateau at the anterior and posterior horns by transverse ligaments [13]. The lateral meniscus covers more of the tibial plateau than the medial meniscus [13]. The meniscus is stabilized within the knee joint by a network of ligaments, including the anterior and posterior cruciate ligaments (ACL and PCL) and medial and lateral collateral ligaments (MCL and LCL), which all connect the femur and tibia at defined locations (Figure 1.1) [5, 13].

The outer periphery of the meniscus is covered by the synovial membrane, which contains blood vessels and nerves [14, 15]. The synovial membrane imparts vasculature to the outer third of the meniscus [14, 15]. The inner third of the meniscus is shielded from the synovial membrane, and therefore is non-vascularized. This limits the ability of the body to repair meniscal damage or injury [15]. The middle third exhibits properties from both the outer and inner region. This regional variation in vasculature is reflected by differences in the structure and composition of the extracellular matrix as well as in the resident cell populations.

## 1.3 Extracellular Matrix

### 1.3.1 Collagen

The extracellular matrix (ECM) of the meniscus is composed largely of collagen (∼75%) that varies in structure and composition across the different regions [5]. The outer region is composed primarily of collagen type I (∼99%) that forms a highly fibrous matrix containing large bundles of circumferentially-aligned fibrils held together by small radial "tie" fibers [5]. The inner region is composed of collagen type I (∼40%) along with collagen type II (∼60%), giving this region more hyaline cartilage-like properties [5]. The surface superficial zone of the meniscus is composed of randomly aligned collagen type II fibers [5]. Other collagen types in the meniscus include III, IV, V, VI, and XVIII, but are present in lower abundance [5].

### 1.3.2 Proteoglycans

Proteoglycans are another major component of the ECM, and vary regionally within the meniscus. Proteoglycans are comprised of a core protein that is decorated with glycosaminoglycans (GAGs) (∼15%), which are long unbranched polysaccharides [5]. GAGs are highly negatively charged making them hydrophilic, attracting water into the tissue such that the meniscus is 70% hydrated [5]. Cells from the inner region tend to produce more GAGs as this region bears more compression during joint loading compared to the outer region. Other components of the meniscus include adhesion glycoproteins (<1%) and elastin (<1%) [5].

## 1.4 Meniscus Cells

The extracellular matrix of the meniscus is produced and maintained by cells that originate from the mesenchymal lineage. However, due to the regional variation in composition and function, meniscus cells display morphological and phenotypic heterogeneity across the different regions to maintain the various structures (Figure 1.2) [5]. Cells in the outer region resemble fibroblast cells in shape and behavior. They are oval and fusiform in shape and have long cytoplasmic extrusions that enhance cell-matrix interactions [16]. These cells mainly produce collagen type I. Cells in the inner region exhibit characteristics of both fibroblasts and chondrocytes, and are often described as fibrochondrocytes [16]. They are round in shape and produce mostly collagen type II and less of collagen type I. These cells also produce much more GAGs compared to cells in the outer region, which gives the inner region more hyaline cartilage-like properties. Cells in the superficial zone are small and circular in shape and behave like progenitor cells with therapeutic and regenerative capabilities [17].

In the meniscus, the cells are sparsely distributed and embedded deep within the dense ECM [17]. Each cell has limited motility within its own matrix and is responsible for the turnover of the matrix within its local microenvironment. Furthermore, meniscal cells are postmitotic with very low replication rates [17]. Therefore, meniscus cells are highly specialized in metabolic processes that produce and

maintain the ECM. These cells respond to a variety of biochemical and biomechanical cues, including growth factors, inflammatory cytokines, and mechanical loading.

Outer and inner meniscal cells reside in different biomechanical environments, and are exposed to different compressive, tensile, and shear stresses of different magnitudes. The cells in the inner region experience tensile stresses in the order of ∼7% of total joint load, while outer cells experience only 2–4% [18]. These differences in biomechanical cues help regulate cellular phenotype, behavior, and synthetic properties in the different regions [19, 20, 21, 22].

### 1.4.1 Cellular Homeostasis

Because the meniscus exhibits a very low cell turnover rate, it depends on intracellular homeostatic mechanisms to maintain functional proteins and organelles to support normal cell function and survival. Autophagy is an essential cellular homeostatic mechanism that facilitates the turnover of proteins, such as aggregate-prone or misfolded proteins and ribosomes, and organelles, including mitochondria and peroxisomes [23]. Autophagy is constitutively active, occurring at low basal levels in mammalian cells [24]. It is a protective mechanism that helps maintain cellular homeostasis, such that loss of constitutive autophagy leads to the accumulation of aggregate-prone and misfolded proteins and defective mitochondria that stimulates the production of reactive oxygen species (ROS) [23]. This leads to altered gene expressions and even autophagic type II programmed cell death, characterized by cytoplasmic vacuolation [23]. In fact, deficiencies in autophagy are involved in several pathophysiologies [25], including cancer [26], neurodegeneration [27, 28], cardiomyopathies [29], and OA [24, 30].

Autophagy is a lysosomal degradation pathway induced by cellular stresses such as nutrient and energy deprivation, hypoxia, or injury (Figure 1.3) [31]. It is characterized by the formation of sequestering vesicles called autophagosomes. When autophagy is constitutively active, mammalian targets of rapamycin (mTOR) form a complex (mTORC1) with unc-51-like kinase 1 (ULK1), 200 kDa family kinase (FAK) interacting protein (FIP200), and autophagy-related protein

13 (ATG13) [24]. Phosophorylation of ULK1 and ATG13 represses autophagy [24]. During cellular stress, autophagy is activated by the inhibition of mTORC1, which results in the dissociation of ULK1. This stabilizes mTORC1 and leads to redistribution of cellular constituents to initiate autophagy [24]. Dissociated ULK1 transduces pro-autophagic signals that initiate the formation of isolated double-membrane structures called phagophores [24]. During autophagy, the cellular constituents are enclosed in phagopores, driven by the production of phosphatidylinositol 3-phosphate (PI(3)P)-enriched membrane domains by beclin-1 with class III phosphatidylinositol-3 kinase (PI3K) on vesicles [24]. This process recognizes and recruits the damaged or dysfunctional proteins and organelles to be autophagocytosed. Next, the phagophores undergo elongation and closure, driven by two ubiquitin-related conjugation systems: ATG-12 to ATG-5, an autophagy regulator, and LC3-I to LC3-II, an autophagy effector [24, 32]. Finally, the enclosed cargo, an autophagosome, fuses with the lysosome and is degraded. The constituents are then released and reutilized as nutrients and energy within the cell.

In articular cartilage, autophagy is regulated by proteins ULK1, Beclin-1, and LC3, mainly in the superficial zone [33]. Carames et al. showed that, in both human and mice articular cartilage, aging and OA is associated with a reduction in ULK-1, Beclin-1, and LC3 [33, 34]. Furthermore, this reduction in autophagy is associated with increased apoptotic cell death as well as cartilage damage [33, 34]. This suggest that basal autophagy decreases with age, which contributes to the accumulation of proteins and organelles and generation of ROS, increasing susceptibility to degeneration and OA in articular cartilage. However, while autophagy activation is present in the meniscus, changes in and the function of autophagy have not been sufficiently investigated during joint aging, injury, and OA.

In addition to autophagy, the unfolded protein response (UPR) is another cellular homeostatic mechanism [35]. UPR assures normal protein folding during protein synthesis in the endoplasmic reticulum (ER) [35]. UPR is activated when misfolded proteins are detected, activating autophagy to remove them. Deficiencies in either UPR or autophagy can lead to deficiencies in the other, thus compromising

cell function and survival [35].

## 1.5 Biomechanical Function and Properties

### 1.5.1 Load Bearing and Transmission

The meniscus plays an important role in providing load bearing and transmission across the knee joint [7, 8, 9, 10]. During normal joint loading, the femoral condyle bears down on the meniscus, which absorbs shock and deforms radially as it is opposed by the anterior and posterior attachments on the tibial plateau [9, 10]. Due to the wedged-shape of the meniscus, the inner region bears the most compressive loads while the outer region experiences tensile hoop stresses [9, 10]. This anisotropic loading condition is reflected by the regional organization of collagen and proteoglycans. The proteoglycan-rich environment of the inner region allows the tissue and cells to withstand high compressive loads, while the circumferentially aligned fibers in the outer region bear tensile loads.

During joint loading, the knee joint bears loads that are 2.7–4.9 times the body weight [36]; the meniscus bears 45–75% of the total knee joint load [37]. The meniscus provides a 1 mm gap between the articulating surface and allows only 10% of these surfaces to come in contact [38]. Therefore, damage or degeneration of the meniscus dramatically increases the stresses on the articular cartilage, which becomes more prone to degeneration, damage, and injury.

### 1.5.2 Biomechanical Properties

The biomechanical functions of the meniscus combine compression, tension, and shear, which have been characterized by bulk mechanical/materials testing. Several studies have reported the intrinsic material properties of both the medial and lateral meniscus from human and animal models at different locations (anterior, central, and posterior), depths (superficial and deep), and orientations (circumferential and radial) (Table 1.1) [39, 40].

In compression, the meniscus exhibits a relatively low compressive modu-

lus (0.09 to 0.16 MPa) compared to articular cartilage [39]. This indicates that the meniscus is less stiff and deforms more readily during joint loading, thus is more efficient in shock absorption compared to articular cartilage. In tension, the menisci exhibit the greatest tensile strength in the circumferential direction, which is at least 3-fold higher compared to the radial direction [40]. In humans, the lateral meniscus has a higher tensile stiffness (∼300 MPa in the central location) compared to the medial meniscus (∼160 MPa at the anterior horn) in the circumferential direction [40]. In comparison to articular cartilage, the meniscus exhibits much higher tensile stiffness, which indicates that the circumferential tensile hoop stresses dominate during joint loading and transmission.

While previous studies examine the bulk mechanical properties of the meniscus, recent studies are interested in examining the biomechanical properties at the micro-to-nanoscale, the length scale of cell-matrix interactions.

### 1.5.3 Atomic Force Microscopy

Recent studies have utilized high resolution force imaging techniques to examine the mechanical properties of cartilaginous tissue at the micro-to-nanoscale. Atomic force microscopy (AFM) is among the most powerful and versatile high resolution force imaging techniques. AFM is a form of scanning probe microscopy that utilizes the interactive forces between a sharp tip at the end of cantilever and the sample as a feedback signal for imaging and force measurements (Figure 1.4) [41, 42]. The deflection of the cantilever is measured continuously, most frequently by deflecting a laser beam off the cantilever for detection by a quadrant photodiode. The interactive forces between the tip and the sample can be calculated using Hooke's law:

$$F = -kx$$

In this equation, $F$ is the force applied by the cantilever, $k$ is the spring constant of the cantilever, and $x$ is the displacement of the cantilever when it interacts with the sample. AFM can be operated in two modes: contact and tapping. In contact mode, a constant interaction force between the cantilever and the surface is

maintained. Tapping mode operates by vibrating the cantilever at its resonant frequency. At close proximity to the surface, the amplitude of vibration is dampened. During imaging, a constant amplitude is maintained.

The spatial resolution of AFM is determined by the size of the cantilever tip, allowing for ∼1 nm spatial resolution. For biological materials, the cantilever tip can be modified with a microbead, to avoid perturbing the membranes. AFM can probe highly localized regions (∼1 nm) using highly sensitive forces (pN) in fluid and dynamic environments. This makes AFM a suitable technique for probing the mechanical properties of biological materials, including tissue, cells, and proteins at the micro-to-nanoscale.

The mechanical properties of cartilaginous tissues have been measured using AFM. McLeod et al. used AFM to measure the mechanical properties of the ECM from porcine articular cartilage in the axial, circumferential, and radial direction [43]. This study revealed new evidence of tissue heterogeneity and anisotropy of the ECM at the microscale. Sanchez-Adams et al. measured the mechanical properties of the ECM and PCM (pericellular matrix) of porcine meniscus, showing regional variations in mechanical properties; stiffness decreases from the outer to inner regions [44].

## 1.6 Meniscus Degeneration

Joint aging or injury, either acute or chronic, can lead to degeneration of the meniscus characterized by the disruption or loss of matrix structure and composition. Aging-related changes are driven by cellular senescence processes, while joint injury can lead to unfavorable changes in the biomechanical properties of the meniscus that promotes degeneration [30]. In the case of the meniscus, tears are a common joint injury that can lead to degenerative changes in the knee [4].

At the macroscopic level, meniscus degeneration is seen typically as fibrillation and lesions at the surface, mostly at the inner region, which is more injury prone [45] (Figure 1.5). However, microscopic histopathologic assessment of the meniscus has shown earlier degenerative changes in the extracellular matrix with

the surface relatively intact. These degenerative changes include reduced cellularity, increased Safranin-O staining, which correlates with reduced proteoglycan content, in the inner region, and loss of collagen fiber organization [45] (Figure 1.6). This suggest that the meniscus degenerates from the interior to the exterior. In contrast, articular cartilage degenerates from the surface inward. Furthermore, other studies have shown increased proteolytic activity due to increased production of matrix degrading enzymes as well as formation of advanced glycation end-products that stiffen the matrix properties [46, 47, 48].

Degenerative changes in the extracellular matrix reflect changes in the cells, including abnormal cell activation and differentiation [3]. This often leads to the disruption of cellular homeostasis resulting in matrix degeneration. An imbalance of anabolic and catabolic processes leads to reduced production of important growth factors and overproduction of matrix degrading enzymes and inflammatory cytokines combining to promote widespread tissue degradation. Aging cells are more susceptible to homeostatic disruption due to cellular senescence that compromises cellular proliferation and biosynthetic capacity as well as a decline in cell function and viability [3].

### 1.6.1 Osteoarthritis

Meniscus degeneration is closely linked to the development and progression of OA, the most prevalent joint disease. OA is characterized by articular cartilage degeneration, although meniscus degeneration is always invariably involved. More than 75% of patients with OA concomitantly suffer from meniscal lesions while 50% of patients with a meniscus injury go on to develop post-traumatic OA within 10 to 20 years [4, 6, 49, 3]. While the exact pathogenic processes of meniscus degeneration are unclear, damage or degeneration of the meniscus disrupts the biomechanical properties and is associated with cell death and abnormal cell activation and differentiation. This disrupts tissue homeostasis which leads to progressive matrix degeneration that ultimately manifests as OA of the whole joint.

## 1.7 Current Diagnosis and Therapeutics

Diagnosis of meniscus injuries and conditions greatly depends on the experience and insight of the physician. Generally, the physician evaluates the patient's history and performs a physical examination that could include joint line palpation [50, 51], McMurray rotation test [52], Apley's grind test [53], and Thessaly test [54, 55, 56]. Diagnostic imaging modalities, such magnetic resonance imaging (MRI), can be used to confirm a diagnosis, such as a meniscal tear [51, 57]. However, due to the intrinsic properties of both the meniscus and articular cartilage, conventional MRI techniques can only detect later stages of tissue degeneration when structural damage is already apparent and irreversible [58]. Current research in MRI technology and techniques focus on enabling high resolution and quantitative imaging assessment of tissue structure and composition at the microscale. This will enable early detection of degenerative changes that precede structural damage and OA in the knee joint.

### 1.7.1 Magnetic Resonance Imaging

MRI is a non-invasive powerful and versatile diagnostic tool capable of acquiring high-contrast images of tissues. Imaging is based on the physical phenomenon of nuclear magnetic resonance, in which atomic nuclei, usually hydrogen, exposed to a magnetic field can absorb and re-emit specific radiofrequencies. The basic principles of MRI measure the spin orientation and magnetic resonance (MR) properties of hydrogen atoms in the tissue body. Briefly, a hydrogen nucleus is composed of one proton and one electron, and therefore has a spinning charge and produces a magnetic moment. Normally, the protons are randomly oriented, but when a magnetic field is applied, the atoms align parallel or anti-parallel to the applied magnetic field. Atoms that align parallel to the field are at a low energy state while atoms that aligned antiparallel are at a high energy state. The protons also spin or precess around the axis of the applied magnetic field. The rate of precession is called the Larmor frequency.

$$\omega = \gamma B$$

In this equation, $\omega$ is the angular frequency, $\gamma$ is the gyromagnetic ratio, and $B$ is the magnetic field strength. Normally, the protons precess randomly, but when a magnetic field is applied, the atoms precess in phase.

During MRI, a RF pulse is applied at the Larmor frequency, which causes some of the atoms aligned parallel to the magnetic field to switch from a low to high energy state, decreasing the longitudinal magnetization. The applied RF pulse also synchronizes the precession of the atoms. As a result, the transverse magnetization is increased. Immediately after the RF pulse, several protons switch back to their favorable low energy state, thus transmitting energy to their surrounding lattice. This change in longitudinal magnetization is quantified by the spin-lattice relaxation time (T1). Concurrently, the atoms that were in phase also begin to de-phase, resulting in a decrease in transverse magnetization quantified as $T2$, the spin-spin relaxation time. However, in reality, the atoms de-phase much quicker than the $T2$ relaxation time due to inhomogeneities in the magnetic field. Therefore, $T2^*$ relaxation refers to combined $T2$ relaxation and the inhomogeneities.

$T1$ and $T2$ relaxation times reflect the structure, composition, and biomechanical properties of the tissue components. In articular cartilage, $T1$ relaxation has been reported to reflect the proteoglycan content as $T1$ values are more sensitive to the structure of macromolecules than of collagen in the ECM. $T2$ relaxation is dependent on the water content imposed by proteoglycans in the ECM. Therefore, $T1$ values decrease while $T2$ values increase from the superficial to deep zones of articular cartilage, consistent with the spatial distribution of proteoglycan content. Studies of healthy versus OA patients also showed that longer $T2$ values reflect more severe degeneration of the articular cartilage associated with OA [59]. However, these quantitative MRI assessments of meniscus degeneration is unclear due to the intrinsic MR properties of the meniscus. The meniscus is composed of a highly structured matrix thus exhibits an extremely short $T2$ and $T2^*$ relaxation times ($\sim$10 ms) that cannot be captured by conventional MRI techniques, which can only capture relaxation times greater than 10 ms [60]. However, recent developments in ultrashort echo time (UTE) MRI enables acquisition of relaxation times between 0.05 to 0.5 ms [61]. This technique is being evaluated on clinical

MR scanners, along with other techniques that provide higher contrast and spatial resolution. Experimental narrow-bore magnets with field strengths of 9.4T and 11.7T have enabled increased signal-to-noise ratio, higher spatial resolution ($\sim$50 $\mu$m), and accelerated acquisition time.

### 1.7.2 Treatment and Repair

Currently, there are no preventative measures or disease-modifying OA drugs available for joint aging and OA. Symptom-modifying drugs help relieve pain and inflammation. Further investigation of mechanisms that maintain joint health are warranted to develop better therapeutic treatments. Current management of meniscus injuries and conditions depends on the location of the injury as self-healing and repair capabilities of the meniscus is dependent on the vasculature. Since the inner region is limited in vasculature, meniscal lesions and tears in this region usually require surgical treatment or repair.

Surgical treatment of meniscal lesions and degeneration is most commonly a partial or total meniscectomy, a procedure that removes damaged or dysfunctional meniscus tissue to allow normal articulation [62]. However, meniscectomies most often lead to uneven load distribution and transmission across the knee joint, resulting in the development or progression of OA within 10 to 20 years post-operation [4, 15, 62, 63, 64].

This has led to the development of meniscus repair techniques that enhance healing in the meniscus. Current repair techniques include fibrin clot injection, synovial abrasion, and vascular access channel creation [65, 66, 67, 68]. Fibrin clot injection containing hematoma chemotactic factors promotes healing when injected in the meniscus [69]. Synovial abrasion also activates hematoma chemotactic factors that stimulate healing in the meniscus [70]. Meniscal lesions in the inner region can be repaired by creating vascular access channels from the vascularized outer region to the non-vascularized inner region [15]. Theoretically, vascular access channels enable the delivery of hematoma chemotactic factors to the inner region to promote healing of lesions, however, the technique has proven to be inadequate. All of these meniscus repair techniques have limited healing capacity,

as the repair tissue, essentially scar tissue, does not stand up to the biomechanical function needed in load bearing tissues in the knee. These repair techniques have a finite, pain-free expectancy of 5 to 7 years post-operation [67]. If the meniscus is damaged or degenerated beyond repair, the meniscus has to be surgically replaced by autografts from non-load bearing tissue, or allografts donated from cadavers [71]. However, the major issues with meniscus replacement transplants are poor integration with host tissue and a finite lifespan of 10 to 15 years[71].

Currently, research in treatments for the meniscus attempts to promote tissue regeneration using cell-based tissue engineering approaches. The present challenge in meniscus tissue engineering is selecting the appropriate combination of cells, scaffolds, and signaling mechanisms that regenerates tissue that is nearly identical to the phenotype and biomechanical properties of native meniscus tissue [72].

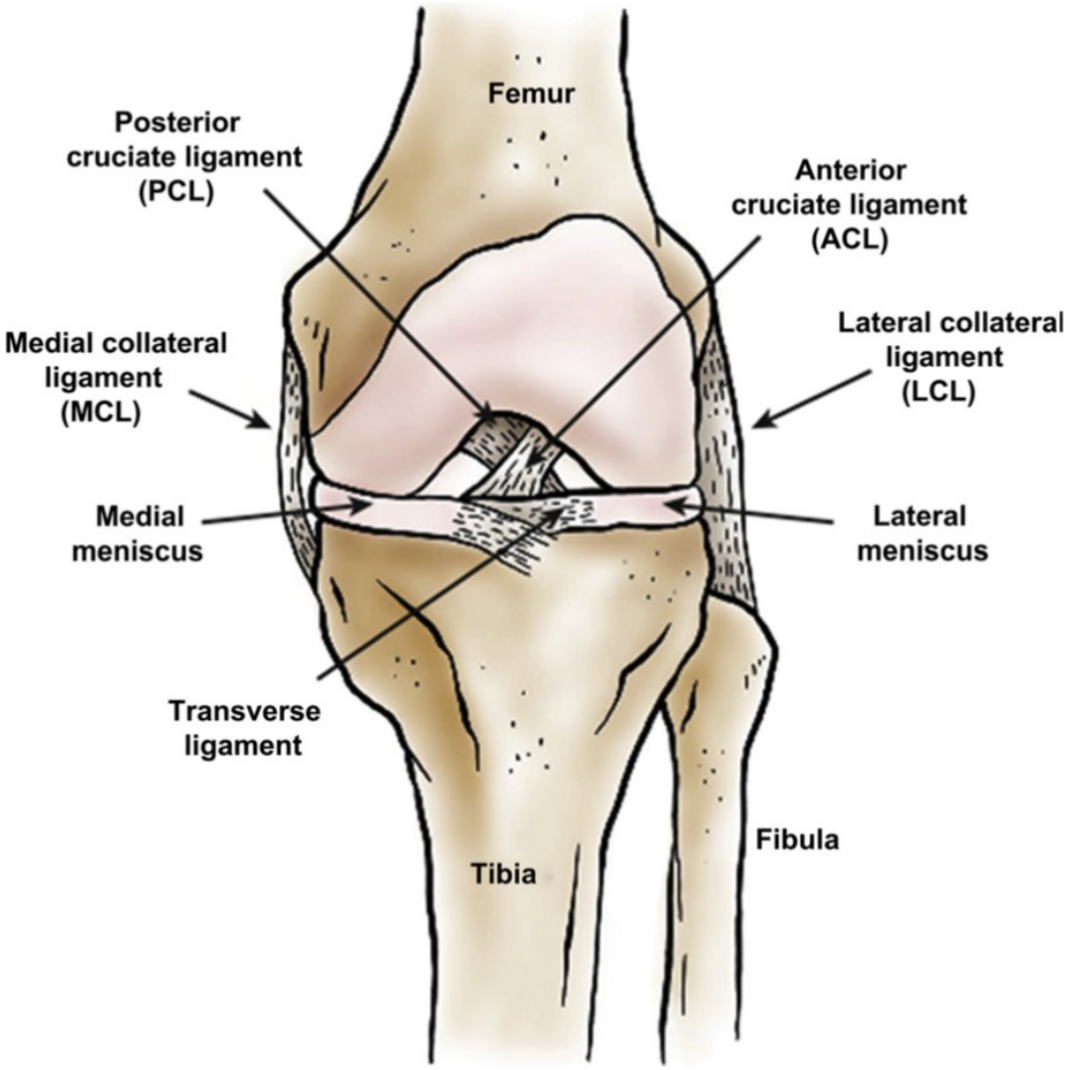


**Figure 1.1**: **Anatomy of the knee joint.** The knee joint contains a medial and lateral meniscus, which are situated between the femur and tibia. The menisci are stabilized by a network of ligaments, which include the anterior and posterior cruciate ligament (ACL and PCL), medial and lateral collateral ligament (MCL and LCL), and transverse ligament. [5]

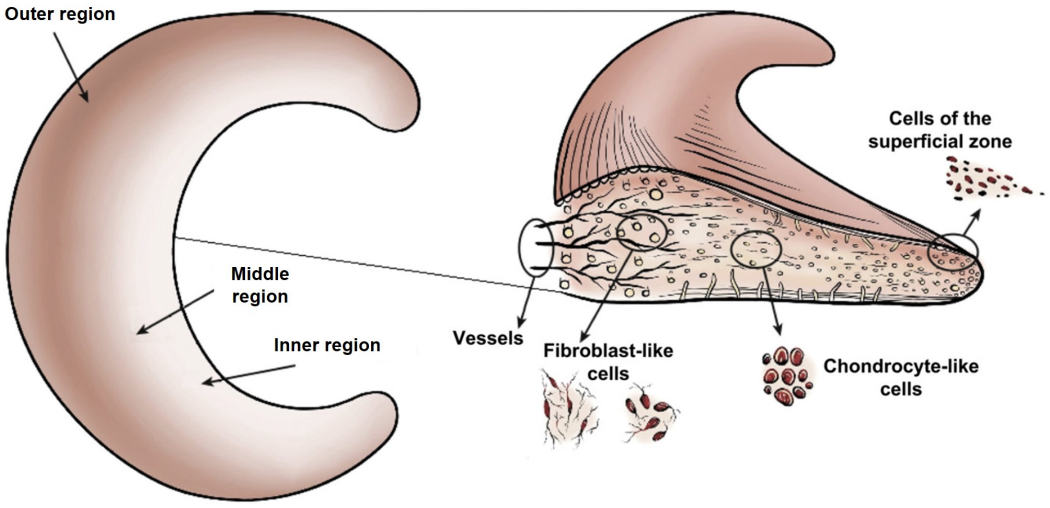


**Figure 1.2**: **Regional variations in the meniscus cell populations. (Left)** The outer region is vascularized (indicated in red) while the inner region is non-vascularized. **(Right)** The outer region contains blood vessels. Cells in the outer region are fibroblast-like while cells in the inner region are chondrocyte-like. Cells in the superficial zone are small and round. [5]

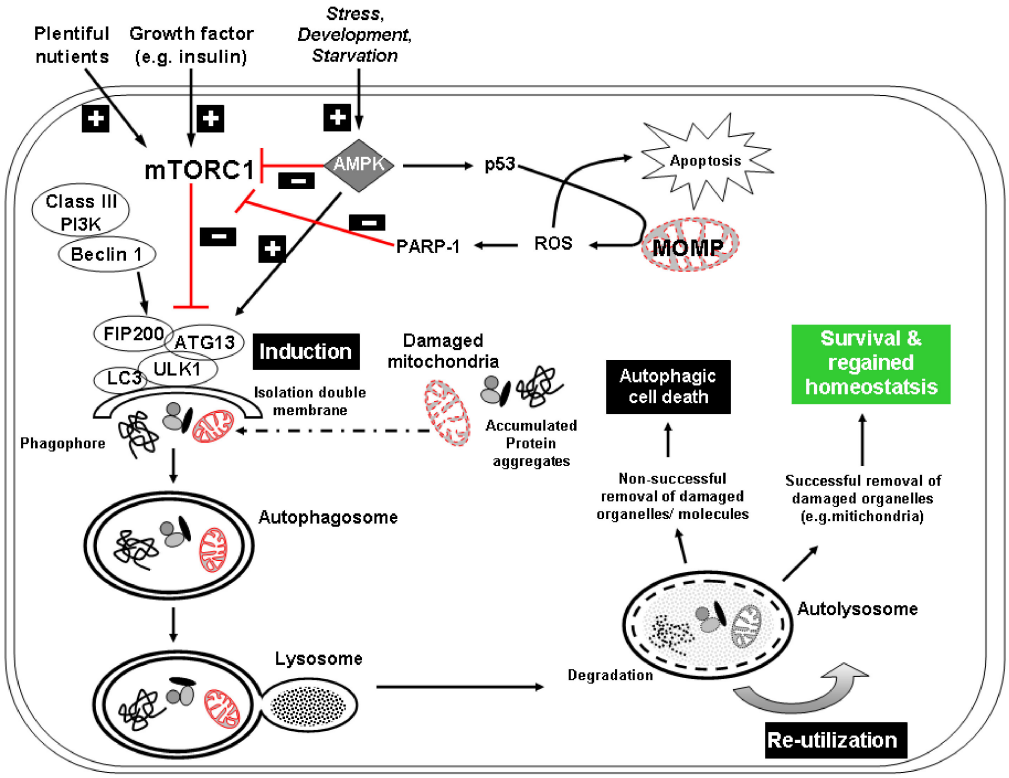


**Figure 1.3**: **Autophagy signaling and regulation.** Autophagy is activated upon cellular stress such as nutrient deprivation and hypnoxia. The formation of a complex with ULK1, FiP200, and ATG13 leads to subcellular redistribution and autophagosome formation. The autophagosome enclosed with the damaged organelles then fuse with the lysosome. Finally, the enclosed constituents are degraded, and reutilized as nutrients and energy. Successful removal of the damaged organelles promote cell survival and regain homeostasis, while non-successful removal results in autophagiac cell death. Reprinted with permission: Grogan et al. 2015 [31].

**Table 1.1: Summary of compressive and tensile properties of human menisci.**

| Tissue | Location | Modulus (MPa) | Reference |
|---|---|---|---|
| **Compressive properties** | | | |
| Human medial menisci | Superficial zone | | |
| | *Anterior* | 0.15 ± 0.03 | [39] |
| | *Central* | 0.10 ± 0.03 | |
| | *Posterior* | 0.11 ± 0.02 | |
| | Deep zone | | |
| | *Anterior* | 0.16 ± 0.05 | [39] |
| | *Central* | 0.11 ± 0.04 | |
| | *Posterior* | 0.09 ± 0.03 | |
| **Tensile properties** | | | |
| Human medial menisci | | | |
| *Circumferential* | *Anterior* | 106.21 ± 77.95 | [40] |
| | *Central* | 77.95 ± 25.09 | |
| | *Posterior* | 82.36 ± 22.23 | |
| *Radial* | *Anterior* | 48.31 ± 24.35 | [40] |
| | *Central* | 46.20 ± 27.56 | |
| | *Posterior* | 32.55 ± 11.27 | |
| Human lateral menisci | | | |
| *Circumferential* | *Anterior* | 124.58 ± 39.51 | [40] |
| | *Central* | 91.37 ± 23.04 | |
| | *Posterior* | 143.73 ± 38.91 | |
| *Radial* | *Anterior* | 48.47 ± 25.67 | [40] |
| | *Central* | 45.86 ± 24.20 | |
| | *Posterior* | 29.85 ± 12.77 | |

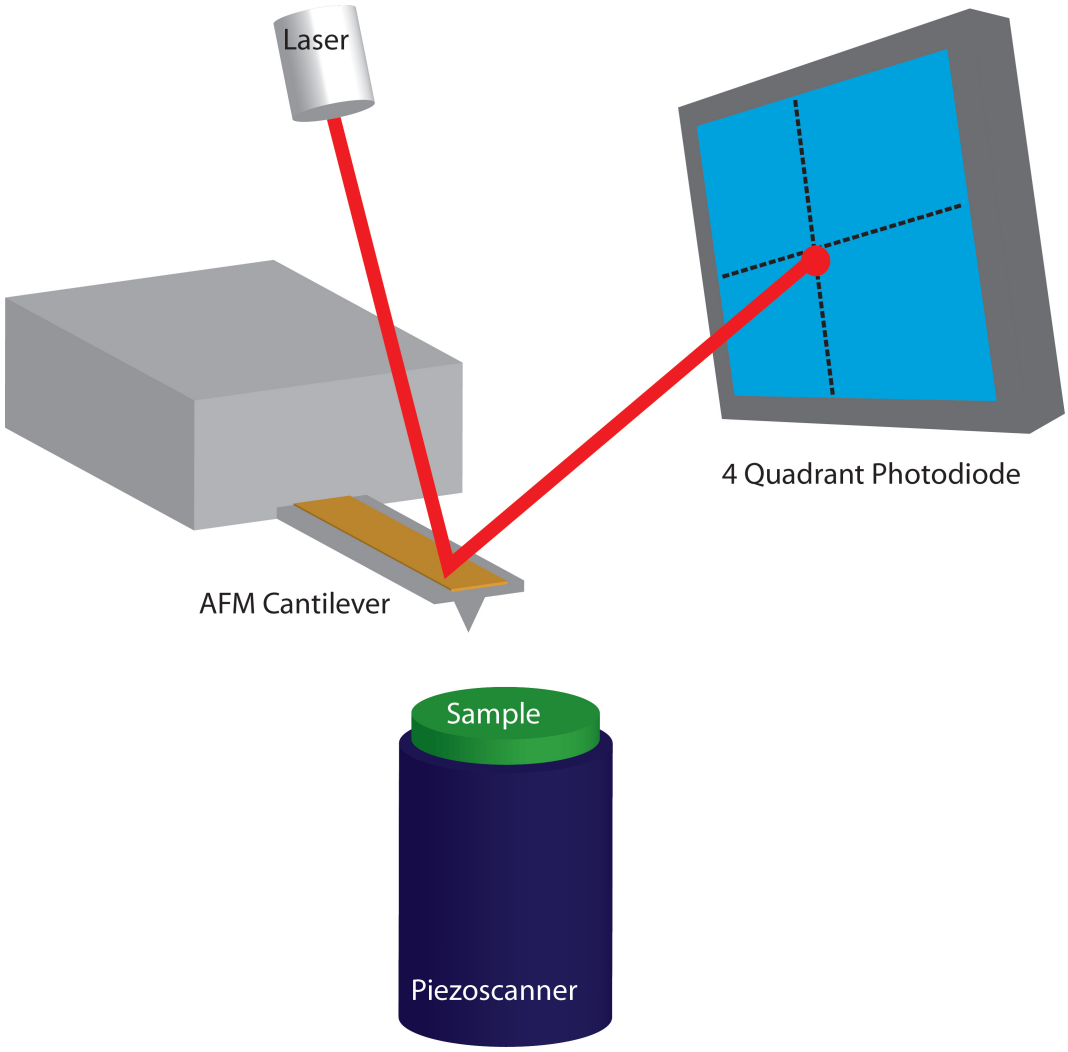


**Figure 1.4**: **Schematic of atomic force microscopy (AFM).** The AFM cantilever approaches the surface of the sample and, upon contact, the cantilever is deflected. The cantilever deflection is recorded using a laser beam that is reflected off the tip of the cantilever onto a 4 quadrant photodiode. Reprinted with permission [42].

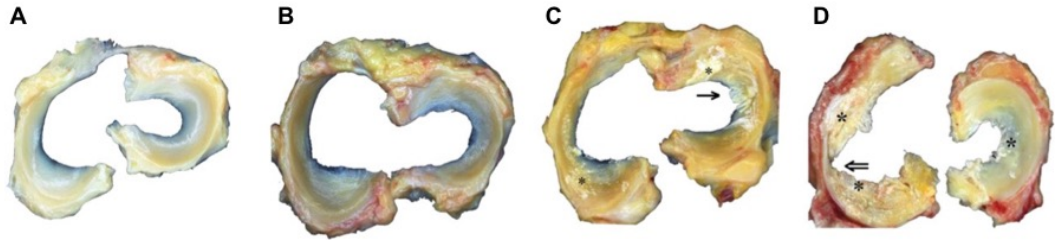


**Figure 1.5**: **Stages of meniscus degeneration at the macroscopic level.** **(A)** Healthy normal meniscus with a smooth, intact surface. **(B)** Mildly degenerated meniscus with fibrillation and fraying at the inner border. **(C)** Moderately degenerated meniscus with a partial tear (arrow) and calcification (asterik). **(D)** Severely degenerated meniscus with a full tear (arrow) and calcification (asterik). Reprinted with permission [45].

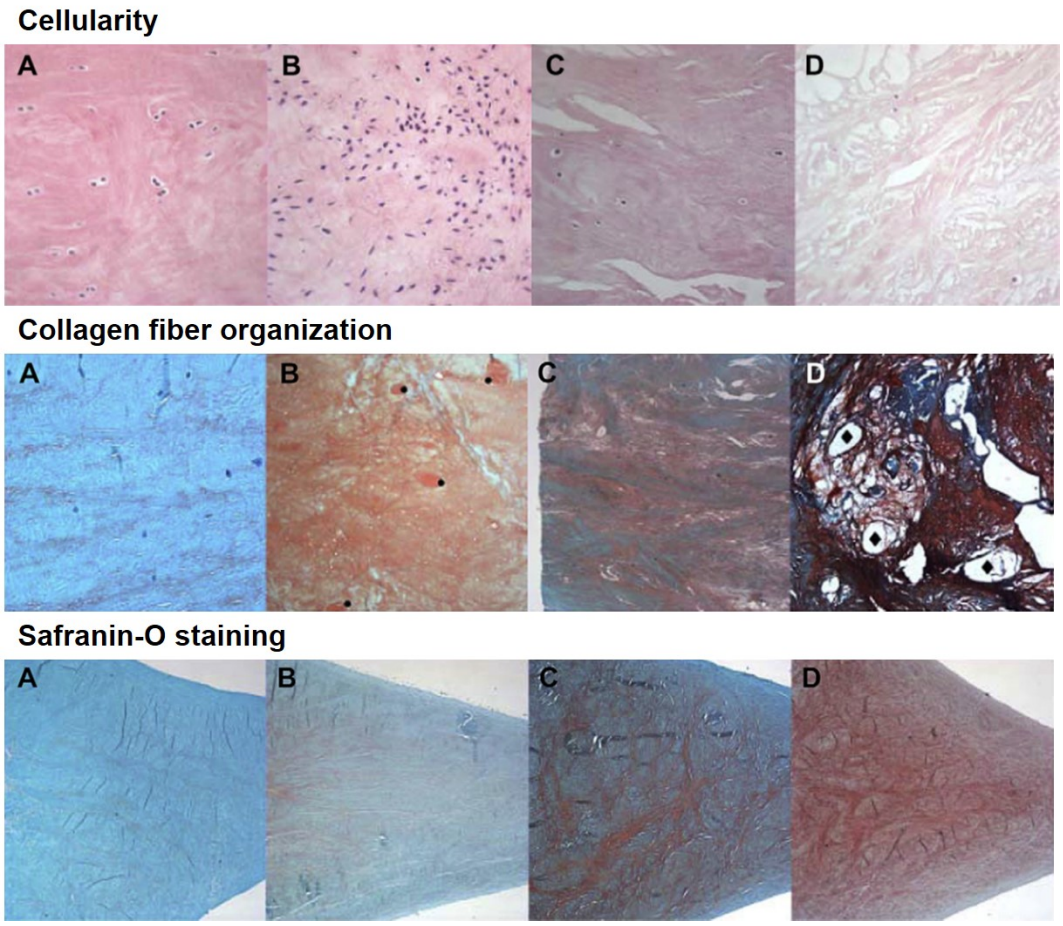


**Figure 1.6**: **Histopathologic features of meniscus degeneration at the microscopic level. (Left to Right)** Showing healthy, mildly, moderately, and severely degenerated menisci. **(Top row)** Degenerative changes in cellularity include diffuse hypercellularity, hypo/acellular regions, and hypocellularity. **(Middle row)** Gradual loss of collagen fiber organization is associated with meniscus degeneration. Histopathological features include diffuse foci (•) and cyst formation (◇). **(Bottom row)** Biochemical changes reflect a reduction in Safranin-O-Fast Green staining intensity. Reprinted with permission [45].

# Chapter 2

# Atomic force microscopy reveals age–dependent changes in nanomechanical properties of the extracellular matrix of native human menisci: implications for joint degeneration and osteoarthritis

## 2.1 Abstract

With aging, the menisci become more susceptible to degeneration due to sustained mechanical stress accompanied by age-related changes in the extracellular matrix (ECM). However, the mechanistic relationship between age-related meniscal degeneration and osteoarthritis (OA) development is not yet fully understood. We have examined the nanomechanical properties of the ECM of normal, aged, and degenerated human menisci using atomic force microscopy (AFM). Nanomechanical profiles revealed a unique differential qualitative nanomechanical profile of healthy young tissue: prominent unimodal peaks in the elastic moduli

distribution among three different regions (outer, middle, and inner). Healthy aged tissue showed similar differential elasticity for the three regions but with both unimodal and bimodal distributions that included higher elastic moduli. In contrast, degenerated OA tissue showed the broadest distribution without prominent peaks indicative of substantially increased heterogeneity in the ECM mechanical properties. AFM analysis reveals distinct regional nanomechanical profiles that underlie aging dependent tissue degeneration and OA.

## 2.2 Introduction

Aging is the leading risk factor for osteoarthritis (OA), a whole joint degenerative disease that affects all articulating tissues, including articular cartilage and menisci in the knee. The menisci play a crucial role in joint loading by providing mechanical stability, smooth articulation, shock absorption, load bearing and transmission in the knee [7, 9, 10, 37, 73, 74, 75]. Damage or degeneration due to aging of the menisci leads to unfavorable changes in joint loading that significantly affect overall joint health by precipitating the onset of OA development. The role of meniscal injuries and surgical removal of the meniscus on the development of post-traumatic OA is well established [4, 62, 76]. However, the mechanistic relationship between age-related meniscal degeneration and OA development is not yet fully understood.

The menisci are two crescent shaped tissue structures wedged between the articulating surfaces of the femoral condyle and tibial plateau. During normal joint loading, the femoral condyle bears down on the menisci concentrating the highest compressive loads in the inner tapered end of the tissue. The forces are transmitted to the outer periphery due to its geometry, which causes the tissue to expand circumferentially. The extrusion is resisted by the anterior and posterior attachments, creating circumferential tensile hoop stresses that distribute the compressive load. This anisotropic biomechanical response is supported by a regionally heterogeneous network of collagenous extracellular matrix (ECM) that varies in microvasculaturity, microstructure, and biocomposition [14, 77]. The inner region is

composed primarily of randomly aligned collagen type II fibrils embedded within an abundance of proteoglycan molecules that help resist high compressive loads [78, 79]. The outer region is more fibrous consisting of both collagen types I and II that form mostly circumferentially aligned fibrils to uphold tensile strength and carry out anisotropic load transmission [78, 79].

Age-related changes are accompanied by molecular and structural changes in the ECM that lead to matrix degeneration [80, 81, 82]. This degenerative process is characterized by an imbalance between anabolic and catabolic processes as cells reduce production of important growth factors and increase production of matrix degrading enzymes and inflammatory cytokines [83, 84]. These age-related biochemical changes have been identified by histological analyses which demonstrate increased Safranin-O staining, reduced cellularity, and loss of collagen fiber orientation [45]. While the biochemical changes have been investigated by histological and immunohistochemical analyses, age-related changes in biomechanical properties have not been documented at the microstructural level in human menisci. Our hypothesis is that aging alters the biomechanical properties of meniscal ECM thus changing the tissue response during joint loading thereby leading to OA development.

To define the earliest age-related biomechanical changes of the ECM, a high resolution force scanning technique is required to measure mechanical properties at the nano-to-microscale, the native length scale of the cells and associated matrix. Recent studies have examined tissue mechanical properties at the nano-to-microscale utilizing atomic force microscopy (AFM) [41]. Cartilaginous tissues, including articular cartilage and porcine menisci, have been evaluated by AFM demonstrating depth-dependent and regional variations in nanomechanical properties [43, 44]. However, the nanomechanical properties of human meniscal tissue, especially in its native and non-fixed condition, have not been reported. Characterizing these nanomechanical properties and identifying key changes with aging, degeneration, and OA will provide important insights into the pathogenesis of joint degeneration and OA, and may lead to novel therapeutic developments for the prevention and treatment of OA. For tissue engineering of menisci, nanome-

chanical characterization is critical for optimal design of materials and scaffolds. In addition, understanding the correlation between biochemical and biomechanical changes may lead to novel targets for pharmacological modulation of meniscal tissue degeneration.

In this study, we have examined nanomechanical properties of the ECM of normal, aged, and osteoarthritic human menisci using AFM. Human meniscal tissue samples were collected from donors of various ages and OA grades to represent meniscus physiology of aging and OA development. Regional ECM nanomechanical properties of individual specimens were measured by AFM-based elastic mapping and correlated with histological Safranin-O staining to identify matrix degeneration [85]. Our results show distinct regional differences in the nanomechanical properties of menisci that correlate well with the aging as well as with the severity of OA.

## 2.3 Materials and Methods

### 2.3.1 Tissue Selection and Processing

This study was approved by the Institutional Review Board at Scripps Health. Human knee joints were collected from tissue banks or from patients undergoing total knee arthroplasty. Subjects were selected by age and OA grade scored by macroscopic assessment of articular cartilage [86]. Briefly, OA grade 0 describes normal (intact smooth surface) articular cartilage, grade 1 thru 3 describes surface irregularities of slight to moderate reductions, and grade 4 describes severe disruption or loss of tissue [86].

In this study, 8 individual specimens were selected to represent normal meniscus physiology and pathophysiology, grouped by age and OA grade (age range 20–90 years; OA grade 0–4). Tissue donors were separated into three groups: specimens from individuals younger than 45 and of OA grade 0 were classified as young normal menisci; specimens from individuals older than 50 with OA grade 1 to 2 were classified as aging normal; and severely degenerated human menisci obtained from OA knee joints (OA grade 4) removed from patients greater than 50

years of age and undergoing total knee arthroplasty were classified as aging OA.

Menisci were dissected from the knee joints and triangular shaped cross-sections in the sagittal plane were harvested from the central portion of the medial menisci (Fig 2.1). The samples were embedded into O.C.T. Tissue Tek (Sakura Finetek, Torrance, CA) and stored at –80 °C for cryopreservation. The O.C.T. embedded samples were then cut using a cryostat microtome into 10 $\mu$m thick sections onto glass slides to be processed for histology and AFM measurements. Same or adjacent tissue sections were evaluated by AFM using histology to locate regions of interest.

10 $\mu$m thick cryosections were thawed and stained with Safranin-O/Fast Green (Sigma-Aldrich, St. Louis, MO) for semi-quantitative evaluation of proteoglycan content associated with matrix degeneration. Each tissue section was examined for Safranin-O staining intensity.

### 2.3.2 Atomic Force Microscopy

Prior to AFM, the tissue sections were thawed, having undergone only one freeze-thaw cycle to minimize the effects of freezing on the tissue structure. Tissue sections were rinsed with PBS to remove O.C.T. Tissue Tek and replenished with fresh PBS (Cellgro, Manassas, VA) to allow the tissue to swell at room temperature. All AFM measurements were carried out using a diBioScope SZ AFM (Bruker Corporation, Santa Barbara, CA) mounted on an Olympus IX71 inverted microscope used to visually position the AFM cantilever with respect to the sample. Colloidal AFM cantilevers (silicon nitride rectangular cantilever tip with a 5 $\mu$m diameter borosilicate glass sphere attached; NovaScan, Ames, IA) were used. The nominal spring constant k of the cantilever was 4.5 N/m and the exact value was determined by the thermal tuning method. The deflection sensitivity was determined by indenting on a glass substrate in fluid. Force-volume (FV) maps were generated from 20 $\times$ 20 $\mu$m$^2$ to 50 $\times$ 50 $\mu$m$^2$ areas of the tissue samples. Each FV map recorded 32 $\times$ 32 pixels (1024 force–displacement curves per map). Each individual force curve constitutes 512 data points. The maximum applied loading force was $\sim$200nN, which resulted in indentation depths of $\sim$1 $\mu$m ( 10%

of the section thickness) at a tip velocity of $\sim$15 $\mu$m/s. Force retraction curves were analyzed using Hertzian contact mechanics to determine the elastic modulus. The Poisson's ratio was assumed to be 0.04.

### 2.3.3 Statistical Analysis

All elastic measurements were summarized in histogram plots to obtain the distribution of values. The bin width was set at 20 kPa while the frequency count was normalized to the total number of measurements per region. A multi-peak Gaussian curve fit was applied to the distribution wherein peaks were located using the peak analysis in OriginPro 7.0 (Northampton, MA). All data are presented as a mean $\pm$ standard deviation. The statistical significance of differences between stiffness values from different regions (outer, middle, and inner) and conditions (normal, aged, and OA) were assessed by Kruskal-Wallis nonparametric test followed by a Wilcoxon test with a Bonferroni correction for age group comparisons in R 3.1.0. $P$-values less than 0.05 were considered statistically significantly different.

## 2.4 Results

### 2.4.1 Nanomechanical properties of ECM of menisci in normal joints

Histological analyses of meniscus specimens from three young normal individuals (20, 31, and 41 years of age) showed healthy, normal well-organized ECM with minimal Safranin-O staining, and intact articular surfaces (Fig 2.2). Individual histograms of regional ECM elastic moduli characterized the nanomechanical profile for healthy, young normal menisci with distinct unimodal peaks in distribution (Figure 2). In general, the outer and middle regions were characterized by a sharp dominant peak at 130 to 150 kPa and the inner region at 70 to 90 kPa. Mean elastic moduli also varied with regions: the outer region with its characteristic fibrous content measured the highest in elastic moduli with a mean value of 205.6 $\pm$ 8.9, with the middle region showing the next highest with a mean value of

188.0 Âś 21.9 kPa (Table 2.1). The inner region displayed the lowest elastic moduli with a mean value of 176.7 ± 28.0 kPa. Each region was statistically different ($P < 0.05$).

### 2.4.2 Nanomechanical properties of ECM of menisci in aged joints

Meniscus specimens representative of normal aging (55 and 56 years of age; OA grade 1 and 2, respectively) exhibited intact articular surfaces, organized matrix, and mild matrix degeneration reflected in the slight to moderate increase in Safranin-O staining compared to healthy normal ECM. Histograms showed a nanomechanical profile that was similar to young, normal menisci with distinct peaks that were comparable in magnitude. However, the elastic moduli of normal aged specimens were more widely distributed, as reflected in the larger standard deviation, and included stiffer values. In addition, the wider distribution contained bimodal peaks varying from 110 to 400 kPa (Fig 2.3). In the sample of 55 years of age (OA grade 1), the outer region exhibited a wider (bimodal) distribution compared to the middle and inner regions (unimodal), which still displayed region-defined nanomechanical properties. However, in the sample of 56 years of age (OA grade 2), region-defined nanomechanical properties became less distinct in nanomechanical properties among the outer (303.0 ± 28.3 kPa), middle (282.4 ± 30.2 kPa), and inner regions (274.0 ± 8.7 kPa).

### 2.4.3 Nanomechanical properties of ECM of menisci in osteoarthritic joints

All OA specimens were harvested from patients with undergoing total knee arthroplasty. Macroscopic and histopathological analyses of the articular cartilage were categorized as OA grade 4, while histological assessment of menisci showed severe matrix degeneration as identified by intense Safranin-O staining throughout the sample. OA menisci specimens exhibited a characteristic wide spread distribution of nanomechanical properties with no dominant peak. The wide distribution

of elastic moduli demonstrates stiffer mean values in the outer (364.3 ± 72.2 kPa), middle (401.9 ± 39.2 kPa), and inner regions (365.9 ± 106.5) (Figure 2.4). The large standard deviations indicate increased nanomechanical heterogeneity that correlated with increased Safranin-O staining intensity in matching sections. Notably, each individual OA sample displayed a unique nanomechanical profile of each region. The regions were not statistically significantly different ($P > 0.05$).

### 2.4.4 Correlation of nanomechanical properties of ECM to histological analyses

The respective nanomechanical profiles were correlated with the histopathological findings in normal, aged, and degenerated OA human meniscal tissue. The correlation of local AFM measurements with matching Safranin-O stained sections corroborated that the ECM regions with strong staining intensity exhibit stiffer values. This pattern was more pronounced in OA samples, as the strong Safranin-O staining in the outer regions was associated with broader and stiffer values (∼300 to 350 kPa) compared to the middle and inner regions (Fig 2.4). Figure 2.5 summarizes the characteristic nanomechanical profile of normal, normal aged, and OA human menisci.

## 2.5 Discussion

Meniscal degeneration due to aging and OA remains poorly understood. In accordance with conventional knowledge (mostly from experimental animal models), studies of macroscopic and histopathological changes of the menisci demonstrate a strong association between age-related meniscal degeneration and OA [81, 82, 87, 88, 89]. This is supported by clinical findings of a high incidence of OA in middle to advanced ages that occurs concomitantly with meniscal lesions [5, 90, 91]. Studies on animal tissues provide for a convenient assessment of anatomical, biochemical, and biomechanical properties of the menisci [15, 44, 81, 82, 92, 93, 94], but are biased due to interspecies variations raised

by significant differences in size, shape, matrix architecture and biochemical content [95].

This study is the first to document age-related biomechanical changes in native human menisci during tissue degeneration and OA development. An experimental profile of human meniscal tissue samples from individuals of various ages and degenerated/diseased conditions were examined to characterize age-related changes. Histological analyses of the samples collectively showed a clear representation of aged-related changes, as evidenced by a marked increase in Safranin-O staining with age. We used AFM-based elasticity mapping of tissue samples to characterize regional nanomechanical properties in normal, aged, and degenerated OA menisci. Overall, these results showed a similar trend in regional nanomechanical properties in healthy young menisci compared to properties previously reported on porcine menisci, although human tissue proved to be less stiff than porcine [44]. Like porcine menisci, the outer region of human menisci is stiffer due to its characteristic collagen fiber I fibrous content, while the inner region is more compliant in line with its rich proteoglycan content. This regional definition of nanomechanical properties is important to the overall health and function of the meniscus, as the results show that the regional properties become less defined with aging and disease (Figure 5). Indeed, regional differences in nanomechanical properties of OA samples proved to be statistically insignificant ($P > 0.05$). Loss of mechanical integrity is likely to compromise the biomechanical function of the tissue, disrupting the region-defined anisotropic biomechanical response of the tissue for efficient load bearing and transmission. These findings suggest that changes in regional nanomechanical properties in the ECM may emerge from earlier biochemical changes that occur during aging and take part in the initiation and progression of OA.

The most striking finding in this study is that normal, aged, and osteoarthritic human meniscal tissue exhibited qualitatively unique nanomechanical profiles. Young, healthy tissues exhibited a unimodal distribution in elastic moduli with each region displaying distinctly sharp peaks: outer (130 to 150 kPa), middle (130 – 150 kPa), and inner (70 – 90 kPa). Normal aged tissue also exhibited simi-

lar unimodal peaks but with a wider distribution (often bimodal) biased towards stiffer values. In general, the bimodal distributions encompassed a narrow first peak and broader second peak, suggesting regions of increased stiffness associated with degeneration. This bimodality was more obvious in some samples compared to others reflective of the severity of degeneration. Within the nanomechanical profiles, age-related changes associated with matrix degeneration were recognized by two features: (i) increased nanomechanical heterogeneity in line with increased Safranin-O staining and (ii) development of matrix stiffening with wider distributions.

Additionally, nanomechanical evaluations of degenerated OA samples were each individually unique in regional properties and distribution profiles. These results demonstrated incremental heterogeneity in nanomechanical properties with aging and OA development. Indeed, OA manifests as a heterogeneous disease with varying clinical features and biochemical characteristics among patients [96, 97].

In general, with increasing age there is stiffening of tissue, which is likely to increase the compressive stiffness of the overall tissue. Eventually, this leads to compromised tensile strength leading to biomechanical failure. Matrix stiffening is most likely due to age-related molecular changes in the ECM, such as abnormal deposition and cross-linking of ECM molecules [98, 99, 100]. These changes are known to alter matrix mechanics which can lead to abnormal cell behavior [101, 102, 103, 104, 105]. Meniscal cells are highly responsive to mechanical stimuli during joint loading [18, 19, 106, 107]. It is possible these changes in the ECM may cause or exacerbate OA-associated phenotypic changes in cells. However, the precise relationship between matrix mechanics and OA development remains to be established.

In summary, we have characterized regional nanomechanical properties of human meniscal tissue, especially ECM changes that occur during aging and OA. Further studies should investigate the correlation between biomechanical properties and biochemical characteristics that reflect meniscal tissue degeneration and OA. Understanding these age-related degenerative changes will provide insight for the development of effective therapeutic strategies to prevent and treat OA.

Chapter 2 in part is a reprint of the material *Kwok J, Grogan S, Meckes B, Arce F.T., Lal R, D'Lima D. Atomic force microscopy reveals age-dependent changes in nanomechanical properties of the extracellular matrix of native human menisci: implications for joint degeneration and osteoarthritis. Nanomedicine: Nanotechnology, Biology, and Medicine. 2014; 10(8): 1777-1785.* The dissertation author was the primary author.

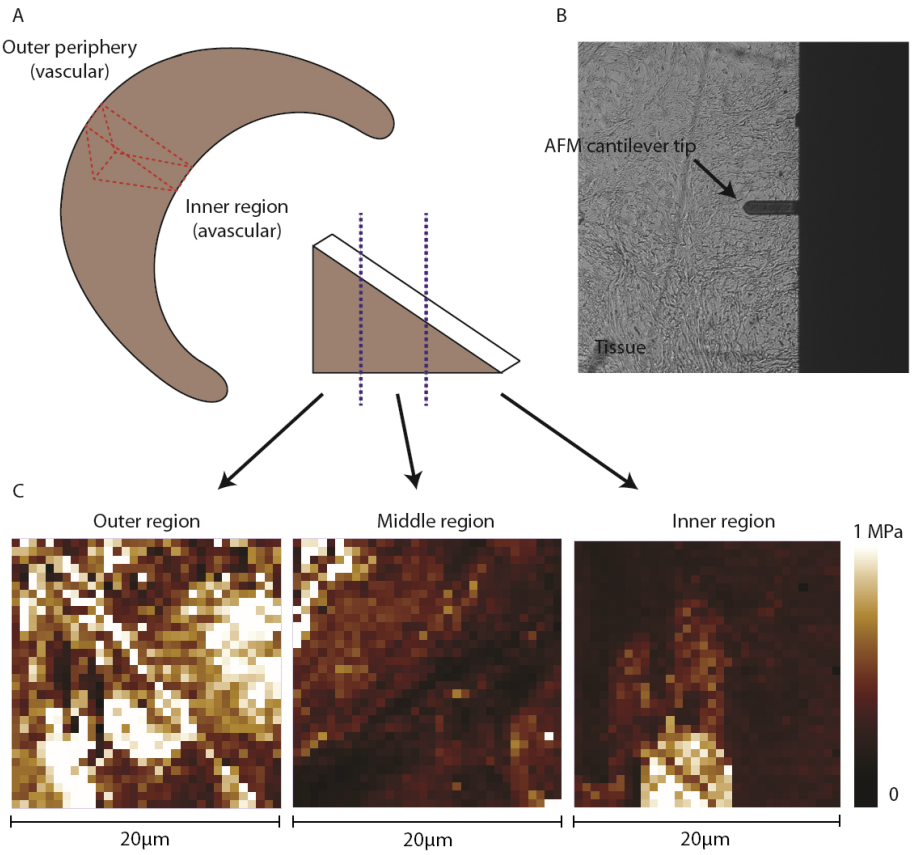


**Figure 2.1**: **AFM schematics for force mapping of human meniscal tissue.** **(A)** Central portion of medial meniscus was sectioned in the sagittal direction (red). The sagittal tissue portion was cut by a cryostat microtome at a thickness of 10 $\mu$m. The regions were defined by the purple line as the outer one-third, middle, and inner one-third of the tissue. **(B)** AFM cantilever tip with a glass microsphere attached (5 $\mu$m in diameter) was used to probe the tissue sample surface of the ECM. **(C)** Representative force maps (scan size of 20 $\mu$m $\times$ 20 $\mu$m) of outer, middle, and inner regions were generated from which the elastic moduli was extracted and plotted in histogram distributions.

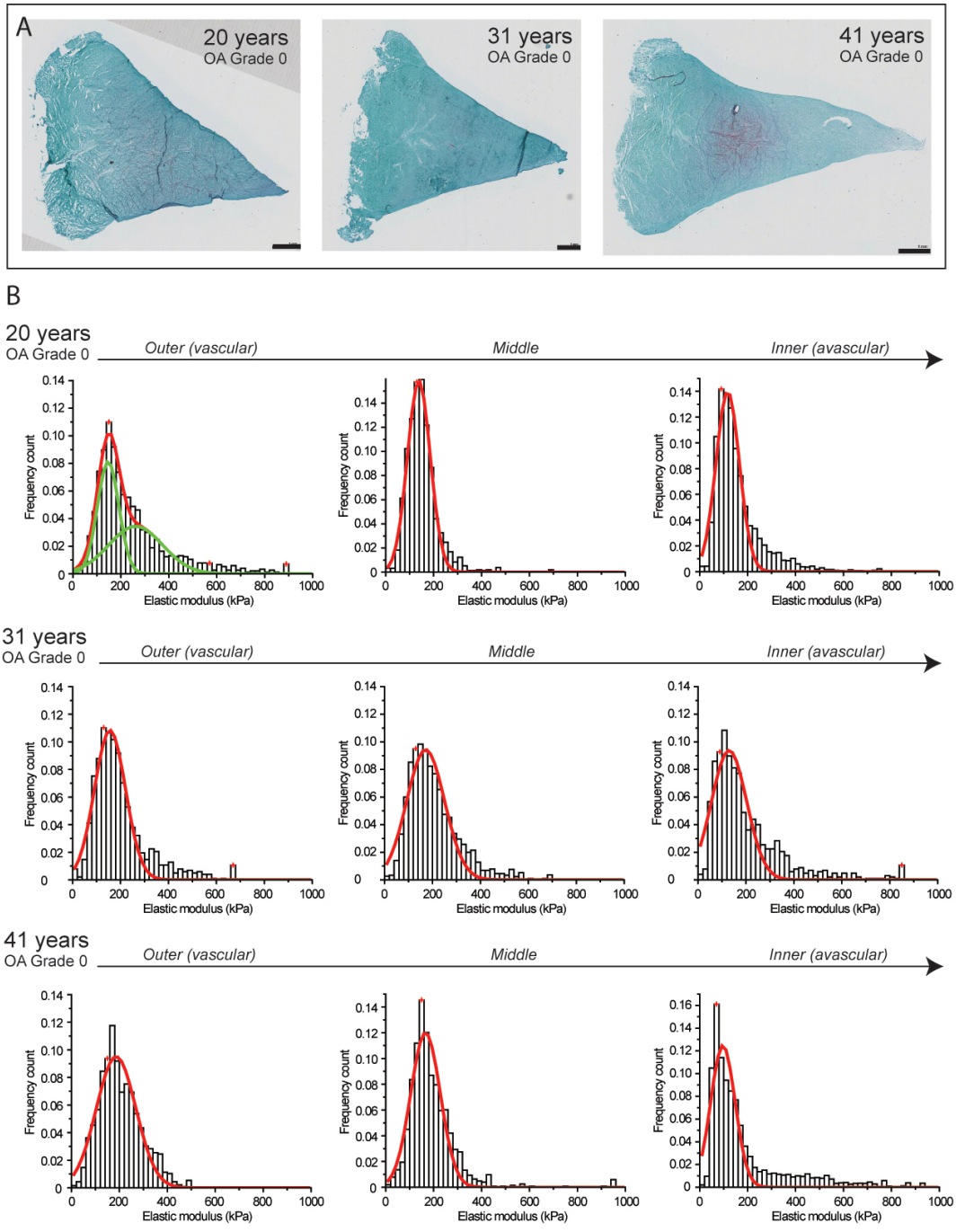


**Figure 2.2**: **Nanomechanical properties of ECM of healthy normal human meniscal tissue with OA grade 0.** **(A)** Histological overview of the samples shows minimal Safranin-O staining (in purple) indicating young, normal meniscal tissue. Scale bar = 1 mm. **(B)** Corresponding stiffness distributions with a multi-peak Gaussian curve fit (in red and green) reveals sharp distinct peaks within each region, representing regional differences across the tissue: outer and middle (peak values from 130 to 150 kPa) and inner region (peak values from 70 to 90 kPa).

**Table 2.1**: **Mean elastic moduli determined from individual donor samples belonging in three groups: normal, aged, and degenerated OA human menisci.**

| Age (years) | Tissue Condition | OA Grade | Elastic Molulus (kPa) | | |
|---|---|---|---|---|---|
| | | | Outer | Middle | Inner |
| 20, 31, 41 | Normal | 0–1 | 205.6 ± 8.9 | 188.0 ± 21.9 | 176.7 ± 28.0 |
| 55, 56 | Normal Aged | 1–2 | 303.0 ± 28.3 | 282.4 ± 30.2 | 274.0 ± 8.7 |
| 61, 75, 90 | Aged OA | 4 (TKA) | 364.3 ± 72.2 | 401.9 ± 39.2 | 265.9 ± 106.5 |

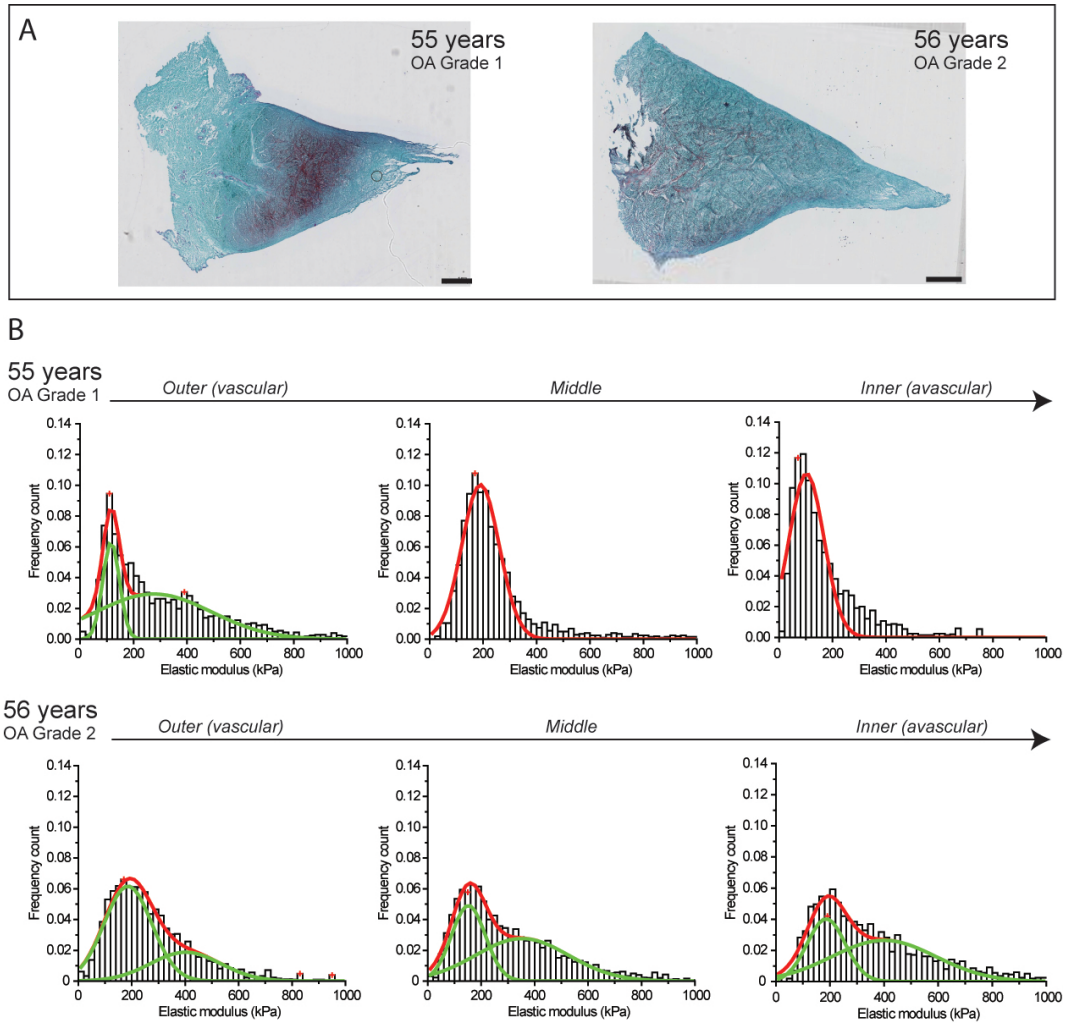


**Figure 2.3**: **Nanomechanical properties of ECM of aged human meniscal tissue with OA grade 1-2. (A)** Histological analyses of normal aging samples show slight to moderate Safranin-O staining (in purple) typical of normal tissue degeneration due to aging. Scale bar = 1 mm. **(B)** Stiffness distribution with multi-peak Gaussian fit curves (in red) revealed both unimodal and bimodal (in green) distributions with regional variations but with a broader distribution that shifts toward stiffer values with increasing age.

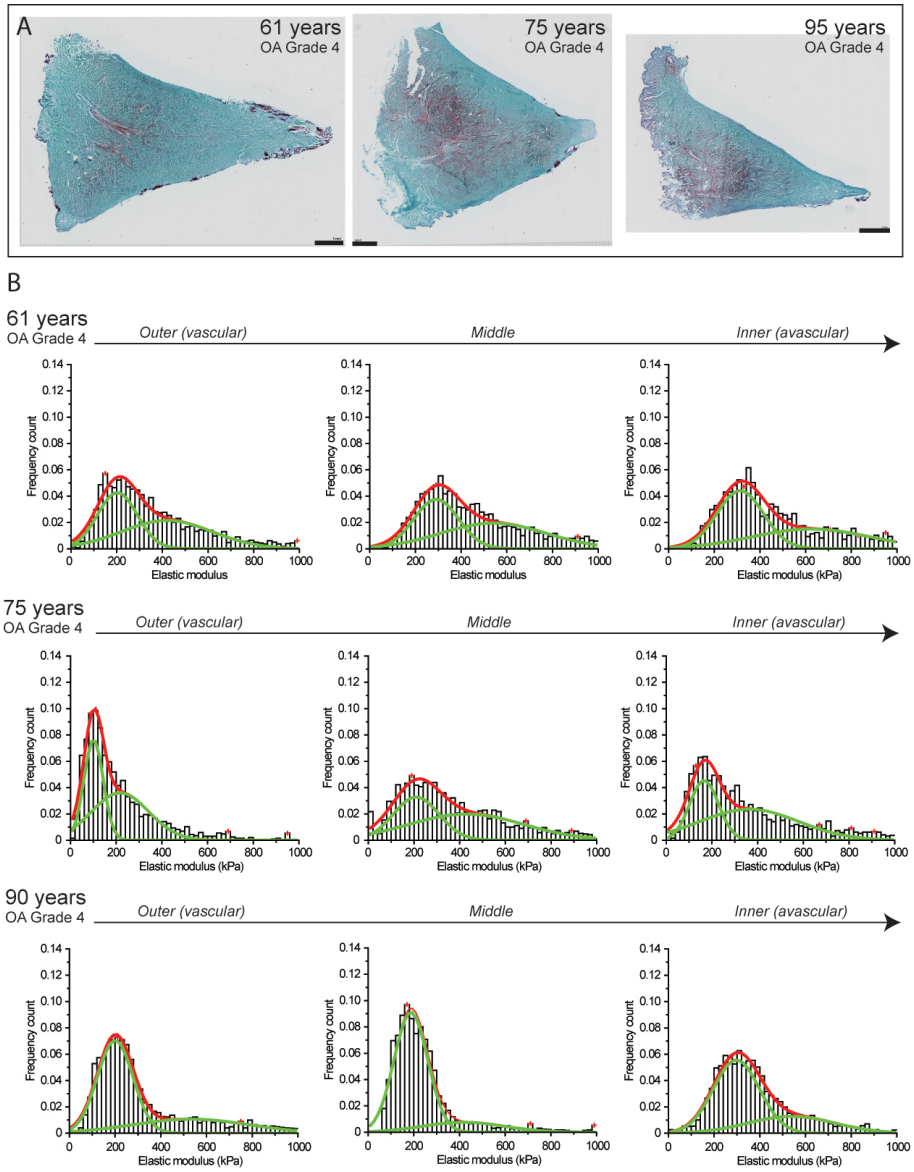


**Figure 2.4**: **Nanomechanical properties of ECM of degenerated human meniscal tissue removed from patients with severe OA undergoing total knee arthroplasty.** **(A)** Histopathology of all three OA samples show a more intense Safranin-O staining (in purple) associated with severe matrix degenerative changes in the ECM. Scale bar = 1 mm. **(B)** Corresponding elastic moduli distributions with multi-peak Gaussian curve fits (in red) demonstrate a significant increase in stiffness with broadened bimodal distributions (in green) and increased nanomechanical heterogeneity across regions (from outer to inner, left to right).

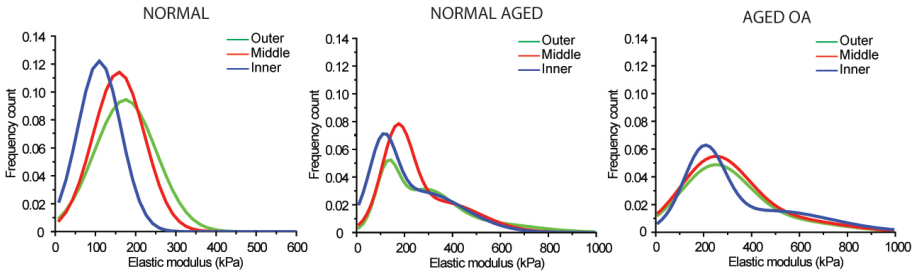


**Figure 2.5**: **Nanomechanical profiles for normal, aged, and degenerated OA human menisci revealed unique qualitative representation of aging and degenerated/diseased conditions.** Healthy normal meniscal tissue presents narrow distinct peaks of the three regions while normal aged and degenerated OA samples display a broadened bimodal distribution indicative of increased mechanical heterogeneity across all regions.

# Chapter 3

# Histopathological Analyses of Murine Menisci: Implications for Joint Aging and Osteoarthritis

## 3.1 Abstract


### 3.1.1 Objective

To establish a standardized protocol for histopathological assessment of murine menisci that can be applied to evaluate transgenic, knock-out/in, and surgically induced OA models.

### 3.1.2 Methods

Knee joints from C57BL/6J mice (6 to 36 months) as well as from mice with surgically-induced OA were processed, and cut into sagittal sections. All sections included the anterior and posterior horns of the menisci and were graded for (1) surface integrity, (2) cellularity, (3) Safranin-O staining distribution and intensity. Articular cartilage in the knee joints was also scored.

### 3.1.3 Results

The new histopathological grading system showed good inter- and intra-class correlation coefficients. The major age-related changes in murine menisci in the absence of OA included decreased Safranin O staining intensity, abnormal cell distribution and the appearance of acellular areas. Menisci from mice with surgically-induced OA showed severe fibrillations, partial/total loss of tissue, and calcifications. Abnormal cell arrangements included both regional hypercellularity and hypocellularity along with hypertrophy and cell clusters. In general, the posterior horns were less affected by age and OA.

### 3.1.4 Conclusion

A new standardized protocol and histopathological grading system has been developed and validated to allow for a comprehensive, systematic evaluation of changes in aging and OA-affected murine menisci. This system was developed to serve as a standardized technique and tool for further studies in murine meniscal pathophysiology models.

### 3.1.5 Keywords

meniscus; aging; osteoarthritis; histopathology

## 3.2 Introduction

Osteoarthritis (OA) is a whole-joint disorder that invariably affects articular cartilage, subchondral bone, menisci, synovium, ligaments, and muscles [97]. Among these joint tissues, articular cartilage is the most susceptible to developing OA and shows the most profound age-related changes. However, the relationship between articular cartilage and meniscus is known to be critical in the dynamics of knee joint loading and transmission [7, 8, 9, 10, 40, 78, 108]. This relationship is emphasized by the fact that meniscal lesions, partial/total meniscectomy, and meniscal degeneration contribute to the development or progression of OA

[4, 6, 88, 109, 110, 111, 112]. Despite its pivotal role in knee joint loading and OA development, the mechanisms of meniscal pathophysiology in aging and OA are not well understood. Better understanding these mechanistic relationships will improve therapeutic strategies for repairing meniscal injuries as well as preventing and treating OA.

Recent progress in understanding the mechanisms related to aging pathology of cartilaginous tissues for the study of human diseases includes the development and use of animal models (i.e., dogs, rabbits, guinea pigs, rats, and mice) [113, 114, 115, 116, 117, 118, 119]. Murine models are the most versatile due to ease of genetic manipulation, leading to a plethora of transgenic and knockout and knockin strains for various biological studies [120]. Furthermore, the availability of murine models allows for extensive studies that answer key questions concerning the spatial and temporal relationships of changes in menisci as well as in correlation with other joint tissues in aging and disease development. The C57BL/6J inbred strain stain of mice has been widely used to create mutants to study developmental biology and OA pathogenesis [33, 121, 122, 123, 124, 125]. C57BL/6J mice spontaneously develop OA as a function of increasing age [126, 127]. OA can also be surgically induced in mice models with destabilization of the medial meniscus (DMM) being the most widely used model [128].

Several histopathological assessment systems exist to evaluate OA-related changes in articular cartilage. The Osteoarthritis Society International (OARSI) histopathology initiative developed a grading system that focuses on specific pathological features in articular cartilage as well as subchondral bone and synovium [113, 114, 115, 116, 117, 118, 119]. Using this grading system, several studies showed that murine OA models exhibited similar histopathological characteristics as humans, including loss of Safranin O staining, fibrillation, and erosion in articular cartilage [115]. However, similar systems for the assessment of aging, degeneration and OA development in mouse menisci are not available. We reported on a grading system for human meniscal pathology [45]. Due to obvious differences between human and murine menisci, a comprehensive system to evaluate the histopathological status of the tissue (i.e., surface, cell morphology, and tissue

composition) at the microscale is required.

The objectives of this study were to (1) establish a standardized protocol for histopathological studies of meniscal physiology in murine menisci for aging and OA, (2) develop and validate a new histopathological grading system for murine menisci to evaluate and assess major changes in aging and OA, and (3) identify major aging-related changes and OA in murine menisci. In this study, we have used C57BL/6J mice to represent normal aging and OA development to develop and validate the histological grading system.

## 3.3 Materials and Methods

### 3.3.1 Mouse Knee Joints

All animal experiments were performed according to protocols approved by the Institutional Animal Care and Use Committee at The Scripps Research Institute (TSRI). Pathogen-free C57BL/6J mice were purchased from TSRI breeding facility. GFP-LC3 transgenic mice with C57BL/6J genetic background [129] were obtained from the RIKEN BioResource Center. The mice were housed in a temperature-controlled environment with 12-hour light/dark cycles and allowed feed and water ad libitum. The mice were sacrificed at various ages and knee joints were collected for analysis. Both male and female mice were included in this study. A total of 62 mice from six different ages were assessed: 6 (n = 13), 18 (n = 16), 24 (n = 12), 27 (n=8), 30 (n = 8), and 36 (n = 5) months old mice.

OA was experimentally induced in 2 months old mice by surgical destabilization of the medial meniscus (DMM). The meniscotibial ligament, which anchors the medial meniscus to the tibial plateau, was transected by microsurgical technique, which induced mechanical instability in the knee joint [128]. These mice were sacrificed at 2-, 4-, 6-, 8, and 12-weeks post-destabilization (10 mice per time point) and the knee joints were collected for analysis.

### 3.3.2 Tissue Processing and Staining

Entire knee joints were collected by a detailed protocol for tissue collection as previously described [130]. Tissue specimens were harvested and fixed using zinc-buffered formalin (Z-Fix; ANATECH LTD, Battle Creek, MI). Knee joints were decalcified in TBD-2 (Shandon Inc., Pittsburgh, PA) for 12 hours on a shaker and then washed.

After fixation, samples were embedded in paraffin. Knee joint sagittal sections (4 $\mu$m thick) were cut from the medial compartment at the junction between the middle region of the menisci and the anterior/posterior horns. These sections were cut until the anterior and posterior horns appeared as triangles between the femoral condyle and tibial plateau. The sections were then stained with Safranin O/Fast Green. All sections Safranin O staining was used to evaluate proteoglycan content and pathological changes.

### 3.3.3 Development of the Histological Grading System

The histological grading system reported in this study was developed by carefully reviewing age-related changes in meniscal sagittal sections (including anterior and posterior locations) of 62 mice sacrificed at various ages (Fig. 3.1). The DMM mice (n = 60) were also reviewed 2-, 4-, 6-, 8, and 12-weeks post-destabilization (Fig. 3.2). Three criteria were selected for histological assessment of menisci: (1) tissue surface structures, (2) cellularity, and (3) Safranin O staining distribution and intensity.

### 3.3.4 Validation of the Histological Grading System

The total sum of the scores of all criteria (structure, cellularity, and matrix staining) can range from 0–24. This score is subdivided into 5 grades representing meniscal degeneration state: score 0–5 = Grade 0, score 6–10 = grade 1, score 11–15 = Grade 2, score 16–20 = Grade 3, score 21–25 = Grade 4.

Three individuals familiar with histopathological grading of joint tissues were given a set of 62 sections to grade using the new histological grading system

for menisci. These sections were selected to cover the spectrum from healthy normal to severely degenerated menisci, and randomized for the graders who were blinded with respect to age or disease state. The three sets of scores were used to assess the interclass reliability of the histological scoring system. In addition, one grader scored the same collection of sections twice (3 weeks apart) to assess the intraclass reproducibility of the grading system.

### 3.3.5 Statistical Analysis

All data was presented as mean ± standard error of the mean. Change in score with age was assessed with linear regression to determine if there was a positive increase in score with age using Excel (Microsoft, Seattle, WA). The statistical significance of differences between age groups were assessed by the Kruskal-Wallis test followed by a Wilcoxon test with a Benjamin and Hochberg correction for multiple comparisons using R Project 3.1.0. The Kruskal-Wallis test assumes that the sample population is not normally distributed. $P$-values less than 0.05 were considered significant. The reliability and reproducibility of the histological grading system was assessed by comparing the scores from all graders for all the histological specimens using interclass/intraclass correlation coefficients (ICCs) according to Shrout and Fleiss' schema using a custom written script in Matlab (MathWorks, Natick, MA) [131]. The ICC is measured for consistency when systematic differences between graders are irrelevant. The 95% confidence intervals were computed using bootstrapping in Matlab.

## 3.4 Results

### 3.4.1 Devlopment of the Histological Grading System

Aging-related changes in the menisci were observed in 6 to 36 month old mice (Fig. 3.1). With increasing age, the femoral (F) and tibial (T) surfaces of the menisci can undergo fibrillation and undulation that increase in severity with aging resulting in partial or total loss of meniscal structure. Cellularity also changes with

aging as reflected by the emergence of areas with hyper- and hypocellularity. Age-related changes in the matrix involve a focal reduction of Safranin O staining, which is normally stained homogeneously at the surface. More severe age-related changes were observed in the anterior horn of the menisci. Based on these observations, a histological grading system of menisci was developed in the context of age-related changes.

For the histological evaluation of meniscus, criteria were selected based on the major age-related changes [45, 122, 132] independently observed in the anterior and posterior regions as well as different regions. These criteria included: (1) surface integrity (femoral and tibial aspects, and inner rim); (2) cellularity (vascular and avascular regions, and superficial zone); and (3) Safranin O staining distribution and intensity (vascular and avascular regions, and superficial zone) (Table 3.1). Each criterion describes four observations, scored 0–3, in varying regions (Fig. 3.3). Following evaluation of each criterion, a total score was calculated representing the pathological state of the meniscus. The presence or absence of blood vessel formation, calcification (ossification), and inflammation were recorded separately.

### 3.4.2 Validation of the Histological Grading System

A total of 62 mouse menisci (normal aging and surgical OA models) were graded independently by three graders using the new histological system. The total scores for all criteria (structure, cellularity, and matrix staining) were summed together which can range from 0 to 24. This range was subdivided into grades 0 through 4 to present progressive stages of meniscal degeneration (Score 0–5 = Grade 0; Score 6–10 = Grade 1; Score 11–15 = Grade 2; Score 16–20 = Grade 3; Score 21–25 = Grade 4). Figure 3 shows representative histopathologic changes of each grade.

Overall there was an age-dependent statistically significant increase in scores ($R^2 = 0.952$) in the C57BL/6J mice as assessed with the new grading system (Fig. 3.4 A). Statistically significant differences in scores were detected starting at 18-months-old mice compared to 6-months ($P < 0.05$). The articular cartilage was

also scored by the OARSI grading system and an age-dependent increase in scores was present as well (Fig. 3.4 C).

Scores for menisci from mice with DMM surgery were significantly higher at 2 weeks compared to normal aging mice without surgery ($P < 0.001$). However, scores for the surgical OA group (DMM model) did not increase further (Fig. 3.4 B) although cartilage scores increased with post-operation time.

Inter-observer variability between three graders was low with an ICC of 0.7423 and 0.6914 for the anterior and posterior regions, respectively (Table 3.2). The ICC between the readers for the surface structural parameter ranged from 0.708 to 0.856 and 0.702 to 0.853 for the anterior and posterior regions, respectively, while the other two parameters (e.g., cellularity and Safranin O staining intensity) revealed lower ICCs. The ICC for the inter-observer variability between the readers was highest for the structural parameter, followed by ICC for overall grade. In addition, one grader repeated the scoring after a minimum period of 3 weeks to assess intra-class grading variations. The absolute agreement between replicate scores was within 0.702 to 0.853. The 95% confidence intervals computed using bootstrapping was 0.7292 and 0.8311 for the anterior region, and 0.6139 and 0.8168 for the posterior region.

### 3.4.3 Analysis of Menisci in Young Mice

Mature C57BL/6J mice at 6 and 12 months of age were examined to identify histological features of normal murine menisci. In these mice, the surface structure was smooth and intact with no or minimal fibrillation or undulation. Cellularity was defined by regions in murine menisci (Fig. 3.5 A). The vascular (outer) regions contained fusiform cells, resembling fibroblast-like cells (Fig. 3.5 B, E). The inner regions contained round and ovoid-shaped cells, resembling the so-called fibrochondrocytes (Fig. 3.5 C, D). These fibrochondrocytes were also found along the superficial zone in the anterior horn, but not in the posterior. In addition, small cyst-like cavities and small ossicles were occasionally observed in the anterior horns of normal mice menisci.

In normal, young mice, a strong correlation between cellular phenotype

and Safranin O staining was observed. The matrix surrounding fibrochondrocytes (avascular and superficial zone) were usually homogeneously stained with Safranin O of moderate intensity (Fig 3.5 C, D). In the vascular regions, only the localized pericellular matrix surrounding fibroblast-like cells were faintly stained by Safranin O while the more distant areas away from the cell were not stained (Fig. 3.5 B, E). Therefore, a normal profile for Safranin O in murine menisci was defined by homogenous staining in avascular and superficial zones with vascular regions devoid of stain. Note, in some 6-month-old mice, this Safranin O staining profile was less defined and more diffuse throughout the menisci. In addition, in some young mice, hypertrophic cells were observed in the avascular zone of the anterior horn.

### 3.4.4 Analysis of Menisci in Aged Mice

The new histological grading system detected moderate meniscal degeneration (Grade 2) by 18 months of age (Fig. 3.4 A). Therefore, age-related changes in murine menisci were identified by examining the histology of 18- to 36-month old mice with no or minimal signs of OA in articular cartilage in comparison to younger mice (6–12 months). In this younger age group, the articular cartilage was relatively intact with low OARSI scores (Fig. 3.4 C).

The aged mice showed mild to moderate levels of meniscal structural changes that include surface fibrillations and undulations. Fibrillations were defined as fraying at the surface while undulations are wave-like or ripple formations at the surface (Fig. 3.6 A, B). These structural changes increased in severity with age. In aged mice, the surface regions became fibrillated and undulated with faint or no Safranin O staining (Fig. 3.6 B).

Compared to young mice, menisci in aged mice also showed a decrease in Safranin O staining intensity in the avascular region and superficial zones. This pattern in Safranin O staining correlated with abnormal phenotypic change mainly in the fibrochondrocytes located in the avascular and superficial zones. Abnormal cell patterns included hypertrophy, cell shrinkage, and cell clustering (Fig. 3.6 C-E). In addition, there were formations of large, irregular cyst-like cavities that are surrounded by structures with a bony spicule appearance (Fig 3.6 F) and

bone marrow-like regions (Fig. 3.6 G). The cavities and ossicles were larger in size in aged mice compared to those observed in young mice. The frequency of the cavities and ossicles were counted with results demonstrating age-dependency for both (Fig. 3.4 D). Less significant changes were found within the posterior horn of menisci though changes in cell size, morphology, and density were most apparent with advanced aged mice.

### 3.4.5 Correlation of Changes in Cartilage and Menisci in Normal Aging Mice

Most changes in articular cartilage occurred at the femoral articular surface in the region covered by the anterior meniscus. Changes in both cartilage and anterior meniscus appeared to be similar and occurred in parallel (Fig. 3.8 A). These changes included alterations in Safranin O distribution, cell reduction, and cell clustering/proliferation. However, the meniscus appeared to better maintain its structure, Safranin O distribution, and cell arrangement compared to articular cartilage. In the 30- and 36-months-old group, most cases showed that articular cartilage underwent more accelerated changes compared to meniscus. This was mainly identified by a greater reduction in Safranin O stain at the femoral surface indicative of focal lesions and degeneration (Fig. 3.8 A). However, a few cases show that the meniscus showed a greater reduction in Safranin O (Fig. 3.8 B).

In the 30- and 36-months-old group, a few mice spontaneously developed OA characterized by severe degeneration of articular cartilage as well as meniscus (Fig. 3.7 A). Both the articular cartilage and meniscus showed an abundant loss of tissue at the superficial zone with fibrillations that extended into the deep zone. This group showed extensive variations in Safranin O staining intensity and distribution. Cellular changes included reduced cell density in many areas as well as the presence of cell clusters, a hallmark of OA that forms in the fibrillated clefts of the superficial zone (Fig. 3.7 B, C). Only in these specimens was cell death (denoted by empty lacuna and pyknotic nuclei) visually prominent in the menisci.

### 3.4.6 Analysis of Menisci in Surgical OA Model

OA was surgically induced by DMM close to the anterior horn (Fig. 3.2). Most of the DMM-related changes presented as an early tissue response within the first 2 weeks after surgery with features not seen in the normal mice or mice with aging-related spontaneous OA. Cells appeared to infiltrate from the synovium through the injury site and spread throughout the tissue as early as 2-weeks post-surgery. Starting at 4-weeks, abnormal histological features similar to age-related changes were observed, including formation of large cyst-like cavities and ossicles. These changes in the cells and extracellular matrix occurred while the meniscus structure and surface remained relatively intact. However, by 12-weeks post-destabilization, all DMM mice developed full-blown OA, defined by severe articular cartilage damage. The histological scores for menisci in the DMM mice did not change significantly over time from 2 to 12 weeks (Fig. 3.4 B).

## 3.5 Discussion

The role of meniscal injuries as well as partial or total meniscectomy in the development OA is well established [111, 133, 134, 62, 49]. However, the mechanistic relationship between age-associated meniscal degradation and OA development is not well understood. Better understanding of meniscal pathophysiology requires mechanistic studies to identify early degradative changes most suitable in animal models. Animal studies in mice could potentially identify key biological processes, which may also be involved in human OA, thus leading to improved therapeutic strategies to treat and repair meniscal injuries as well as to prevent and treat OA in the knee.

A prerequisite for mechanistic studies is a grading system that allows quantification of histopathological changes in mouse menisci. Here, we have developed and validated a grading system for mouse menisci that evaluates aging-associated or experimental OA-related changes. We used C57BL/6J transgenic mice from age 6 to 36 months as this strain of mice most commonly used in studies of joint aging and OA [121, 33, 123, 135, 136]. At 6 months, these mice reach skeletal maturity

and exhibit healthy normal physiology at large. Therefore these mice are used to characterize the healthy, normal meniscus state. These mice can spontaneously develop OA in cartilage with the meniscus showing minimal signs of degeneration. Hence, a DMM mice model was used to induce severe degeneration in menisci for histological assessment and to determine the effects of an unstable meniscus on the development of OA.

There are obvious differences between human and murine menisci, notably their distinct Safranin O staining profiles. In human menisci, young healthy tissues show little to no Safranin O staining, which then increases with age and degradation [45]. In murine menisci, Safranin O staining is present in both young and old mice, though staining intensity and distribution varies with age and degradation. In young, healthy mice, Safranin O staining is concentrated mainly at the superficial zone in the anterior meniscus. In the posterior meniscus, Safranin O staining appears mainly in the inner region. In aged mice, the distribution of Safranin O staining appears disrupted with reduced intensity of staining, which could indicate early signs of degradation. In general, menisci in OA affected mouse knees tend to have much less Safranin O staining compared to human OA menisci.

In murine menisci, there is a strong correlation between cell type and Safranin O staining which is also age-dependent. The rounded 'fibrochondrocytes' reside in areas with dense Safranin O staining, while only the pericellular matrix is stained around the fusiform fibroblast-like cells. In aged mice, strong staining intensity usually correlates with abnormal age-related cellular changes in cell size, morphology, and distribution (e.g., cell shrinkage and cell clustering) (Fig. 3.6). These changes can occur with the articular cartilage surfaces remaining relatively intact. The relationship between meniscus and articular cartilage was also observed in the Safranin O staining profiles, which show a strong correlation between the intensity of staining in articular cartilage and meniscus.

In mice with OA-like cartilage changes, the menisci were severely degraded with numerous and deep fibrillations at the surface and loss of tissue structure. Besides the obvious structural changes, OA-related cellular changes in meniscus include cell clustering in the fibrillated clefts of the superficial zone, which is almost

identical to those seen in articular cartilage [33, 122, 132, 137]. The differences between age-associated versus OA-associated cell clustering are unknown. The DMM mice represent secondary OA induced by injury and abnormal mechanical loading [128]. All of these mice developed an injury-repair response that appeared to take place in three stages over the course of 12-weeks post DMM surgery [138, 139, 140, 141, 142, 143]. A large infiltration of cells at the injury site from the synovium indicated an acute inflammatory response, which was absent in mice with normal knees and aging-related OA [128, 144]. The inflammation was present already at 2-weeks and persisted through 12-weeks post-destabilization. It spread throughout the tissue, indicating a pathologic healing process. Cellular abnormalities, including the formation of cyst-like cavities and ossicles as well as changes in Safranin O staining profile were noted as early as 4 weeks post-surgery. These changes are presumed to be part of an injury-induced repair response associated with abnormal cell proliferation and matrix deposition [138, 139]. Ultimately, this led to the third stage defined by severe meniscal degradation, which evidently influenced the state of articular cartilage. At 12-weeks post-destabilization, all DMM mice developed full-blown OA, defined by severe degradation of articular cartilage as well as meniscus.

Meniscal surfaces often remained intact while distinct age-related changes in Safranin O staining and cellularity was observed within the tissue substance. This indicates that degeneration of menisci possibly initiates within the tissue substance before detection of changes in the surface. This phenomenon was more evident in the DMM model in which dramatic changes in the cells and extracellular matrix occurred with most of the surface structure remaining intact. This result was in direct contrast to degradation of articular cartilage, where changes progressed from the surface to the mid and deep zones. In general, the anterior menisci appeared to undergo more change in cellular and matrix components than the posterior menisci. In the DMM mice, the prominent changes in the anterior segments were also likely due to the location of the surgical injury in the medial meniscus, as shown in the sections (Fig. 3.2). Meniscal surface fibrillations were first seen at the inner rim, which progresses to loss of meniscal tissue, mainly in the avascular

region. Signs of aging and degeneration included formation of cyst-like cavities, inflammation, bony spicules, and bone marrow-like regions. We also observed the presence of hypertrophic-like single cells in regions intensely stained with Safranin O, indicative of abnormal proliferation and hypertrophic differentiation.

A limitation of this study is that only one strain of mice was included in the histological analysis. C57BL/6J transgenic strain is commonly used to study joint aging and OA, as it is known to spontaneously develop OA with aging [115, 128]. Therefore, the present study was developed to quantitatively assess age-related degenerative changes in menisci that accompany OA development. Analysis of knee joints from other mice strains that do not develop OA with aging may reveal differences between aging and osteoarthritic meniscal degeneration. This study also examines only the anterior and posterior locations of the menisci for convenience in establishing a standard protocol for histological analysis of menisci.

In summary, we present a comprehensive meniscus grading system for mouse models undergoing normal aging, aging-related and surgical OA. Previous studies used individual histological grading systems for mouse articular cartilage to evaluate mechanistic studies of articular cartilage pathophysiology [115]. With a standard grading system, outcomes of similar studies can be directly compared to identify mechanisms of meniscal pathophysiology. This system may be useful to characterize the molecular mechanisms that are reflected in the reported age-related changes in the structure, cells, and matrix. This system can also be used to establish the temporal relationship of and identify cause and effect mechanisms of age-associated changes in the menisci. This system was developed to serve as a standardized technique and tool for further studies in murine meniscal pathophysiology models. Further development of this system could integrate evaluations of all joint tissues, including synovium, ligaments, bone, and cartilage regions covered or not covered by the meniscus.

Chapter 3 in part is a reprint of the material *Kwok J, Onuma H, Olmer M, Lotz M, Grogan S P, D'Lima D D. Histopathological analyses of murine menisci: implications for joint aging and osteoarthritis. Osteoarthritis and Cartilage. 2015; Accepted.* The dissertation author was the primary author.

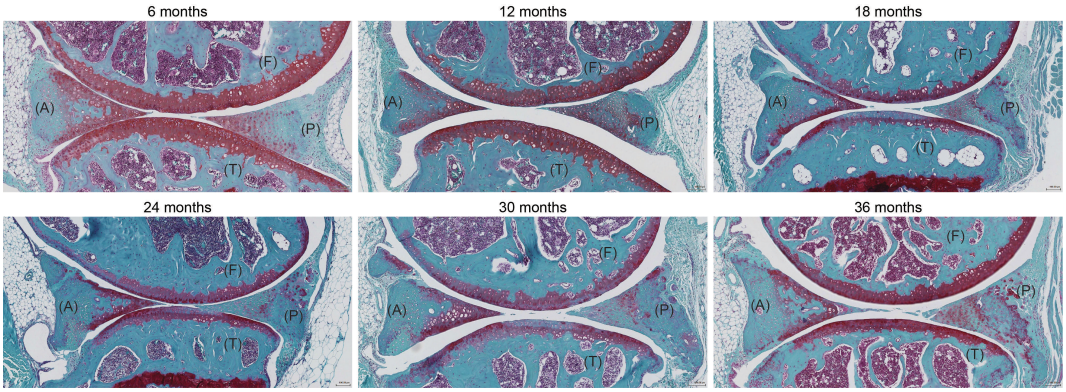


**Figure 3.1**: **Representative images of normal aging in C57BL/6J mice knee joints (6 to 36 months old).** Images show the femur (F), tibia (T) as well as anterior (A) and posterior (P) location of the menisci (Safranin O staining).

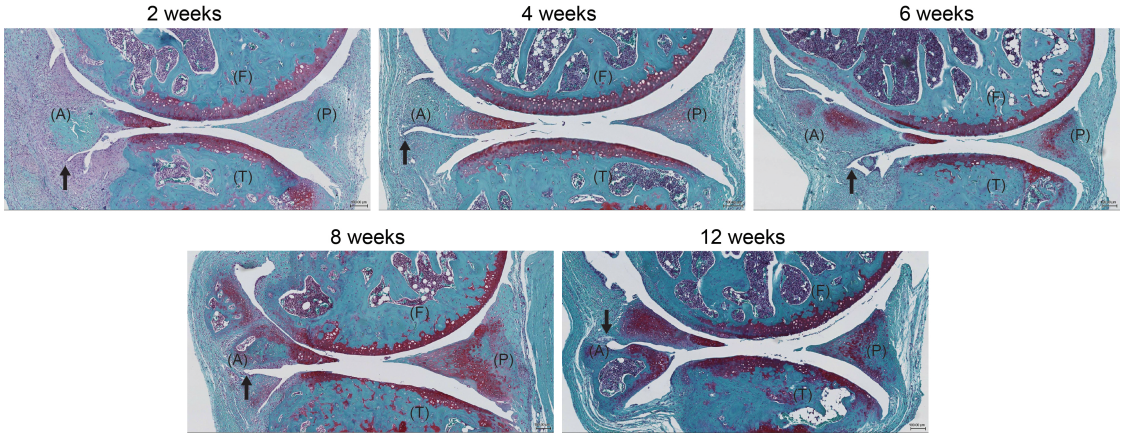


**Figure 3.2**: **Representative images of the surgical/injury DMM model of C57BL/6J mice knee joints (2-, 4-, 6-, 8- and 12-weeks post-destabilization).** Images show the femur (F), tibia (T) as well as anterior (A) and posterior (P) location of the menisci (Safranin O staining). The transection of the meniscotibial ligament (black arrow) intersects the medial menisci, leading to joint stability, meniscal degeneration, and development of OA in articular cartilage.

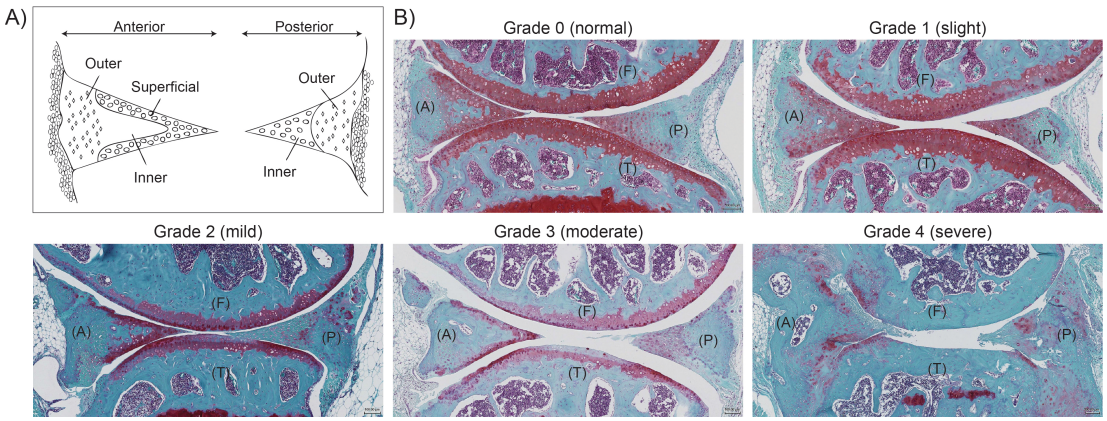


**Figure 3.3**: **Regional assessment of menisci scored by histological assessment. (A)** Diagram demonstrating the different regions of the anterior and posterior portions to be scored by histological assessment. **(B)** Representative images of histopathological grade 0 through 4, showing the femur (F), tibia (T) as well as anterior (A) and posterior (P) location of the menisci (Safranin O staining). Grades were converted from the total scores from the histological assessment: Grade 0 = 0–4, Grade 1 = 5–9, Grade 2 = 10–14; Grade 3 = 15–19; Grade 4 = 20–24.

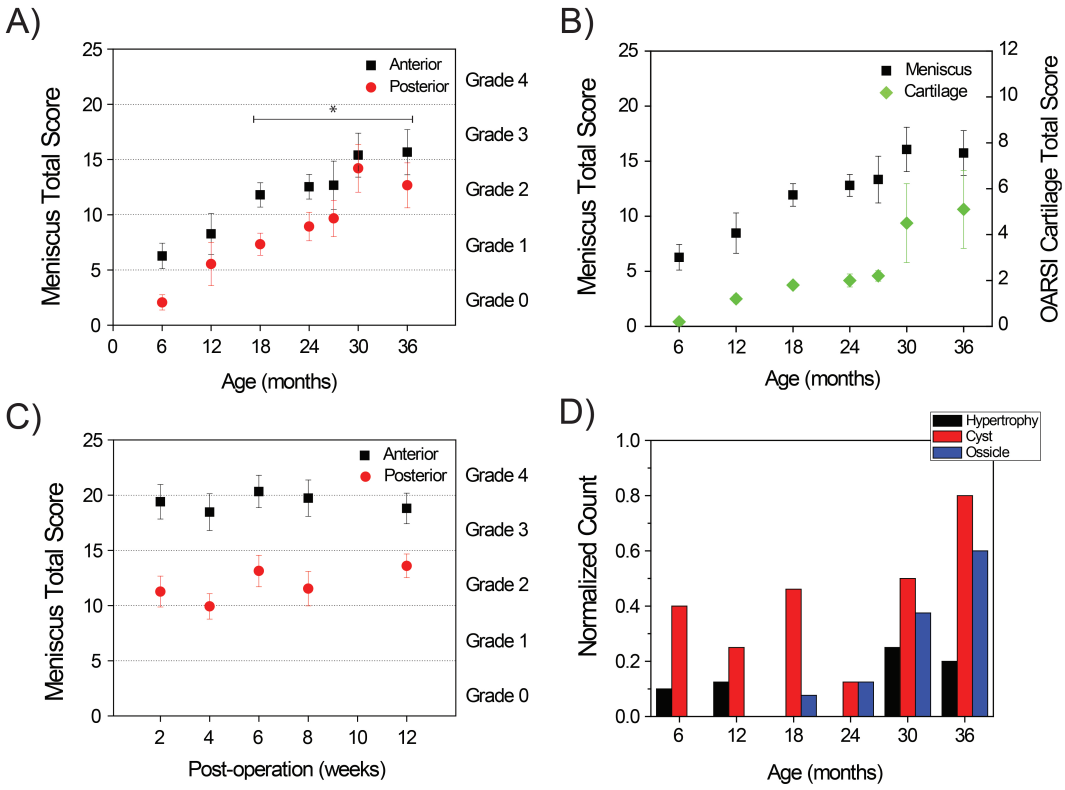


**Figure 3.4**: **Meniscus total scores and grades for menisci (anterior and posterior) obtained with new grading system. (A)** C57BL/6J normal aging mice (asterisk = P $<$ 0.05 versus 6 months old mice) and **(B)** surgically-induced OA mice (DMM model). **C)** Meniscus total scores were compared with articular cartilage scoring by OARSI method. D) Frequency counts of hypertrophy, cyst and ossicle formation in anterior meniscus showing increased incidences with aging.

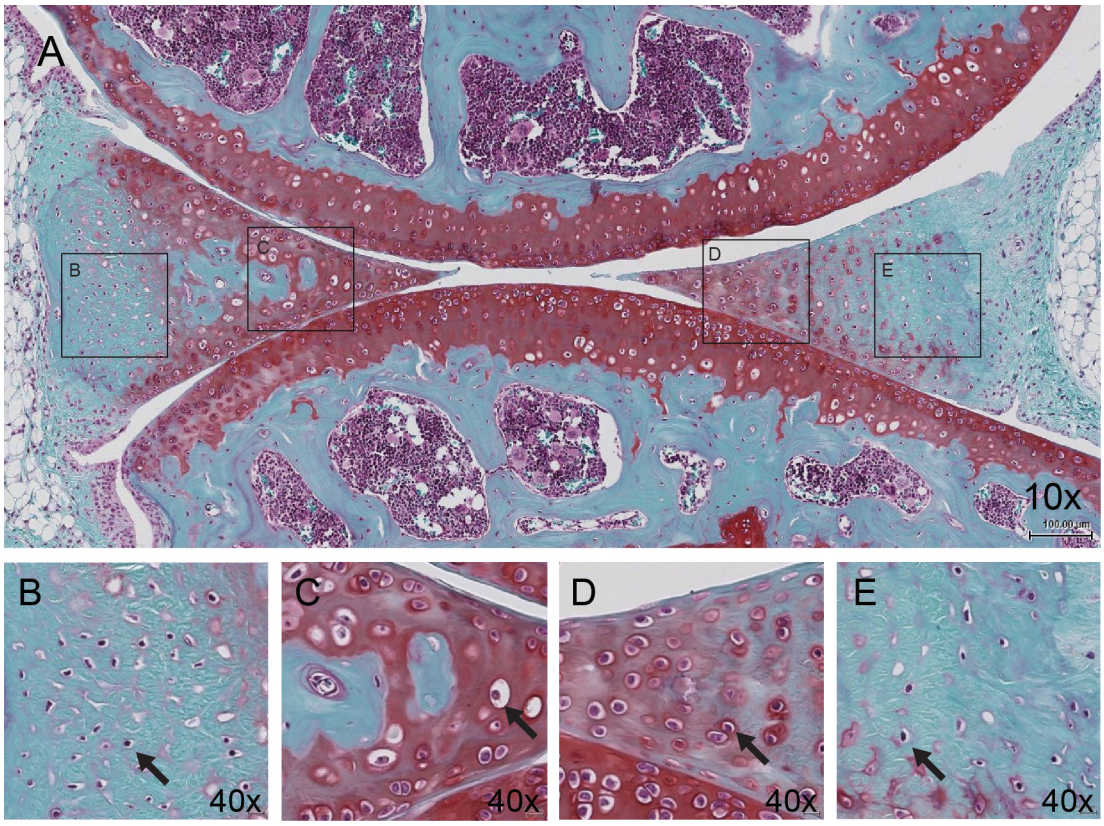


**Figure 3.5**: **Normal pattern of matrix staining and cellularity in young mice (6 months).** A very similar pattern was found in 12 months old mice. A) Minimal to no staining in the outer region and moderate staining in the inner region diffused in the superficial and deep zone. Outer meniscal cells resemble (B, E) fibroblast cells and inner meniscal cells resemble (C, D) fibrochondrocytes (black arrows).

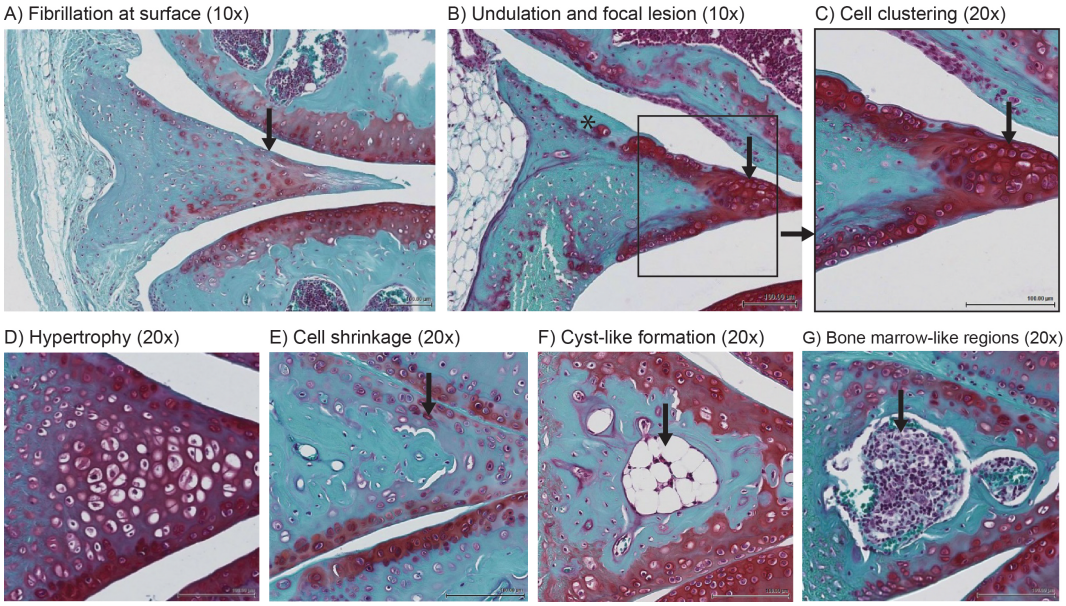


**Figure 3.6**: **Age-related abnormal changes to tissue structure, cells and extracellular matrix in aged mice (24 to 36 months old).** Structural changes include **(A)** fibrillation (indicated by arrow) and **(B)** undulation mainly at the femoral aspect surface (asterisk indicates surface defects with faint or no Safranin O staining). Hypercellular changes included (C) cell clustering (shown in inset and indicated by arrow) and **(D)** hypertrophy. Hypocellularity was observed through **(E)** reduced cell density and cell shrinkage (indicated by arrow). **(F)** Cyst-like formation (indicated by arrow) and **(G)** bone marrow-like regions were also observed more frequently in aged mice (indicated by arrow).

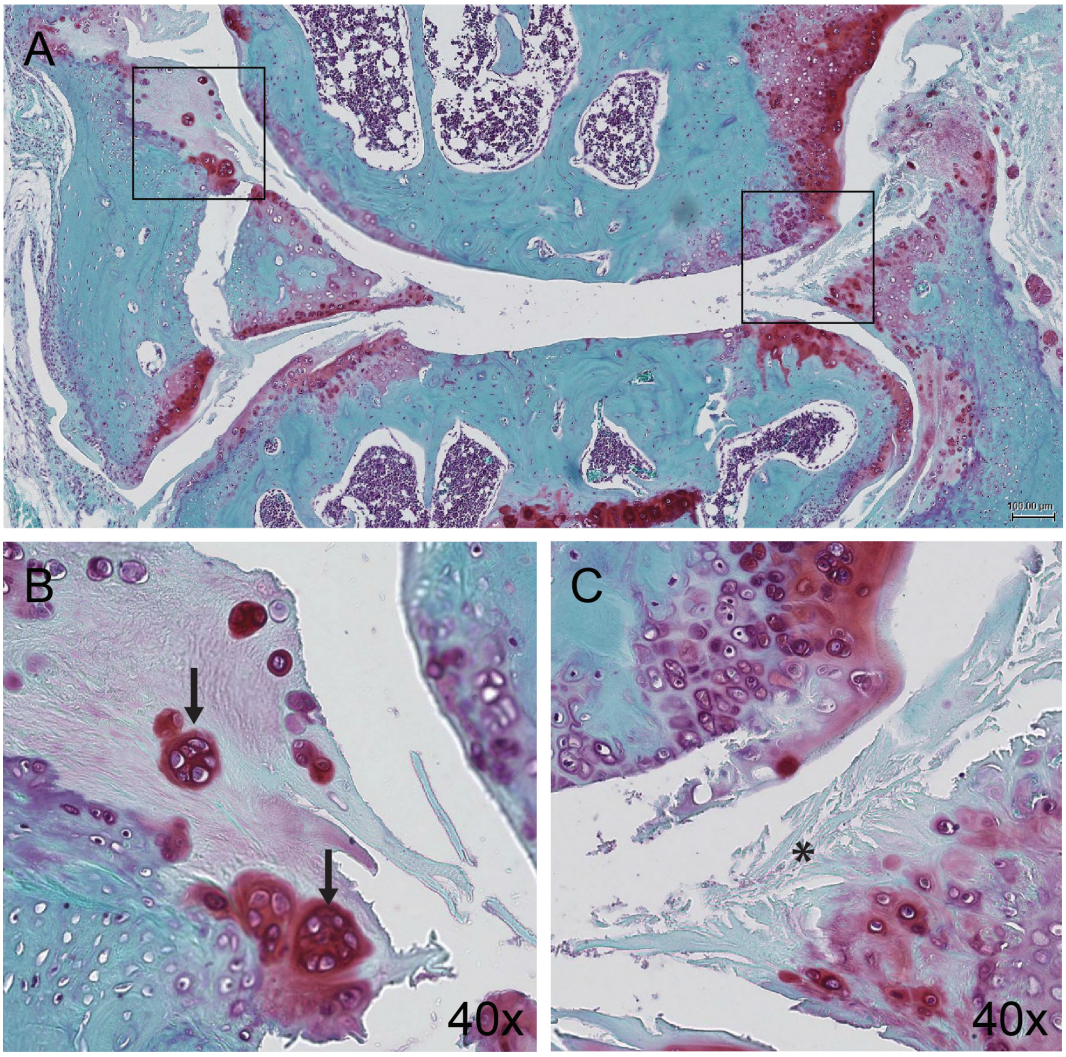


**Figure 3.7**: **(A)** OA manifestation in the meniscus and articular cartilage (36 months) characterized by **(B)** cell clusters (black arrow) and **(C)** severe disruption of meniscal tissue (asterisk) and articular cartilage.

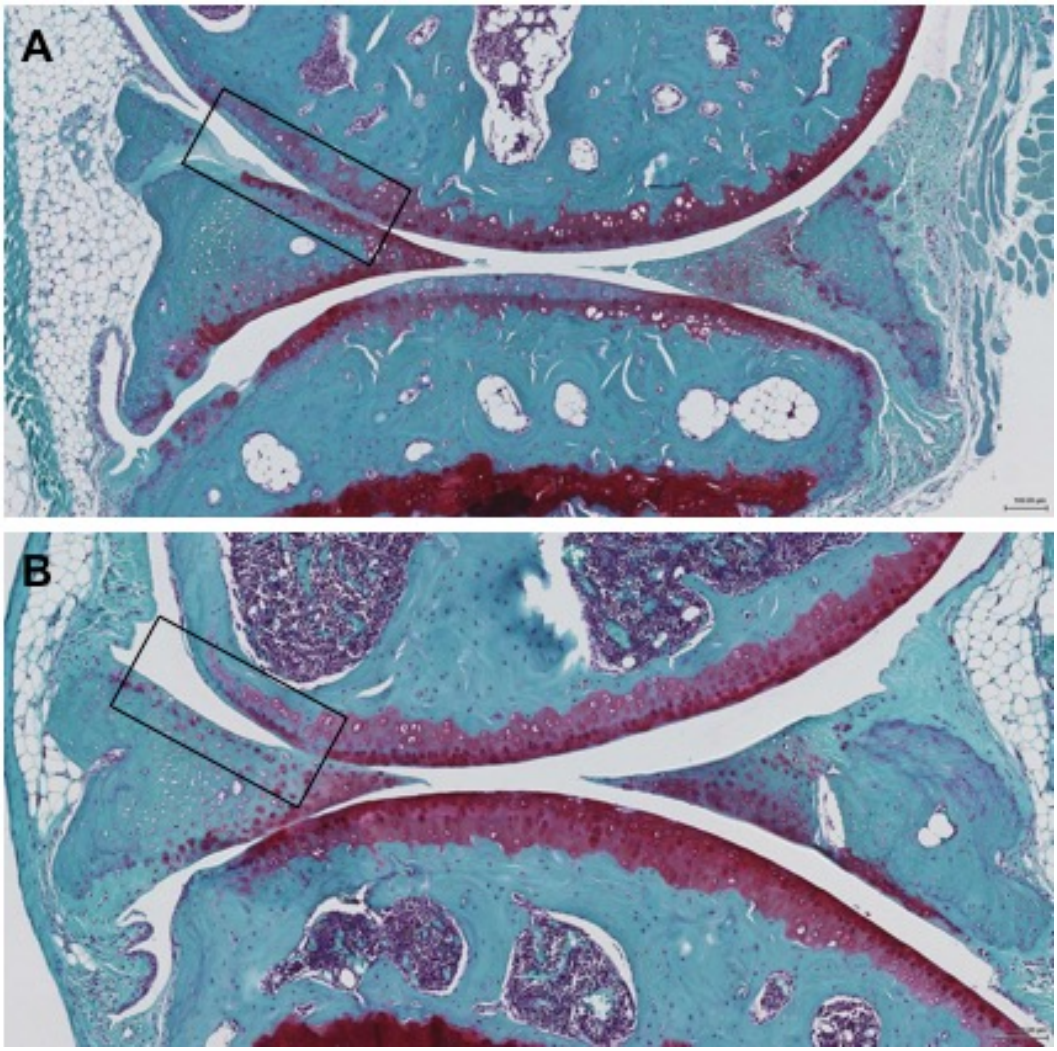


**Figure 3.8**: **Spatial and temporal relationship between articular cartilage and meniscus.** **(A)** In most cases, there is a greater reduction in Safranin O staining in articular cartilage (boxed in black). **(B)** A few cases showed greater reduction in the meniscus (boxed in black).

**Table 3.1**: **Criteria, scores, and observations for histological assessment of menisci.** The range of possible total score is 0-25.

| Criteria | Score | Anterior | Posterior |
|---|---|---|---|
| Tissue Surface Structure | | | |
| Femoral and tibial side, | 0 | Smooth | Smooth |
| inner rim | 1 | Slight fibrillation and undulating | Slight fibrillation or undulating |
| | 2 | Moderate fibrillation or undulating | Moderate fibrillation or undulating |
| | 3 | Severe fibrillation or undulating | Severe fibrillation or undulating |
| | | - Distuption or total loss of tissue | - Disruption or total loss of tissue |
| Cellularity | | | |
| Outer Region | 0 | Normal distribution of fusiform cells | Normal distribution of fusiform cells |
| | 1 | Hypercellularity | Hypercellularity |
| | 2 | Diffused hypocellularity | Diffused hypocellularity |
| | | - Few empty lacuna | - Few empty lacuna |
| | 3 | Hypocellularity | Hypocellularity |
| | | - Empty lacunae, cyst, matrix separation | - Empty lacunae, cyst, matrix separation |
| Inner Region | 0 | Normal distribution of round cells | Normal distribution of round cells |
| | 1 | Hypercellularity | Hypercellularity |
| | 2 | Diffused hypo/acellular zones | Diffused hypo/acellular zones |
| | 3 | Hypocellularity | Hypocellularity |
| | | - Empty lacunae, cyst | |
| Superficial Zone | 0 | Normal distribution of round cells | – |
| | 1 | Hypercellularity | – |
| | | - Cell clustering | – |
| | 2 | Diffused hypocellularity | – |
| | | - Cell shrinkage | – |
| | 3 | Hypocellularity | – |
| Matrix Staining | | | |
| Outer Region | 0 | Normal - slight staining of PCM | Normal - slight staining of PCM |
| | 1 | Slightly disrupted | Slightly disrupted |
| | 2 | Moderately disrupted | Moderately disrupted |
| | 3 | Severely disrupted | Severely disrupted |
| Inner Region | 0 | – | Normal - slight staining of ECM |
| | 1 | – | Slightly disrupted |
| | 2 | – | Moderately disrupted |
| | 3 | – | Severely disrupted |
| Superficial Zone | 0 | Normal - homogeneous staining of ECM | – |
| | 1 | Slightly disrupted | – |
| | 2 | Moderately disrupted | – |
| | 3 | Severely disrupted | – |

**Table 3.2**: **Validation of reliability and reproducibility quantified by ICC for histological grading of menisci.**

| Anterior | Intra-class (3 graders) | Inter-class (1 grader) |
|---|---|---|
| Grade | 0.7423 | 0.8933 |
| Structure | 0.7484 | 0.8387 |
| Cellularity | 0.5784 | 0.8580 |
| Matrix Staining | 0.4816 | 0.8802 |

| Posterior | Intra-class (3 graders) | Inter-class (1 grader) |
|---|---|---|
| Grade | 0.6914 | 0.8040 |
| Structure | 0.7635 | 0.7970 |
| Cellularity | 0.5641 | 0.8091 |
| Matrix Staining | 0.4263 | 0.9365 |

# Chapter 4

# Compromised autophagy precedes meniscus degeneration and cartilage damage

## 4.1 Abstract

### 4.1.1 Objective

Autophagy is a cellular homeostatic mechanism facilitates normal cell function and survival and is activated in response to injury. The objectives of this study are to determine whether altered autophagic response is involved in meniscal injury and to monitor changes in autophagy in menisci during joint aging, degeneration, injury, and OA.

### 4.1.2 Methods

Constitutive activation of autophagy was measured in reporter GFP-LC3 transgenic mice. Meniscal injury was represented by a surgical model of post-traumatic OA in mice by destabilizing the medial meniscus in C57BL/6J transgenic mice. The autophagic response in meniscus was analyzed by confocal microscopy, immunohistochemistry and associated histopathological changes, such as cellular-

ity, matrix staining, and structural damage. These observations were compared to autophagic changes in articular cartilage.

### 4.1.3 Results

In the meniscus, basal autophagy activation was detected at a lower level compared to articular cartilage. With increasing age, the expression of autophagy proteins were reduced. Age-related changes included reduced cellularity, the presence of focal lesions, and general degeneration of both meniscus and cartilage tissue. In the surgical OA murine model, meniscal injury induced autophagy in the meniscus while it was suppressed in cartilage. Cartilage displayed a greater loss of autophagic activity and a higher degree of degeneration compared to meniscus. Systematic administration of rapamycin induced autophagy activation and reduced degenerative changes that manifest as OA in both meniscus and cartilage.

### 4.1.4 Conclusion

Altered autophagic responses accompany aging and degeneration of both menisci and cartilage while maintenance of autophagic activity is critical for joint health and function.

## 4.2 Introduction

Knee meniscal injuries and degeneration are linked to osteoarthritis (OA), the most prevalent joint disease [145, 146, 147, 148]. OA is characterized by degradation loss of articular cartilage, but its pathogenic process most always involves the meniscus. More than 75% of patients with OA concomitantly suffer from meniscal lesions while 50% of patients with a meniscal injury will go on to develop post-traumatic OA within 10 to 20 years [6, 149]. While the exact pathogenic process of meniscal degeneration are unclear, it is suspected that injury or damage to the meniscus disrupts the biomechanical environment at the cellular level [4]. This disruption in tissue homeostasis leads to widespread matrix degeneration that

ultimately manifests as OA of the whole joint [24].

Autophagy is an important cellular homeostatic mechanism that helps maintain normal cellular function and survival under stress-induced conditions, including injury [150]. This catabolic process regulates energy and nutrients though the removal of damaged or dysfunctional proteins and organelles. Defects in autophagy leads to the accumulation of aggregate-prone proteomes and organelles that can result in oxidative stress [151], abnormal gene expression [24], and even cell death [152]. Aging increases the susceptibility of autophagy defects, thus autophagy is involved in many pathogenic processes, including cancer [153], neurodegeneration [27], and musculoskeletal disorders. In osteoarthritis, a reduction in autophagy activity in articular cartilage has been identified as part of the pathogenic process of degeneration [33, 34].

Autophagy is a lysosomal degradation pathway that is activated in response to cellular stress such as nutrient deprivation and hypoxia [154]. Mammalian target of rapamycin complex 1 (mTORC-1) is a key upstream regulator of autophagy as it inhibits serine/threonine-protein kinase (ULK1), a key initiator of autophagy [155]. ULK1 transduces pro-autophagic signals to initiate the formation of phagophores, isolated double-membrane structures [156]. During autophagy, cellular constituents are enclosed by phagophores as they undergoes elongation and closure, driven by two ubiquitin-related conjugation systems: LC3-I to phosphatidylethanolamine, resulting in the formation of LC3-II, and ATG-12 to ATG-5 [32, 157]. Finally, autophagosomes, the double-membrane enclosures, fuse with lysosomes and the enclosed constituents are degraded and released for reutilization as nutrients and energy [154].

Since cartilage as a tissue has a relatively low turnover rate as its resident chondrocyte population cannot be replenished via the vasculature, autophagy is essential for maintaining tissue homeostasis. We previously reported low levels of basal autophagy activation in articular cartilage in normal young, skeletally mature mice under physiological conditions [34]. Articular cartilage showed an age-dependent reduction in the expression of autophagy proteins, ATG-5 and LC3, in both human and mice [33, 34, 158]. This was accompanied by reduced cellularity

and increased apoptotic cell death as well as matrix degeneration and OA development. When aged mice were treated with rapamycin, a pharmacological activator of autophagy, cellularity was preserved and severe damage and degeneration was prevented in the articular cartilage [136]. These observations were also made in a surgically-induced OA mice model. Together, these findings suggest that autophagy plays an important role in joint aging and OA development. Autophagy may also play a role in the relationship between meniscal injury and degeneration, cartilage damage and post-traumatic OA. However, very little is known about autophagy in meniscal cells, and the role of autophagy in meniscus in health, injury, and degeneration.

This study was carried out in parallel to previous studies that examined defective autophagy in articular cartilage during aging and OA [34]. This study was designed to specifically analyze autophagy in the meniscus. The objectives of this study were to determine the changes in and function of autophagy in meniscus 1) during normal aging, 2) in development of joint degeneration following a meniscal injury, and 3) effect of inducing autophagy with a pharmacological activator of autophagy (rapamycin).

## 4.3 Materials and Methods

### 4.3.1 Mice and Tissue Collection

All animal experiments were performed according to protocols approved by the Institutional Animal Care and Use Committee at The Scripps Research Institute. Reporter mice that ubiquitously express green fluorescence protein (GFP) fused to LC3 with a C57BL/6J genetic background (GFP-LC3 transgenic mice) were obtained from the RIKEN BioResource Center [129]. Pathogen-free C57BL/6J mice were also purchased from the breeding facility at Scripps. Both male and female mice were included in this study. Five mice were used per each age group (6, 18, 24, 30 months). Mice were housed in a temperature-controlled environment with 12-hour light/dark cycles, and received food and water ad libitum. Mice were euthanized at the various ages and knee joints were collected for

analysis.

### 4.3.2 Surgically-induced Meniscal Injury in Mice

Five pathogen-free C57BL/6J mice at 2 months old were subjected to surgical transection of the medial meniscotibial ligament and medial collateral ligament in the right knee. A detailed protocol for the surgical procedure has been previously described [128]. The left knee was not subjected to surgery to be used as a control. The mice were euthanized at 10 weeks post-operation and knee joints were harvested for analysis.

### 4.3.3 Rapamycin Treatment

Rapamycin was obtained from LC Laboratories (Woburn, Massachusetts, USA) and dissolved in dimethyl sulphoxide (DMSO) at 25 mg/ml and stored at –20 °C. For injection, the stock solution was diluted in PBS at 1 mg/kg body weight/dose in a total injection volume of 0.3 ml. Mice received daily intraperitoneal injections for 10 weeks and control mice received the DMSO vehicle at 0.4% in a total injection volume of 0.3 ml.

### 4.3.4 Histological Analysis of Knee Joints

A detailed protocol for tissue collection has been previously described [34]. Briefly, knee joints were fixed with zinc buffered formalin (Z-Fix; Anatech) and then decalcified in a Shandon TBD-2 decalcifier for 12 hours on a shaker. Knee joints were washed and stored in PBS at 4 °C, and then cut into ∼70 $\mu$m sections using a Leica VT 1000 S Vibratome. Knee joints were also embedded in paraffin for histology and immunochemistry.

Knee joint serial sections (4 $\mu$m) were stained with Hemoxylin and Eosin (H&E) to evaluate cellularity. Images were taken under 40× magnification and the total number of cells per 100 $\mu m^2$ in each section was counted. Sections were also stained with Safranin O-fast green for histological analysis using a semi-quantitative grading system for meniscal degeneration (Chapter 3). Briefly, three

parameters, tissue structure, cellularity, and Safranin O staining were scored to determine the degenerative states of meniscus as follows: 0 = absent, 1 = slight (grade 1), moderate (grade 2), or severe (grade 3).

### 4.3.5 Immunohistochemistry

Knee joint serial sections (4 $\mu$m thick) were first deparaffinized in xylene substitute Pro-Par Clearant (Anatech) and then rehydrated in a series of graded ethanol and water. Sections were blocked with 5% serum for 30 minutes at room temperature and then incubated with ATG-5 antibody (1:500 dilution; Novus Biologicals), LC3-antibody (1:1,000 dilution; MBL International), and poly(ADP-ribose) polymerase (PARP) p85 (Promega) overnight at 4 °C. After washing with PBS, sections were incubated with biotinylated goat anti-rabbit secondary antibody for 30 minutes at room temperature and then with Vectastain ABC-AP alkaline phosphatase (Vector Laboratories) for 30 minutes at room temperature. Slide were washed and developed in alkaline phosphatase substrate for 10 to 15 minutes.

### 4.3.6 Immunostaining and Fluorescent Imaging of Autophagosome Formation

A detailed protocol for immunostaining of knee joint vibratome sections has been previously described [34]. Briefly, sections are incubated with Hoechst 33342 (1:1,000 dilution; Life Technologies) for 1 hour at room temperature to label nuclei. For localization of LC3, sections were incubated with anti-LC3 antibody (1:5,000 dilution; MBL International) in PBS with 1% normal goat serum and 0.3% Triton X-100 for 1 hour at room temperature and 2 days at 4 °C on a vertical shaker. Sections were also incubated with Alexa Fluor 568–conjugated goat anti-rabbit antibody (1:400 dilution) in PBS/0.3% Triton X-100/1% NGS for 1 hour at room temperature. After incubation, sections were mounted with ProLong Gold antifade reagent (Life Technologies) for confocal microscopy.

### 4.3.7 Quantification of Atg5 and LC3 expressing cells

For each mice, images of anterior and posterior menisci, and articular cartilage (regions covered by menisci) were taken at the tissue surface ($\sim$100 $\mu$m in depth) under 40$\times$ magnification. The total number of ATG-5 and LC3 expressing cells per 100 $\times$ 100 $\mu m^2$ area were counted. The results were reported as percentage of ATG-5 positive cell density per 100 $\mu m^2$ area.

### 4.3.8 Stastical Analysis

Statistically significant differences between two groups were determined with the Mann-Whitney-Wilcoxon test. Statistically significant differences between multiple comparisons were determined using a Kruskal-Wallis test. $P$ values less than 0.05 were considered significant. The results are reported as mean $\pm$ standard deviation.

## 4.4 Results

### 4.4.1 Autophagosome Formation in Menisci and Age-Related Changes

GFP-LC3 transgenic mice were used in this study. These mice ubiquitously express GFP-LC3, which serves as a specific biomarker for autophagic vesicles. The accumulation of GFP puncta indicates the formation of autophagosomes, which can be individually detected as discrete signals of high fluorescence. These signals were analyzed based on the average number of vesicles per cell (Fig. 4.1 A).

We first analyzed autophagosome formation in menisci from young, skeletally mature mice (3–6 months old; n = 5). The GFP-LC3 signals were detected at the meniscal surface, which indicated basal levels of autophagy activation in normal menisci under physiological conditions. These signals were greater in young mice compared to old mice (28–30 months; n = 5). The average number of vesicles per meniscal cell was higher in young mice (4.09 $\pm$ 0.12) compared to old mice (2.17 $\pm$ 0.04), indicating an age-dependent reduction in autophagy activation (Fig. 4.1 B).

To determine the relationship between autophagy activation in menisci and articular cartilage, we compared the autophagosome formation in meniscus to that in articular cartilage. In young mice, the average number of autophagic vesicles per cell was two-fold lower in meniscal cells compared to chondrocytes. This indicated a lower basal level of autophagy activation in menisci compared to articular cartilage. In old mice, the average number of vesicles per cell was reduced to ($2.17 \pm 0.04$) and ($4.28 \pm 0.40$) in meniscus and articular cartilage, respectively, while articular cartilage still maintained higher levels of autophagy activation.

### 4.4.2 Aging-Related Changes in Autophagy Protein Expression

To evaluate the molecular mechanisms of autophagy activation, we performed immunohistochemistry for autophagy markers ATG-5, an autophagy regulator, and LC3, an autophagy effector, in knee joints from mice ages 6, 18, 24, and 30 months. The amount of ATG-5 and LC3 expression correlates with the extent of autophagy activation. ATG-5 and LC3 were expressed mostly in cells in the superficial layer and much weaker in cells in the deep zone of young menisci (Figure 2A). ATG-5 and LC3 expressions were greater in the posterior region of menisci compared to the anterior. The percentage of ATG-5 and LC3 positive cells in the superifical layer decreased with increasing age. The percentage of ATG-5-positive cells were significantly reduced ($P < 0.05$) at 24 months in the anterior region while LC3-positive cells were significantly reduced ($P < 0.05$) at 30 months (Figure 4.2 B). No significant age-related changes in the percentage of ATG-5 and LC3 positive cells were found in the posterior region. In addition, age-dependent reduction of ATG-5 and LC3 positive cells was accompanied by a decrease in total cell density, which was statistically significant ($P < 0.05$) at 24 months.

These findings were similar to those found in articular cartilage [15]. ATG-5 and LC3 expressing cells were primarily located in the superficial layers in young cartilage and were fewer in number in aged mice (Fig. 4.2 A). In aged mice, there was less atuophagy activation, reflected by fewer cells and lower GFP signals, in articular cartilage compared to meniscus (Fig. 4.2 A: 30 months old), suggesting a

spatial and temporal relationship in autophagy deficiencies across the knee joint.

### 4.4.3 Autophagy in Relationship to Meniscal Degeneration

To examine a possible relationship between autophagy deficiencies and meniscal degeneration, we performed histopathological analysis of meniscal degeneration in the mice using a semi-quantitative grading system that we had developed (Chapter 3). The three criteria were scored (0 to 3): tissue structure (smooth, fibrillation, and undulating), cellularity (normal, hypercellularity, and hypocellularity), and matrix staining of Safranin O/Fast Green (normal and disrupted staining). The total score was summed and categorized into grades 0 to 4 indicative of the degree of meniscal degeneration (Grade 0 – normal menisci; Grade 1 indicates – early degeneration; Grade 2 – mild degeneration; Grade 3 – moderate degeneration; and Grade 4 – severe degeneration). We graded each murine menisci, (n = 12; 4 per age group) both the anterior and posteior sections, using this histopathological grading system. The grades correlated with ATG-5 and LC3 expression in the menisci (Fig. 4.3 A). The results show that with increasing grade, indicating advancing degeneration, there is a reduction in autophagy protein expression (Fig. 4.3 B). The reduction of ATG-5 expression was statistically signifcant ($P < 0.05$) at Grade 2 (moderate degeneration) in the anterior menisci, and at Grade 3 (severe degeneration) in the posterior. Histological hallmarks of degeneration include surface fibrillation and undulation where there was faint or no Safranin O staining in the extracellular matrix. Loss of Safranin O staining corresponds to a loss of glycosaminoglycan (GAG) matrix content.

### 4.4.4 Autophagy Changes in Response to Meniscal Injury in Experimental Osteoarthritis

To identify differences in aging-related autophagy function from that in response to meniscal injury, we examined mice knee joints injured by surgical destabilization of the medial menisci near anterior in the right leg. The left leg was not operated on and served as a control. The knee joints were harvested 10-

weeks after the injury and analyzed by histology and immunohistochemistry for ATG-5 and LC3.

Medial meniscal destabilization resulted in a rapid development of OA, as reflected by structural damage to menisci and articular cartilage compared to the control knee joints (without injury/surgery) (Fig. 4.4 A). Articular cartilage appeared to be more severely damaged than menisci. Injury led to a significant increase ($P < 0.05$) in the ATG-5 expression around the injury site in menisci in the anterior horn, while ATG-5 expression was reduced in the posterior region. Autophagy protein expression was almost completely depleted in articular cartilage (Fig. 4.4 B). Compared to normal aging, ATG-5 expressing cell density was much greater in menisci from the injured mice. These findings demonstrate that autophagy in meniscal cells is rapidly activated in response to acute local injury, and suggests that depletion of autophagy in articular cartilage may render it more susceptible to structural damage compared to menisci.

### 4.4.5 Effect of Rapamycin Treatment on Autophagy in Preventing Post-Traumatic Osteoarthritis

To determine whether the induction of autophagy can reduce meniscal degeneration and OA, we treated injured mice with rapamycin, a pharmacological activator of autophagy. Rapamycin directly inhibits the mTOR signaling pathway and induces activation of autophagy [159, 160]. Previously, we investigated the potential of rapamycin as a disease-modifying drug for OA [136]. Rapamycin significantly reduced cartilage degradation and synovial inflammation in mice subjected to DMM. In this study, we examined the menisci from the same mice. The results showed that rapamycin further induced ATG-5 expression in knee joint following injury by DMM with a signficant increase in ATG-5 positive cells in the posterior meniscus and articular cartilage (Fig. 4.5 B). Rapamycin treatment appeared to preserve meniscus structure and protected the articular cartilage from damage and OA development (Fig. 4.5 A). These new findings suggest a therapeutic potential of rapamycin as a disease-modifying drug that modulates meniscus and perhaps knee joint tissues collectively in a manner that prevents post-traumatic OA following

meniscal injury.

## 4.5 Discussion

The meniscus plays an important role in knee joint load bearing and transmission [7, 108], shock absorption [10], and mechanical stability [8]. These biomechanical functions protect the articular cartilage from degeneration, damage, and injury. The conventional wisdom is that articular cartilage degeneration is central to the pathogenesis of primary OA. However, meniscal degeneration invariably accompanies moderate or severe OA, and meniscal injury is a common cause for post-traumatic OA [4, 6, 49, 62, 147, 148, 149]. We previously established a role for dysfunctional autophagy in cartilage mechanical injury and OA [33, 34, 161]. In this study, we investigated the role of autophagy response to meniscal injury, aging, and OA. The primary mechanism of the tissue degradation process is abnormal cell function and cell death as a result of homeostatic imbalance which invariably involves autophagy [152, 162]. Autophagy, an essential cellular homeostasis mechanism, protects against cell dysfunction by regulating nutrients and energy and by removing damaged or dysfunctional proteins and organelles [163]. Thus, defects in autophagic response can lead to uncontrolled cellular dysfunction that ultimately manifests as widespread tissue and organ failure in the form of OA [164, 165, 166].

In our previous study, we evaluated the defects in autophagy in articular cartilage degradation and its implications for joint aging and OA in C57BL/6J transgenic mice [34]. Normal cartilage in mice exhibited a steady level of constitutive autophagy, progressing to an aging-dependent reduction in autophagy activation that preceded cell death [34]. The defects in autophagy was most profound in the superficial and upper middle zones, where OA-like structural damages first appears, suggesting that autophagy plays a major role in matrix degradation, cell death, and OA development in cartilage.

The purpose of the present study was to analyze the role of autophagy in meniscal degeneration during aging and injury in mice. Herein, we used the

same GFP-LC3–transgenic reporter mice [34] to establish the baseline constitutive level of autophagy activation in normal menisci. However, meniscal cells exhibited lower constitutive autophagy activation compared to chondrocytes, reflected in the quantitative analysis of autophagosome formation (Fig. 4.1). This difference between meniscal cells and chondrocytes may be due to differences in cell phenotype and mechanical loading profiles between the two tissues, especially as the tissues degenerate.

Autophagic cells, expressing ATG-5 and LC3, in menisci appeared to be fibrochondrocytes, or chondrocyte-like in shape. These cells were primarily located in the superficial layer while very few were found in the deep zone. A similar pattern of autophagy activation existed in the superficial and middle zones of articular cartilage, suggesting that chondrocyte-like cells are primarily responsible for autophagy activation in the knee joint. This observation might be due to similar phenotypes between fibrochondrocytes and chondrocyte, however this is unknown.

Similar to articular cartilage [34], autophagy activity in menisci also reduced with age, as reflected by reduced expression of autophagy proteins, ATG-5 and LC3 (Fig. 4.2). The deficiency in autophagy was invariably associated with meniscal degeneration characterized by our previously reported histological grading system (Kwok et al. Osteoarthritis and Cartilage. 2015. In Press). Higher grades, and more severe degeneration was observed in mice menisci exhibiting lower levels of autophagy proteins compared to menisci with higher expression (Fig. 4.3). Autophagy defects corresponded with structural changes of degeneration that included surface fibrillation and undulation, while histological analysis revealed loss of proteoglycan content and a reduction in cellularity. These observations support a major role for autophagy in meniscal degeneration during aging.

We also evaluated the temporal relationship between autophagy activation in articular cartilage and menisci during aging. In most of the mice knee joints, reduced expression of LC3 in articular cartilage preceded the reduction in meniscus, and cartilage damage was relative greater than meniscal degeneration. It is possible that the autophagy in articular chondrocytes is more susceptible to suppression or dysregulation during aging than in meniscal cells. In fact, this was also observed

in the presence of surgically induced meniscal injury, where autophagy suppression was more profound in articular cartilage than in menisci.

In addition to aging, we previously reported that mechanical injury can also suppress autophagy in articular cartilage [161]. On the other hand, in menisci, injury increased autophagy with visible damage to both the meniscus and cartilage. In contrast to aging, ATG-5 expressing cells were located throughout the menisci and were especially numerous in the region near the site of injury. The increase cells exhibiting high levels of autophagy could be a result of hypercellularity or hypertrophy within the menisci, or cell infiltration from the synovium; the latter being a consequence of the inflammatory and repair response observed at the meniscal injury site.

These observations motivated the further study to examine whether systematic administration of pharmacological autophagy activator, rapamycin, can reduce the severity of meniscal degeneration in injured mice as previously demonstrated for articular cartilage degeneration [136]. While rapamycin treatment resulted in profound changes in articular cartilage, only a slight reduction was observed in the severity of meniscal degeneration, which was associated with minimal change in autophagy protein expression in anterior menisci. These findings suggest that pharmacological activation of autophagy, while not directly reducing meniscal degeneration, may be effective not only in primary OA, but also in preventing or delaying the progression of secondary cartilage degeneration resulting from meniscal injury [30].

The potential mechanisms by which autophagy declines with aging and injury could be related to cellular stresses, namely increased production of free radicals, including reactive oxidative and nitrogen species [24]. In particular, the effects of nitric oxide (NO), an inorganic, gaseous free radical, on autophagy pathways seem to play a critical role in regulating several catabolic processes such as the synthesis of collagen and proteoglycan [167, 168, 169, 170]. Elevated levels of NO have been reported to inhibit autophagy during aging [171, 172] and disease, including OA in articular cartilage [170] and meniscus [173]. Furthermore, NO production has been reported to be higher in articular cartilage compared to menisci

and synovium, respectively [174, 175]. Since articular cartilage seems to be the main source of NO in the knee joint, it is possible that the higher NO production corresponds to higher basal autophagy in cartilage compared to menisci, as shown in the present study. This might also increase the susceptibility for autophagy suppression in articular cartilage with aging, injury, and OA, but warrants further investigation.

One limitation of this study is that the knee joint anatomy, physiology, and biomechanics of mice is different from human [39, 95]. The spatial and temporal associations between autophagy, cell density, and degeneration in cartilage with similar changes in meniscus require further experiments to establish cause and effect. Lastly, our model of meniscal injury was surgically induced and not one of traumatic disruption.

In summary, this study is the first to characterize autophagy in menisci. Baseline autophagic activity was lower in meniscal tissue relative to articular cartilage and suffered an age-related reduction which was associated with histologic evidence of meniscal degeneration. Autophagy was significantly increased in response to meniscal injury. Treatment with rapamycin did not further induce autophagy expression in anterior menisci but reduced the severity of meniscal degeneration and the development of post-traumatic OA. The results link compromised autophagy to meniscal degeneration and to overall joint degeneration.

Chapter 4 is a publication in preparation. *Kwok J, Carames B, Olmer M, Kiosses W, Grogan S, Lotz M, D'Lima D. Compromised autophagy precedes meniscus degeneration and cartilage damage.* The dissertation author is the primary author.

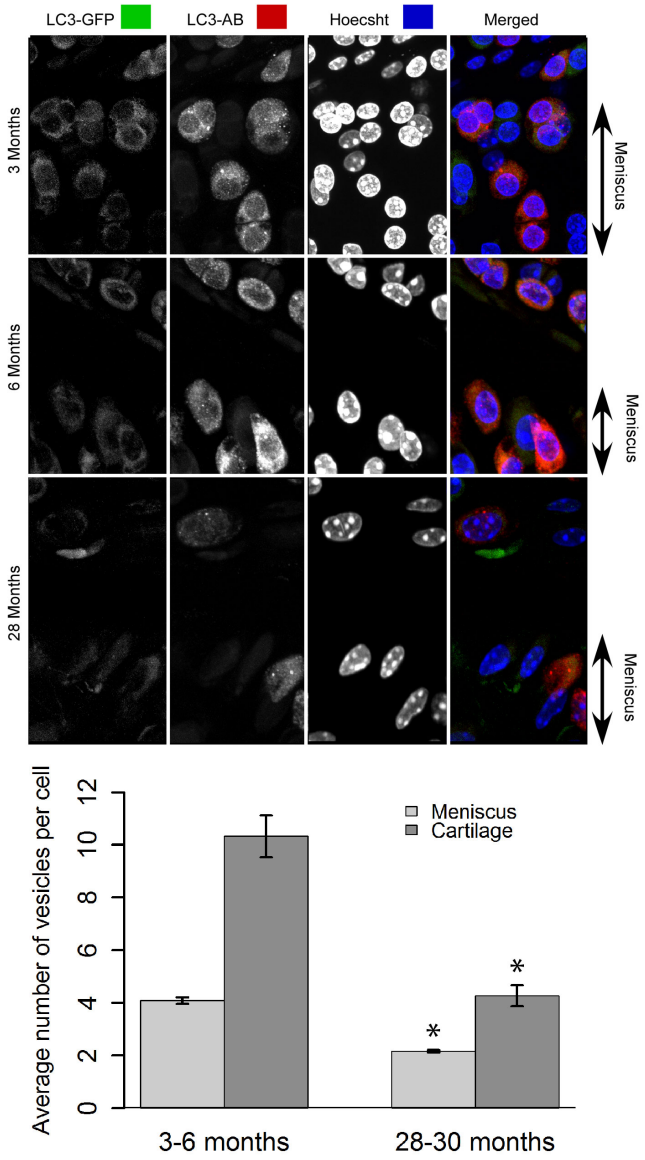


**Figure 4.1**: **Autophagosome formation in meniscus from GFP-LC3 transgenic mice.** Vibratome cut sagittal sections (70 $\mu$m) of mice knee joints were stained with anti-LC3 antibody (AB) and Hoechst 33342 to label nuclei and analyzed by confocal microscopy. **(A)** Representative images of GFP-LC3 signal in 3, 6 and 28 month old mice showing the surface superficial layer of meniscus for each condition. Original magnification 63×. **(B)** Quantitative analysis of autophagosomes in superficial meniscal cells presented as average number of autophagic vesicles per cell. Values are presented as SEM ± mean of five mice per group. $^* = P < 0.05$ versus 6 month old mice.

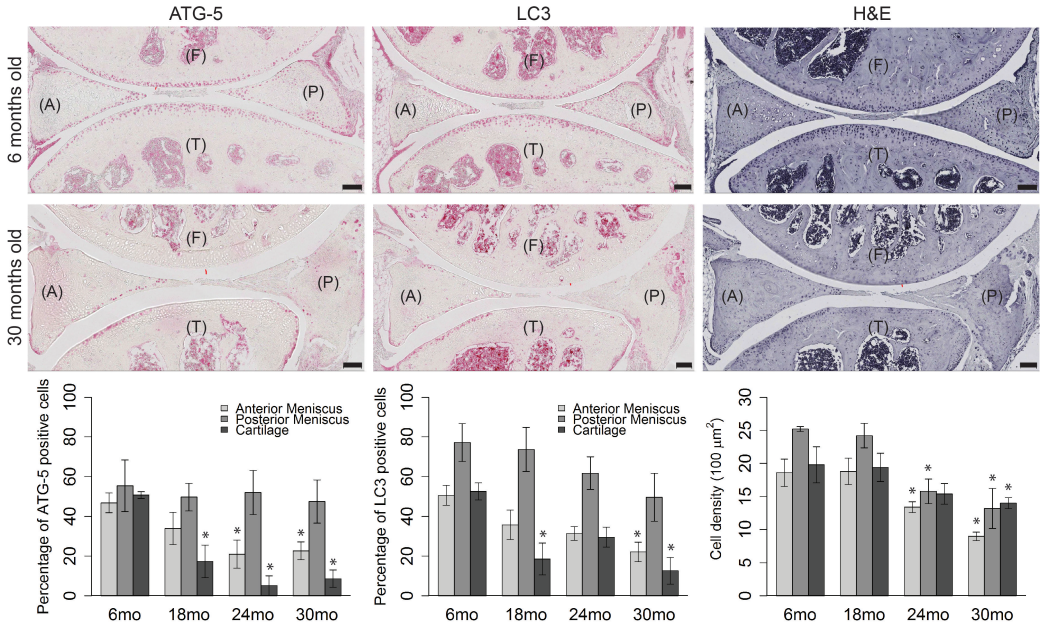


**Figure 4.2**: **Age-related changes in ATG-5 and LC3 expression and cellularity.** Immunohistochemistry for ATG-5 and LC3 were performed on mice knee joint sections. **(A)** Representative images of knee joints from 6 and 30 month old mice stained with ATG-5, LC3, and H&E. Original magnification 10×. **(B)** Percentage of ATG-5 positive cell density per 100 $\mu$m$^2$ area. H&E stained sections were analyzed by total cell density per 100 $\mu$m$^2$ area. Results show a significant decrease in ATG-5 and LC3 cell number and reduced cellularity (H&E). Values are the mean of 5 mice per group. $^* = P < 0.05$ versus 6 month old mice.

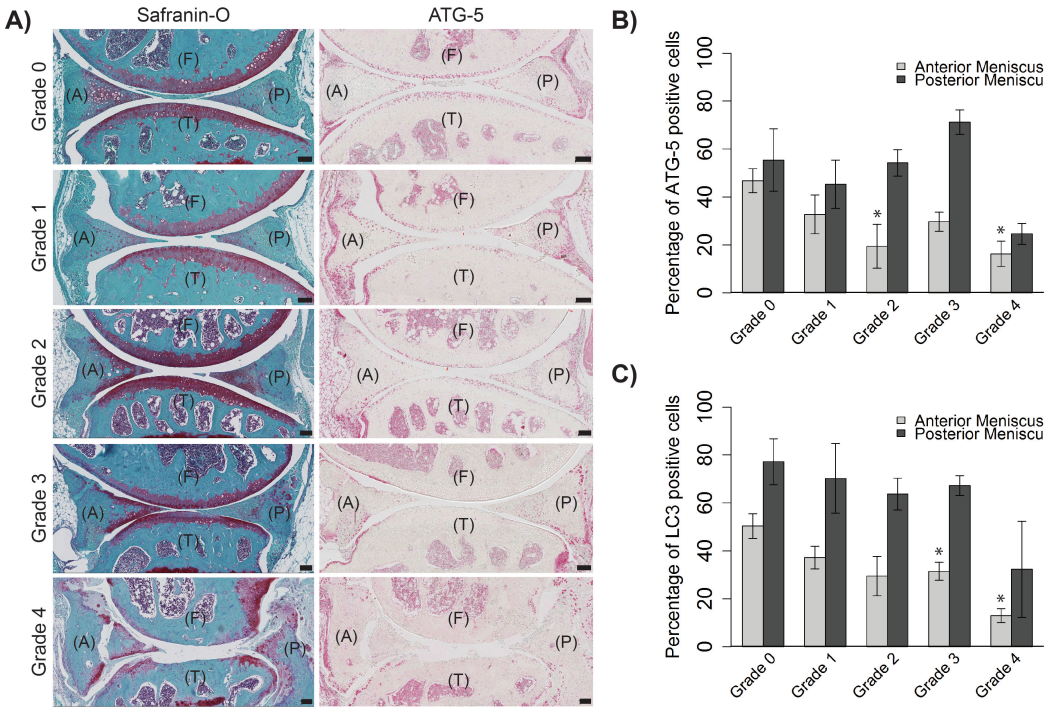


**Figure 4.3**: **Changes in ATG-5 expression associated with meniscal degeneration.** Mice knee joints were analyzed by a semi-quantitative histological grading system for meniscal degeneration in mouse models. Grades are defined from 0 to 4 ranging from healthy normal tissue to severe degeneration. **(A)** Representative images of mice knee joints stained with Safranin-O and ATG-5. Original magnification 10×. **(B)** Correlation of grading with the percentage of ATG-5 positive cell density per 100 $\mu m^2$ area.. Results show a significant decrease in ATG-5 positive cells in the anterior meniscus with advancing degeneration. Values are the mean of 5 mice per group. $^* = P < 0.05$ versus Grade 0 (healthy, normal menisci).

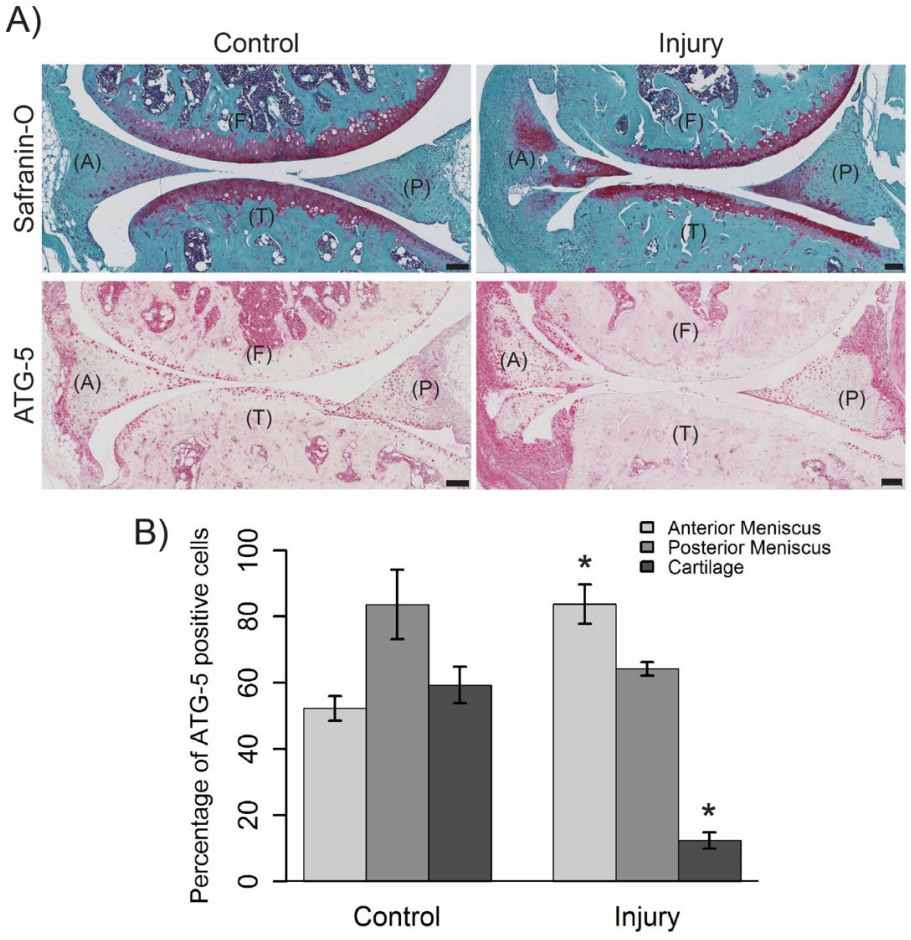


**Figure 4.4**: **Autophagic response following meniscal injury.** 2 month old C57BL/6J transgenic mice were subjected to surgical transection of the medial meniscotibial ligament and medial collateral ligament in the right knee. The left knee was not subjected to surgery to be used as a control. The knee joints were analyzed by Safranin-O staining and immunohistochemistry for ATG-5. **(A)** Representative images of the control and injured mice knee joints stained with Safranin-O and ATG-5. (B) Percentage of ATG-5 positive cell density per 100 $\mu m^2$ area. Results show a significant increase in ATG-5 expressing cells in the anterior meniscus and articular cartilage. Values are the mean of 5 mice per group. $^* = P < 0.05$ versus control.

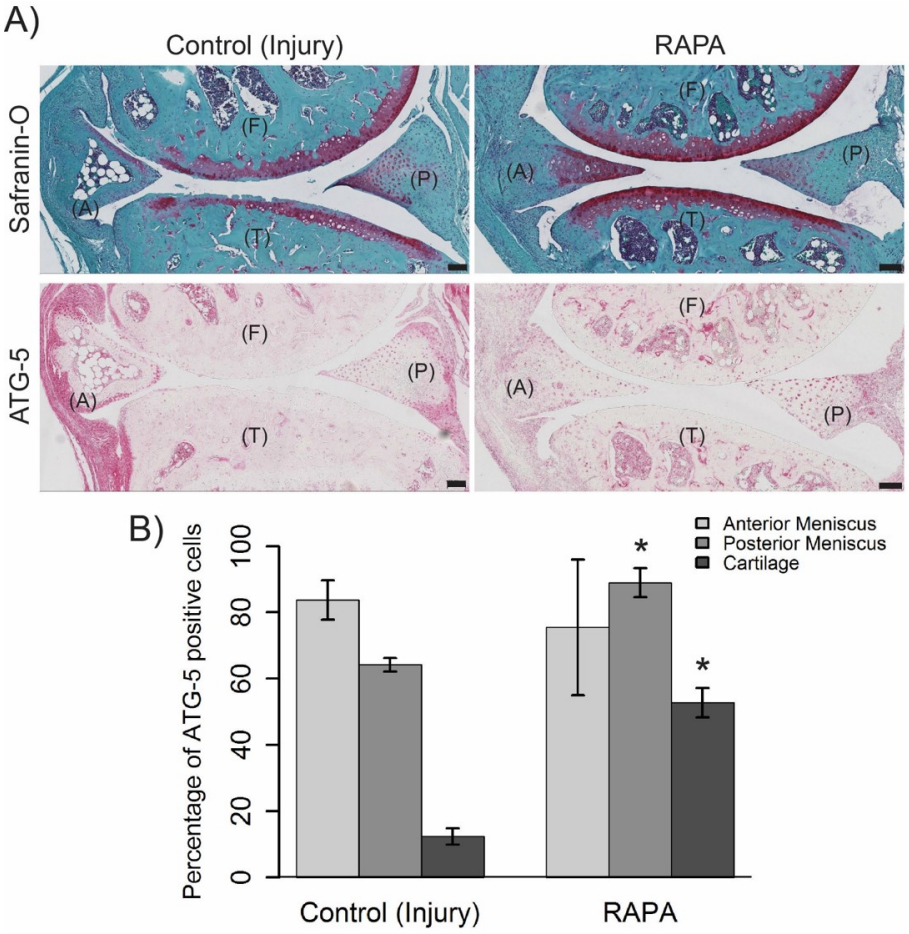


**Figure 4.5**: **Effect of rapamycin treatment on meniscal injury and degeneration.** C57BL/6J transgenic mice with surgically induce meniscal injuries were systematically administrated rapamycin. The knee joints were analyzed by Safranin-O staining and immunohistochemistry for ATG-5. **(A)** Representative images of the control and rapamycin (RAP) treated mice knee joints stained with Safranin-O and ATG-5. **(B)** Percentage of ATG-5 positive cell density per 100 $\mu m^2$ area. Results show a significant increase in ATG-5 expressing cell number in the posterior meniscus and articular cartilage. Values are the mean of 5 mice per group. $^* = P < 0.05$ versus control.

# Chapter 5

# Qualitative and quantitative UTE MRI for morphological and functional assessment of regional variations in meniscus during joint aging, degeneration, and osteoarthritis

## 5.1 Abstract

Meniscal lesions usually result from long-term tissue degeneration, which contributes to the development or progression of osteoarthritis (OA). Clinical magnetic resonance imaging (MRI) can be used to diagnose meniscal lesions and later stages of osteoarthritis, only after established structural damage which is typically irreversible. The short relaxation times, $T2^*$ ($\sim$10 ms) of the tissue limits the detection of early meniscus degeneration. Recent developments in ultrashort echo time (UTE) imaging, however, enables the acquisition of short and ultrashort $T2^*$, which is associated with bound and free water concentrations in the tissue. In this

preliminary study, human menisci from various ages and stages of degeneration were assessed using UTE MR imaging. Nonslice selective two-dimensional UTE MR sequences analyzed by multiexponential models for components of $T2^*$ were used to assess the functional properties of menisci. High resolution 11.7T MR imaging was used to capture morphological changes in the meniscus with aging and degeneration. These sequences have the clinical potential of detecting meniscus degeneration at the early stages and may be more sensitive to monitoring the progression of tissue degeneration.

## 5.2 Introduction

The knee meniscus is a highly ordered structure consisting of a collagen-based matrix and proteoglycans, where composition varies from region to region. The outer region is mainly composed of collagen type I fibers, while the inner region contains both collagen type I and II as well as more proteoglycans [10, 79]. Due to the negative charge of the proteoglycan molecules, the meniscus has a high water content and is $\sim$70% hydrated [5, 10]. This regional organization of structure and composition supports important biomechanical functions in the knee joint, including load bearing, transmission, and shock absorption [7, 108]. Changes in the meniscus tissue upon aging or due to traumatic knee injury compromises the tissue structure and function, thus increasing the susceptibility of the meniscus to further injury including the development of tears and lesions, which then procedes to osteoarthritis. After injury or OA, the structural damage is irreversible and likely will require surgical intervention. Early detection of meniscus degeneration would allow for early intervention and prevention of further meniscus degeneration and lesions to reduce the risk of developing OA.

While meniscal lesions and late stages of osteoarthritis can be detected by conventional magnetic resonance imaging (MRI), early degenerative changes in the meniscus are virtually undetectable as the tissue mostly generates short relaxation time, $T2$ ( 10 ms) [60]. The MR signals from the meniscus characteristically decay much faster than the echo times (TEs) used in conventional MRI, such that

majority of the signals recovered are from the long $T2$ components [176]. This generates little signal for high contrast imaging. In addition, conventional MRI uses half-pulse excitations that are highly sensitive to eddy currents, thus resulting in out-of-slice excitation and low signal-to-noise ratio (SNR) [177].

With the advent of ultrashort echo time (UTE) MR imaging, tissues with predominantly short (0.5–10 ms) and ultrashort (0.05 to 0.5 ms) relaxation times, $T2^*$, can be evaluated. UTE MR imaging uses slice selective two-dimensional (2D) sequences containing a half-pulse excitation followed by a 2D radial ramp sampling that minimizes the TEs by eliminating phase encoding used in conventional MRI [60, 176, 177, 178]. Recent studies in multiexponential $T2^*$ analysis in articular cartilage has shown that short $T2^*$ components are predicative of bound water to the matrix, while long $T2^*$ components are predictive of free water [179]. However, multiexponential $T2^*$ analysis has not been thoroughly evaluated in menisci, particularly in the different regions nor at various stages of degeneration.

In this preliminary in vitro study, the potential for clinically relevant MRI of early meniscus degeneration and progression is assessed. A two-dimensional (2D) UTE sequence for both single component and bicomponent $T2^*$ analysis was used to assess the functional properties that pertain to bound and free water concentration in the different regions of human menisci from increasing ages and degeneration. In addition, high resolution 11.7T MRI was used to assess the morphology of the collagen matrix and vasculature. The objective was to generate preliminary results in order to design a more definitive study to identify correlations between MR properties with histological and biomechanical properties as well as establish MRI changes due to aging and degeneration.

## 5.3 Materials and Methods

### 5.3.1 Tissue Collection

Fresh human knee joints were obtained from donor tissue banks, approved by Institutional Review Board at Scripps Health. Subjects were selected by age and grade scored by macroscopic assessment of the meniscus [45]. Meniscus specimens

from patients undergoing total knee arthroplasty (TKA) at Scripps Health were also obtained. At total of 6 meniscus specimens were collected and processed for MR imaging and histology. For each specimen, a sagittal section (3–5 mm thick) was cut from the central portion of the medial meniscus. The sections were stored in DMEM at 4 °C until MRI.

### 5.3.2 UTE MR Imaging and Assessment

A General Electric 3.0T Signa HDx MR scanner (GE Healthcare, Milwaukee, MI) with a maximum gradient strength of 40 mT/m and slew rate of 150 mT/m/s was used for imaging and data acquisition. A custom Transmit-Receive (T/R) switch was added to the receiver preamplifiers for fast switching between the end of radiofrequency (RF) excitation and data acquisition which enables UTE imaging. A custom birdcage T/R coil (1 inch in diameter) was added for signal excitation and reception. For UTE imaging of menisci, each specimen was placed in a 20 mL syringe filled with perfluorooctyl bromide solution to minimize susceptibility effects tissue-air junctions. The syringe was then placed in the center of the birdcage coil to minimize coil RF inhomogeneities.

A nonslice selective two dimensional (2D) UTE sequence using a short rectangular hard pulse excitation (32 $\mu$s in duration) followed by a 2D radial ramp sampling was used. A short rectangular pulse was used to enhance the signal-to-noise (SNR) ratio and eliminate errors due to the eddy currents associated with the gradient pulse sequences used in conventional half-pulse excitation. Together, with the 2D radial ramp sampling and fast T/R switching, this MR sequence achieves an ultrashort nominal TE of 8 $\mu$s. Images were acquired using a pulse repetition time of 425 ms, field of view of 5 $\times$ 5 cm$^2$, reconstruction matrix of 256 $\times$ 256, and 6 sets of dual TEs of 0.03, 0.2, 0.4, 0.8, 2.2, 6.6 ms and 10, 14, 18, 22, 26, and 30 ms. Only one excitation (number of excitation (NEX) = 1) was needed.

Both monoexponential and biexponential models were used to analyze the apparent transverse relaxation times ($T2^*$). The biexponential model assumes both a short and long $T2^*$ component. Short $T2^*$ components are predicative of bound water, while long $T2^*$ components are predictive of free water. In this model,

the UTE MR signals taken at increasing TEs were measured and then normalized before fitting to a bicomponent function given by the following equation:

$$S_N^*(t) = F_S \times e^{-t/T2_S^*} + F_L \times e^{-t/T2_L^*}$$

where $F_S$ and $F_L$ are the fractions of short $T2_S^*$ and long $T2_L^*$ components [180]. The noise is estimated using a voxel by voxel basis on the bicomponent model developed by Sijbers et al. [181, 182, 183]. This noise corrected model is considered the most accurate and precise method for calculating $T2^*$, especially for low SNR images [183].

Monoexponential and biexponential $T2^*$ analyses were computed using custom written script in MATLAB (The MathWorks, Natick, MA). The script allows for specific region of interests to be selected for analysis and then executes regional averages of $T2^*$ values. In this study, we selected the outer and inner regions as well as the global meniscus for analysis.

### 5.3.3 High Resolution 11.7T MR Imaging

A Bruker Biospec 117/16 USR system (Bruker Corporation, Billerica, MA) with a maximum field strength of 11.7T and a 155 mm bore as well as a maximum gradient strength of 740 mT/m and slew rate of 6,600 T/m/s was used for high resolution MR imaging. Images were acquired using a repetition time of 3000 ms, slice thickness of 5 mm, flip angle of 90°, and acquisition matrix of 300 x 200.

### 5.3.4 Histological

After MRI, the same specimen or tissue from an adjacent region were processed histology. Briefly, the samples were fixed in a zinc buffered formalin (Z-Fix; Anatech) and then decalcified in a Shandon TBD-2 decalcifier for 12 hours on a shaker. The samples were then embedded in paraffin and cut into 4 $\mu$m thick sagittal sections. For histology, the samples were de-paraffinzed and then stained with Safranin O–Fast Green. The samples were then graded for degeneration using a semi-quantitative histopathological grading system for meniscus developed by Pauli et al. [45].

### 5.3.5 Stastical Analysis

Statistically significant differences between 2 groups were determined by Student's unpaired t-test. Statistically significant differences between multiple groups were determined by analysis of variance (ANOVA) with Tukey's multiple comparisons test. $P$-values less than 0.05 were considered significant. Linear regression was utilized to assess wether changes in the long and short $T2^*$ components occured with age or degenaration state. The slopes of the regression lines were assessed for significance with $P$-values less than 0.05 considered significant.

## 5.4 Results

### 5.4.1 Quantitative UTE $T2^*$ Analysis

Through UTE MR imaging, the $T2^*$ components were measured in six menisci from patients of different ages (27 – 69 years old) and at various states of degeneration (Grade o to Grade 3, Table 1). Both single component and bicomponent, short and long $T2^*$ (both fractions and values), were assessed in the global, outer, and inner regions of menisci (Fig. 5.1). Single component analysis showed no signifcant differences in $T2^*$ values with neither age or degeneration. Globally, we approached a significant difference in the short and long fractions when expressed as a percentage ($P = 0.06$). However, we found no significant age-related changes in $T2^*$ components in the global area, or in the outer, and inner regions of the meniscus (Fig. 5.2). No significant differences were found in the short and long $T2^*$ components of increasing degenerative grades either. This is most likely due to the small number of samples scanned so far (n = 6) (Fig. 5.3). However, in general, there was an increase in long $T2^*$ components (fractions and values) in the outer region with increasing age and degeneration, while changes in the inner region displayed variations between samples. This indicates the free water concentration is reduced with increasing age and degeneration. Changes in short $T2^*$ also varied between samples with no significant trend. Compared to the outer region, the inner region consists of lower short and long $T2^*$ components, thus is

more hydrated. Histological analysis of the samples showed a general increase in degeneration with increasing age (Fig. 5.4).

### 5.4.2 High resolution 11.7T MR imaging

Imaging healthy meniscus with the 11.7T MR scanner revealed distinct morphological features, including vasculature (yellow arrow) and collagen fibers in the different orientations, including circumferential (red arrow), radial (green arrow), and lamellar (blue arrow) (Fig. 5.5). Severe collagen disorganization can be observed in the assessment of a meniscus retrieved from a TKA (Fig. 5.6). MR images taken within TEs of 3.63 to 8.21 ms appear to give the highest resolution and contrast.

## 5.5 Conclusion

Meniscal tears represent the most common intra-articular injury and, in most cases, require surgical intervention [5]. Meniscal lesions usually result from long-term degeneration, which ultimately leads to OA. While meniscal lesions and late stages of OA are detectable by conventional MRI, early to moderate meniscus degeneration is virtually undetectable. This occurs due to the meniscus MR spectrum being primarily composed of short $T2$ components that decay much faster than the TEs used in conventional MR imaging, thus the MR signals are invisible with traditional techniques. New developments in MRI enable the detection of ultrashort TEs (0.05 to 5 ms), potentially leading to the identification of early meniscus degeneration. Recent studies have already evaluated degenerative changes in articular cartilage, quantifying bound and free water concentrations, associated with degeneration and OA [59, 60, 177].

In this preliminary in vitro study, we evaluated changes in MR properties in human menisci associated with aging and degeneration. From general observations, long $T2^*$ components tend to increase with advancing age and degeneration, while short $T2^*$ components vary between samples with no significant trends for age or degeneration. This indicates that the free water concentration, quantified by long

$T2^*$ components, is reduced with age and degeneration as expected. Age-related reduction in proteoglycan content has been shown to reduce tissue hydration during degeneration and OA [79]. In addition, short and long $T2^*$ components are greater in the inner region compared to the outer region, which indicate that the inner region is more hydrated than the outer region. This also reflects the abundance of proteoglycans in the inner region compared to the outer region.

Future directions involve a larger study to fully determine aging-related changes in MR properties associated with degeneration. Furthermore, the correlation of MR properties with more specialized histologic imaging (immunohistochemistry and polarized microscopy) and biomechanical properties could provide insight to the biochemical and biomechanical changes associated with aging and degeneration.

Chapter 5 is a publication in preparation. *Kwok J, Shao H, D'Lima D D, Du J. Qualitative and quantitative UTE MRI for morphological and functional assessment of regional variations in meniscus during joint aging, degeneration, and osteoarthritis.* The dissertation author is a primary author.

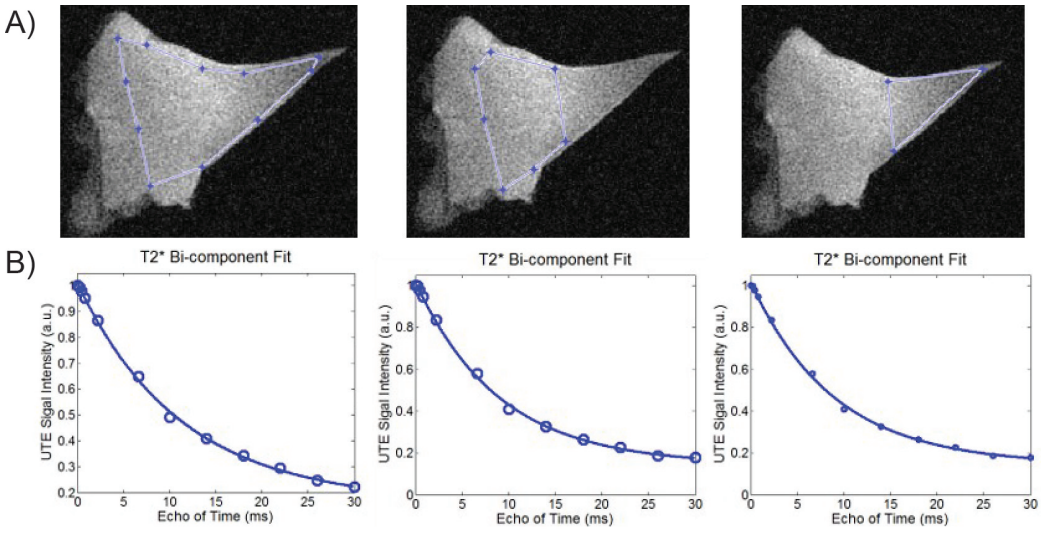


**Figure 5.1**: **Schematic for UTE bicomponent $T2^*$ analysis of human menisci.** **(A)** Regions of interest (outlined in blue) analyzed by UTE MRI included the global, outer, and inner regions, respectively. **(B)** UTE signals from global, outer, and inner region assessment showed rapid decay of $T2^*$ signal with increasing echo time.

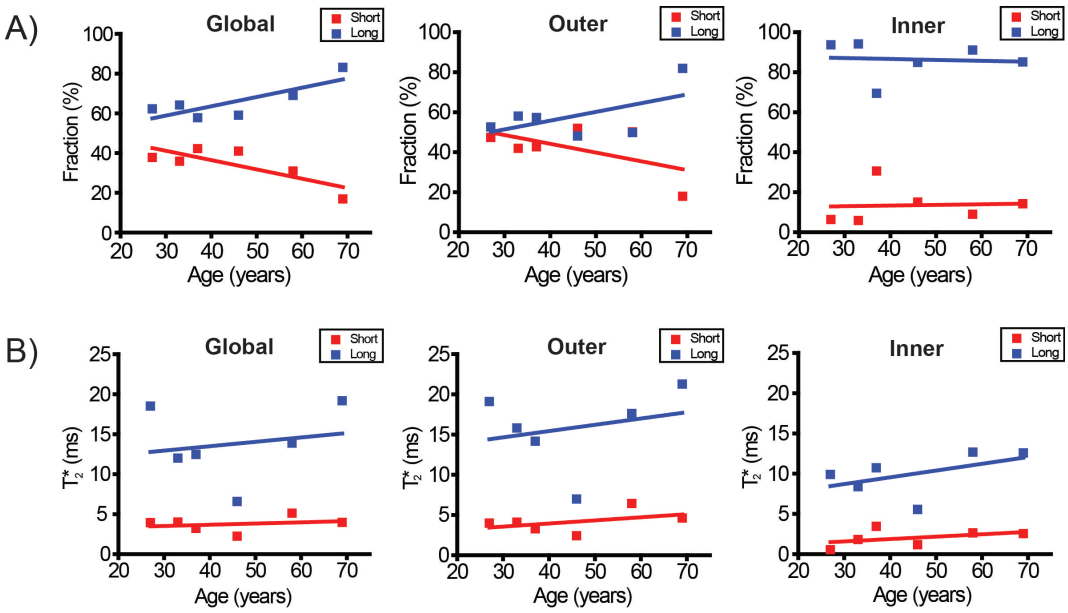


**Figure 5.2**: **UTE bicomponent $T2^*$ analysis of human menisci from various ages.** **(A)** Short and long fractions. **(B)** Short and long $T2^*$ values.

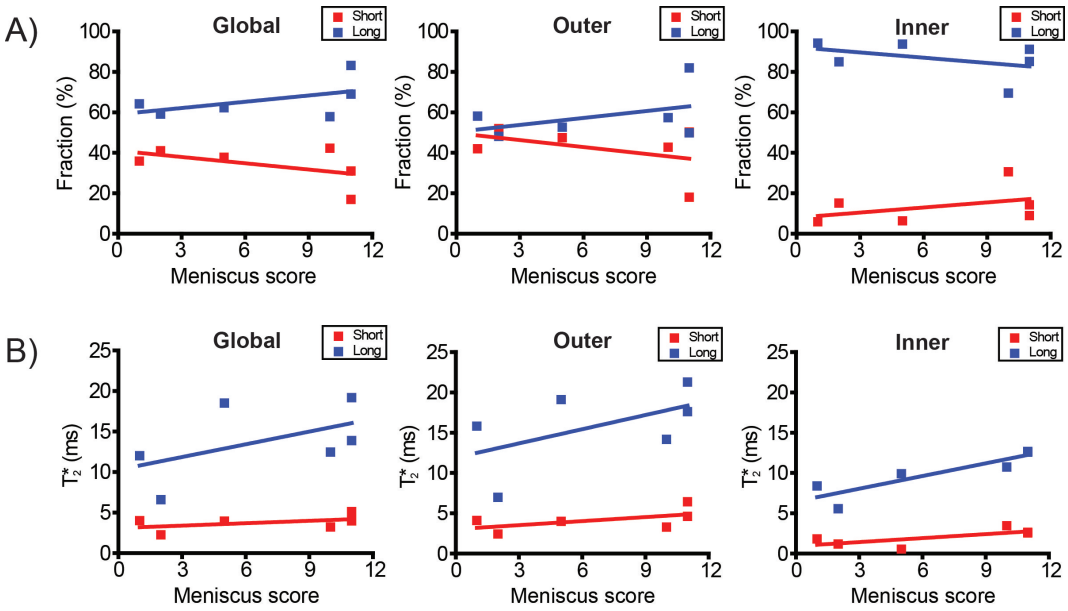


**Figure 5.3**: **UTE bicomponent $T2^*$ analysis of human menisci from various stages of degeneration graded by meniscus scores.** **(A)** Short and long fractions. **(B)** Short and long $T2^*$ values.

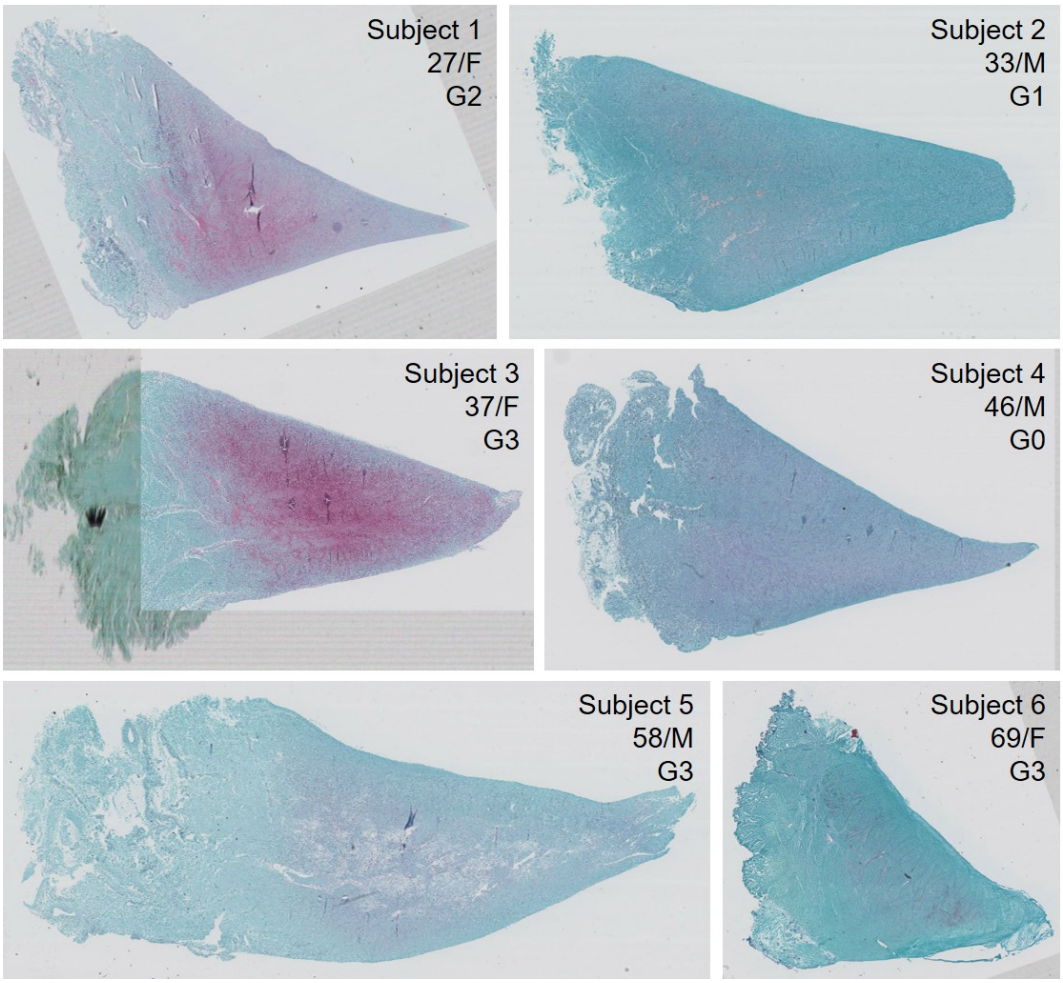


**Figure 5.4**: **Histopathological analysis of human meniscus specimens.** Safranin-O staining shows increase in degeneration with aging.

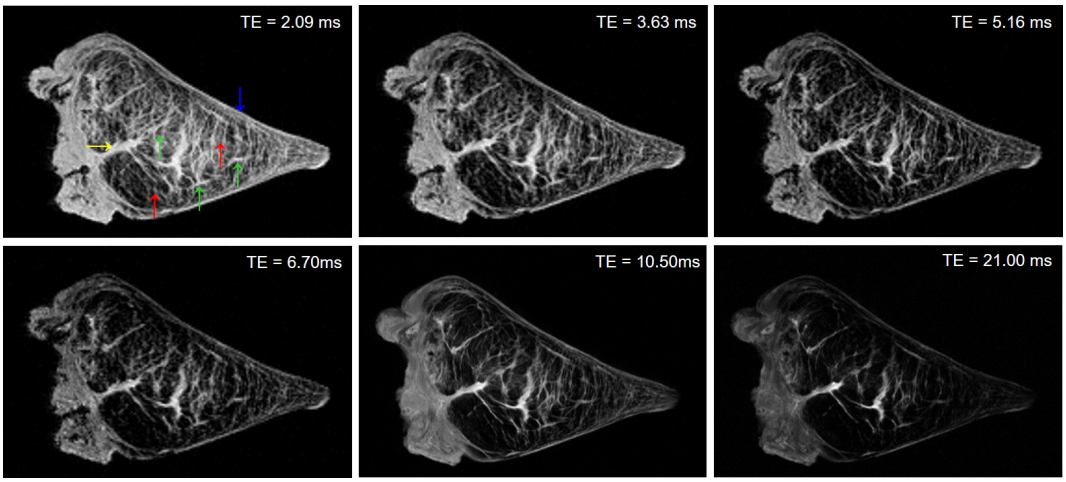


**Figure 5.5**: **High resolution 11.7T images of a healthy normal meniscus.** Representative images of healthy normal meniscus taken at varying TEs from 2.09 to 21.00 ms, showing the vasculature (yellow arrow), circumferential (red arrows), radial (green arrows), and lamellar (blue arrow) collagen fibers.

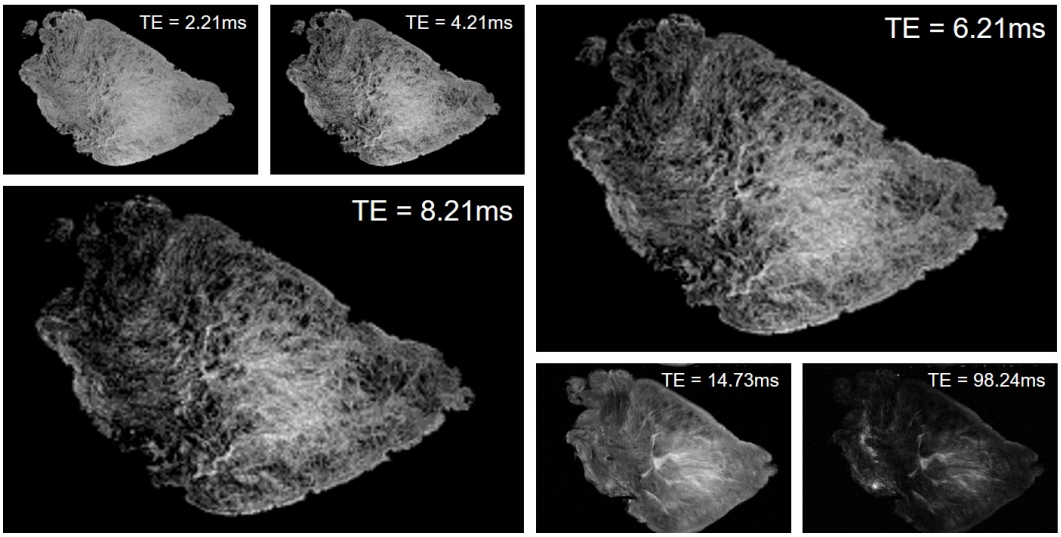


**Figure 5.6**: **High resolution 11.7T images of a degenerated meniscus.** Representative images of degenerated meniscus taken at varying TEs from 2.21 to 98.24 ms, showing disrupted structure and organization within the deep zone.

**Table 5.1**: **Summary of UTE bicomponent $T2^*$ analysis of human menisci from various ages.** Both short and long $T2^*$ components were presented as fractions or actual $T2^*$ value assessed in the (top) global, (middle) outer, and (bottom) inner regions.

Global

| | | Monoexponential $T2^*$ | Biexponential $T2^*$ | | | |
|---|---|---|---|---|---|---|
| | | | Short $T2^*$ Component | | Long $T2^*$ Component | |
| Age | Meniscus Score | $T2^*$ (ms) | Fraction (%) | $T2^*$ (ms) | Fraction (%) | $T2^*$ (ms) |
| 27 | 5 | 8.54±0.43 | 37.74±65.06 | 3.95±0.94 | 62.26±64.94 | 18.51±7.41 |
| 33 | 1 | 7.82±0.25 | 35.84±53.48 | 4.00±0.89 | 64.16±46.52 | 12.01±2.85 |
| 37 | 10 | 7.01±0.33 | 42.25±52.56 | 3.22±0.48 | 57.75±47.44 | 12.45±1.84 |
| 46 | 2 | 4.26±0.16 | 40.96±50.65 | 2.25±0.15 | 59.04±49.35 | 6.59±0.34 |
| 58 | 11 | 9.47±0.21 | 31.00±52.88 | 5.12±2.08 | 68.97±47.12 | 13.88±4.84 |
| 69 | 11 | 12.71±0.48 | 16.88±66.84 | 3.98±1.10 | 83.12±33.16 | 19.17±2.87 |

Outer

| | | Monoexponential $T2^*$ | Biexponential $T2^*$ | | | |
|---|---|---|---|---|---|---|
| | | | Short $T2^*$ Component | | Long $T2^*$ Component | |
| Age | Meniscus Score | $T2^*$ (ms) | Fraction (%) | $T2^*$ (ms) | Fraction (%) | $T2^*$ (ms) |
| 27 | 5 | 7.41±0.36 | 47.37±66.58 | 3.99±0.62 | 52.63±33.42 | 19.1±7.80 |
| 33 | 1 | 7.88±0.33 | 41.93±57.89 | 4.1±0.76 | 58.07±42.11 | 15.8±4.84 |
| 37 | 10 | 7.40±0.38 | 42.69±54.06 | 3.28±0.45 | 57.32±45.94 | 14.17±2.16 |
| 46 | 2 | 4.06±0.16 | 51.9±50.76 | 2.42±0.10 | 48.08±49.24 | 6.98±0.35 |
| 58 | 11 | 9.43±0.19 | 50.18±54.26 | 6.42±2.48 | 49.82±45.74 | 17.60±15.96 |
| 69 | 11 | 13.44±0.49 | 18.01±69.16 | 4.61±1.53 | 81.93±30.84 | 21.28±5.1 |

Inner

| | | Monoexponential $T2^*$ | Biexponential $T2^*$ | | | |
|---|---|---|---|---|---|---|
| | | | Short $T2^*$ Component | | Long $T2^*$ Component | |
| Age | Meniscus Score | $T2^*$ (ms) | Fraction (%) | $T2^*$ (ms) | Fraction (%) | $T2^*$ (ms) |
| 27 | 5 | 9.09±0.38 | 6.33±54.98 | 0.53±0.16 | 93.67±45.02 | 9.91±0.26 |
| 33 | 1 | 7.81±0.15 | 5.87±52.34 | 1.81±1.25 | 94.13±47.66 | 8.38±0.46 |
| 37 | 10 | 7.64±0.25 | 30.59±51.25 | 3.45±1.25 | 69.41±48.75 | 10.73±2.11 |
| 46 | 2 | 4.66±0.17 | 15.07±50.18 | 1.18±0.17 | 84.93±49.82 | 5.552±0.15 |
| 58 | 11 | 10.81±0.27 | 8.93±57.14 | 2.64±0.97 | 91.07±42.86 | 12.68±0.85 |
| 69 | 11 | 14.94±0.60 | 14.19±57.26 | 2.55±0.25 | 85.12±42.74 | 12.57±0.37 |

# Bibliography


[1] Helmick CG, Felson DT, Lawrence RC, Gabriel S, Hirsch R, Kwoh CK, Liang MH, Kremers HM, Mayes MD, Merkel PA, Pillemer SR, Reveille JD, Stone JH, National Arthritis Data W (2008) Estimates of the prevalence of arthritis and other rheumatic conditions in the United States. part I. Arthritis Rheum 58: 15-25.

[2] Kotlarz H, Gunnarsson CL, Fang H, Rizzo JA (2009) Insurer and out-of-pocket costs of osteoarthritis in the US: evidence from national survey data. Arthritis Rheum 60: 3546-53.

[3] Lotz MK, Kraus VB (2010) New developments in osteoarthritis. posttraumatic osteoarthritis: pathogenesis and pharmacological treatment options. Arthritis Res Ther 12: 211.

[4] Lohmander LS, Englund PM, Dahl LL, Roos EM (2007) The long-term consequence of anterior cruciate ligament and meniscus injuries: osteoarthritis. Am J Sports Med 35: 1756-69.

[5] Makris EA, Hadidi P, Athanasiou KA (2011) The knee meniscus: structure-function, pathophysiology, current repair techniques, and prospects for regeneration. Biomaterials 32: 7411-31.

[6] Roos H, Adalberth T, Dahlberg L, Lohmander LS (1995) Osteoarthritis of the knee after injury to the anterior cruciate ligament or meniscus: the influence of time and age. Osteoarthritis Cartilage 3: 261-7.

[7] Seedhom BB (1976) Loadbearing function of the menisci. Physiotherapy 62: 223.

[8] Walker PS, Erkman MJ (1975) The role of the menisci in force transmission across the knee. Clin Orthop Relat Res : 184-92.

[9] Proctor CS, Schmidt MB, Whipple RR, Kelly MA, Mow VC (1989) Material properties of the normal medial bovine meniscus. J Orthop Res 7: 771-82.

[10] Fithian DC, Kelly MA, Mow VC (1990) Material properties and structure-function relationships in the menisci. Clin Orthop Relat Res 252: 19-31.

[11] McDermott ID, Sharifi F, Bull AM, Gupte CM, Thomas RW, Amis AA (2004) An anatomical study of meniscal allograft sizing. Knee Surg Sports Traumatol Arthrosc 12: 130-5.

[12] Shaffer B, Kennedy S, Klimkiewicz J, Yao L (2000) Preoperative sizing of meniscal allografts in meniscus transplantation. Am J Sports Med 28: 524-33.

[13] Brantigan OC, Voshell AF (1941) The mechanics of the ligaments and menisci of the knee joint. J Bone Joint Surg Am 23: 44-66.

[14] Arnoczky SP, Warren RF (1982) Microvasculature of the human meniscus. Am J Sports Med 10: 90-5.

[15] Arnoczky SP, Warren RF (1983) The microvasculature of the meniscus and its response to injury. an experimental study in the dog. Am J Sports Med 11: 131-41.

[16] Hellio Le Graverand MP, Ou Y, Schield-Yee T, Barclay L, Hart D, Natsume T, Rattner JB (2001) The cells of the rabbit meniscus: their arrangement, interrelationship, morphological variations and cytoarchitecture. J Anat 198: 525–535.

[17] Verdonk PC, Forsyth RG, Wang J, Almqvist KF, Verdonk R, Veys EM, Verbruggen G (2005) Characterisation of human knee meniscus cell phenotype. Osteoarthritis Cartilage 13: 548-60.

[18] Upton ML, Guilak F, Laursen TA, Setton LA (2006) Finite element modeling predictions of region-specific cell-matrix mechanics in the meniscus. Biomech Model Mechanobiol 5: 140-9.

[19] Upton ML, Chen J, Guilak F, Setton LA (2003) Differential effects of static and dynamic compression on meniscal cell gene expression. J Orthop Res 21: 963-9.

[20] Upton ML, Chen J, Setton LA (2006) Region-specific constitutive gene expression in the adult porcine meniscus. J Orthop Res 24: 1562-70.

[21] Upton ML, Hennerbichler A, Fermor B, Guilak F, Weinberg JB, Setton LA (2006) Biaxial strain effects on cells from the inner and outer regions of the meniscus. Connect Tissue Res 47: 207-14.

[22] Bursac P, Arnoczky S, York A (2009) Dynamic compressive behavior of human meniscus correlates with its extra-cellular matrix composition. Biorheology 46: 227-37.

[23] Klionsky DJ, Emr SD (2000) Autophagy as a regulated pathway of cellular degradation. Science 290: 1717-21.

[24] Lotz MK, Carames B (2011) Autophagy and cartilage homeostasis mechanisms in joint health, aging and OA. Nat Rev Rheumatol 7: 579-87.

[25] Levine B, Kroemer G (2008) Autophagy in the pathogenesis of disease. Cell 132: 27-42.

[26] Jin S, White E (2007) Role of autophagy in cancer: management of metabolic stress. Autophagy 3: 28–31.

[27] Hara T, Nakamura K, Matsui M, Yamamoto A, Nakahara Y, Suzuki-Migishima R, Yokoyama M, Mishima K, Saito I, Okano h, Mizushima N (2006) Suppression of basal autophagy in neural cells causes neurodegenerative disease in mice. Nature 441: 885-9.

[28] Komatsu M, Kominami E, Tanaka K (2006) Autophagy and neurodegeneration. Autophagy 2: 315–317.

[29] Tanaka Y, Guhde G, Suter A, Eskelinen EL, Hartmann D, Lullmann-Rauch R, Janssen PM, Blanz J, von Figura K, Saftig P (2000) Accumulation of autophagic vacuoles and cardiomyopathy in LAMP-2-deficient mice. Nature 406: 902–906.

[30] Lotz M, Carames B (2012) Autophagy: a new therapeutic target in cartilage injury and osteoarthritis. J Am Acad Orthop Surg 20: 261-2.

[31] Grogan SP, Lotz MK, D'Lima DD (2015) Post-traumatic arthritis: pathogenesis, diagnosis, and management. Chapter 16 Periarticular tissue response to joint injury. 185-199. Springer.

[32] Kabeya Y, Mizushima N, Ueno T, Yamamoto A, Kirisako T, Noda T, Kominami E, Ohsumi Y, Yoshimori T (2000) LC3, a mammalian homologue of yeast Apg8p, is localized in autophagosome membranes after processing. EMBO J 19: 5720-8.

[33] Carames B, Taniguchi N, Otsuki S, Blanco FJ, Lotz M (2010) Autophagy is a protective mechanism in normal cartilage, and its aging-related loss is linked with cell death and osteoarthritis. Arthritis Rheum 62: 791-801.

[34] Carames B, Olmer M, Kiosses WB, Lotz MK (2015) The relationship of autophagy defects to cartilage damage during joint aging in a mouse model. Arthritis Rheumatol 67: 1568-76.

[35] Ron D, Walter P (2007) Signal integration in the endoplasmic reticulum unfolded protein response. Nat Rev Mol Cell Biol 8: 519-29.

[36] Paul JP (1976) Force actions transmitted by joints in the human body. Proc R Soc Lond B Biol Sci 192: 163–172.

[37] Shrive NG, O'Connor JJ, Goodfellow JW (1978) Load-bearing in the knee joint. Clin Orthop Relat Res : 279–287.

[38] Walker PS, Hajek JV (1972) The load-bearing area in the knee joint. J Biomech 5: 581–589.

[39] Sweigart MA, Zhu CF, Burt DM, deHoll PD, Agrawal CM, Clanton TO, Athanasiou KA (2004) Intraspecies and interspecies comparison of the compressive properties of the medial meniscus. Ann Biomed Eng 32: 1569-1579.

[40] Tissakht M, Ahmed A (1995) Tensile stress-strain characteristics of the human meniscal material. J Biomech 28: 411-422.

[41] Binnig, Quate, Gerber (1986) Atomic force microscope. Phys Rev Lett 56: 930–933.

[42] Meckes BR (2015) Design and development of integrated multi-modal scanning probe microscopy for scanning probe microscopy for structure-function imaging of ion channels and receptors. Ph.D. thesis, University of California, San Diego.

[43] McLeod MA, Wilusz RE, Guilak F (2013) Depth-dependent anisotropy of the micromechanical properties of the extracellular and pericellular matrices of articular cartilage evaluated via atomic force microscopy. J Biomech 46: 586–592.

[44] Sanchez-Adams J, Wilusz RE, Guilak F (2013) Atomic force microscopy reveals regional variations in the micromechanical properties of the pericellular and extracellular matrices of the meniscus. J Orthop Res 31: 1218–1225.

[45] Pauli C, Grogan SP, Patil S, Otsuki S, Hasegawa A, Koziol J, Lotz MK, D'Lima DD (2011) Macroscopic and histopathologic analysis of human knee menisci in aging and osteoarthritis. Osteoarthritis Cartilage 19: 1132-41.

[46] Bluteau G, Conrozier T, Mathieu P, Vignon E, Herbage D, Mallein-Gerin F (2001) Matrix metalloproteinase-1, -3, -13 and aggrecanase-1 and -2 are differentially expressed in experimental osteoarthritis. Biochim Biophys Acta 1526: 147-58.

[47] Verzijl N, DeGroot J, Thorpe SR, Bank RA, Shaw JN, Lyons TJ, Bijlsma JW, Lafeber FP, Baynes JW, TeKoppele JM (2000) Effect of collagen turnover on the accumulation of advanced glycation end products. J Biol Chem 275: 39027-31.

[48] DeGroot J, Verzijl N, Budde M, Bijlsma JW, Lafeber FP, TeKoppele JM (2001) Accumulation of advanced glycation end products decreases collagen turnover by bovine chondrocytes. Exp Cell Res 266: 303-10.

[49] Roos H, Lauren M, Adalberth T, Roos EM, Jonsson K, Lohmander LS (1998) Knee osteoarthritis after meniscectomy: prevalence of radiographic changes after twenty-one years, compared with matched controls. Arthritis Rheum 41: 687-93.

[50] Konan S, Rayan F, Haddad FS (2009) Do physical diagnostic tests accurately detect meniscal tears? Knee Surg Sports Traumatol Arthrosc 17: 806-11.

[51] Ercin E, Kaya I, Sungur I, Demirbas E, Ugras AA, Cetinus EM (2012) History, clinical findings, magnetic resonance imaging, and arthroscopic correlation in meniscal lesions. Knee Surg Sports Traumatol Arthrosc 20: 851-6.

[52] Akseki D, Ozcan O, Boya H, Pinar H (2004) A new weight-bearing meniscal test and a comparison with McMurray's test and joint line tenderness. Arthroscopy 20: 951-8.

[53] Smith BW, Green GA (1995) Acute knee injuries: Part I. History and physical examination. Am Fam Physician 51: 615-21.

[54] Karachalios T, Hantes M, Zibis AH, Zachos V, Karantanas AH, Malizos KN (2005) Diagnostic accuracy of a new clinical test (the Thessaly test) for early detection of meniscal tears. J Bone Joint Surg Am 87: 955-62.

[55] Mirzatolooei F, Yekta Z, Bayazidchi M, Ershadi S, Afshar A (2010) Validation of the Thessaly test for detecting meniscal tears in anterior cruciate deficient knees. Knee 17: 221-3.

[56] Goossens P, Keijsers E, van Geenen RJ, Zijta A, van den Broek M, Verhagen AP, Scholten-Peeters GG (2015) Validity of the Thessaly test in evaluating meniscal tears compared with arthroscopy: a diagnostic accuracy study. J Orthop Sports Phys Ther 45: 18-24, B1.

[57] Ryzewicz M, Peterson B, Siparsky PN, Bartz RL (2007) The diagnosis of meniscus tears: the role of MRI and clinical examination. Clin Orthop Relat Res 455: 123-33.

[58] Subhas N, Sakamoto FA, Mariscalco MW, Polster JM, Obuchowski NA, Jones MH (2012) Accuracy of MRI in the diagnosis of meniscal tears in older patients. AJR Am J Roentgenol 198: W575-80.

[59] Du J, Carl M, Bae WC, Statum S, Chang EY, Bydder GM, Chung CB (2013) Dual inversion recovery ultrashort echo time (DIR-UTE) imaging and quantification of the zone of calcified cartilage (ZCC). Osteoarthritis Cartilage 21: 77–85.

[60] Du J, Takahashi AM, Chung CB (2009) Ultrashort TE spectroscopic imaging (UTESI): application to the imaging of short T2 relaxation tissues in the musculoskeletal system. J Magn Reson Imaging 29: 412–421.

[61] Holmes JE, Bydder GM (2005) MR imaging with ultrashort TE (UTE) pulse sequences: Basic principles. Radiography 11: 163-174.

[62] Fairbank TJ (1948) Knee joint changes after meniscectomy. J Bone Joint Surg Br 30B: 664-70.

[63] Levy IM, Torzilli PA, Warren RF (1982) The effect of medial meniscectomy on anterior-posterior motion of the knee. J Bone Joint Surg Am 64: 883-8.

[64] Levy IM, Torzilli PA, Gould JD, Warren RF (1989) The effect of lateral meniscectomy on motion of the knee. J Bone Joint Surg Am 71: 401-6.

[65] Cooper DE, Arnoczky SP, Warren RF (1990) Arthroscopic meniscal repair. Clin Sports Med 9: 589-607.

[66] Cooper DE, Arnoczky SP, Warren RF (1991) Meniscal repair. Clin Sports Med 10: 529-48.

[67] DeHaven KE, Arnoczky SP (1994) Meniscus repair: basic science, indications for repair, and open repair. Instr Course Lect 43: 65-76.

[68] McAndrews PT, Arnoczky SP (1996) Meniscal repair enhancement techniques. Clin Sports Med 15: 499-510.

[69] Henning CE, Lynch MA, Yearout KM, Vequist SW, Stallbaumer RJ, Decker KA (1990) Arthroscopic meniscal repair using an exogenous fibrin clot. Clin Orthop Relat Res : 64–72.

[70] Henning CE, Lynch MA, Clark JR (1987) Vascularity for healing of meniscus repairs. Arthroscopy 3: 13–18.

[71] Arnoczky SP, Warren RF, McDevitt CA (1990) Meniscal replacement using a cryopreserved allograft. an experimental study in the dog. Clin Orthop Relat Res : 121-8.

[72] Baek J, Chen X, Sovani S, Jin S, Grogan SP, D'Lima DD (2015) Meniscus tissue engineering using a novel combination of electrospun scaffolds and human meniscus cells embedded within an extracellular matrix hydrogel. J Orthop Res 33: 572-83.

[73] Ahmed AM, Burke DL (1983) In-vitro measurement of static pressure distribution in synovial joints–Part I: Tibial surface of the knee. J Biomech Eng 105: 216–225.

[74] Radin EL, de Lamotte F, Maquet P (1984) Role of the menisci in the distribution of stress in the knee. Clin Orthop Relat Res : 290–294.

[75] Shoemaker SC, Markolf KL (1986) The role of the meniscus in the anterior-posterior stability of the loaded anterior cruciate-deficient knee. effects of partial versus total excision. J Bone Joint Surg Am 68: 71–79.

[76] Krause WR, Pope MH, Johnson RJ, Wilder DG (1976) Mechanical changes in the knee after meniscectomy. J Bone Joint Surg Am 58: 599–604.

[77] Day B, Mackenzie WG, Shim SS, Leung G (1985) The vascular and nerve supply of the human meniscus. Arthroscopy 1: 58–62.

[78] Aspden R, Yarker Y, Hukins D (1985) Collagen orientations in the meniscus of the knee joint. J Anat 140: 371.

[79] McDevitt CA, Webber RJ (1990) The ultrastructure and biochemistry of meniscal cartilage. Clin Orthop Relat Res : 8–18.

[80] Adams ME, Billingham ME, Muir H (1983) The glycosaminoglycans in menisci in experimental and natural osteoarthritis. Arthritis Rheum 26: 69–76.

[81] Hellio Le Graverand MP, Vignon E, Otterness IG, Hart DA (2001) Early changes in lapine menisci during osteoarthritis development: Part II: molecular alterations. Osteoarthritis Cartilage 9: 65–72.

[82] Hellio Le Graverand MP, Vignon E, Otterness IG, Hart DA (2001) Early changes in lapine menisci during osteoarthritis development: Part I: cellular and matrix alterations. Osteoarthritis Cartilage 9: 56–64.

[83] Herwig J, Egner E, Buddecke E (1984) Chemical changes of human knee joint menisci in various stages of degeneration. Ann Rheum Dis 43: 635-40.

[84] Ishihara G, Kojima T, Saito Y, Ishiguro N (2009) Roles of metalloproteinase-3 and aggrecanase 1 and 2 in aggrecan cleavage during human meniscus degeneration. Orthop Rev (Pavia) 1: e14.

[85] Rosenberg L (1971) Chemical basis for the histological use of safranin o in the study of articular cartilage. J Bone Joint Surg Am 53: 69–82.

[86] Pauli C, Whiteside R, Heras FL, Nesic D, Koziol J, Grogan SP, Matyas J, Pritzker KPH, D'Lima DD, Lotz MK (2012) Comparison of cartilage histopathology assessment systems on human knee joints at all stages of osteoarthritis development. Osteoarthritis Cartilage 20: 476–485.

[87] Burman MS, Sutro CJ (1933) A study of the degenerative changes of the menisci of the knee joint, and the clinical significance thereof. J Bone Joint Surg Am 15: 835-861.

[88] Englund M (2009) The role of the meniscus in osteoarthritis genesis. Med Clin North Am 93: 37-43, x.

[89] Loeser RF (2010) Age-related changes in the musculoskeletal system and the development of osteoarthritis. Clin Geriatr Med 26: 371–386.

[90] Bhattacharyya T, Gale D, Dewire P, Totterman S, Gale ME, McLaughlin S, Einhorn TA, Felson DT (2003) The clinical importance of meniscal tears demonstrated by magnetic resonance imaging in osteoarthritis of the knee. J Bone Joint Surg Am 85-A: 4–9.

[91] Englund M, Guermazi A, Gale D, Hunter DJ, Aliabadi P, Clancy M, Felson DT (2008) Incidental meniscal findings on knee MRI in middle-aged and elderly persons. N Engl J Med 359: 1108-15.

[92] Cox JS, Nye CE, Schaefer WW, Woodstein IJ (1975) The degenerative effects of partial and total resection of the medial meniscus in dogs' knees. Clin Orthop Relat Res : 178–183.

[93] McDevitt CA, Muir H (1976) Biochemical changes in the cartilage of the knee in experimental and natural osteoarthritis in the dog. J Bone Joint Surg Br 58: 94–101.

[94] Nakano T, Dodd CM, Scott PG (1997) Glycosaminoglycans and proteoglycans from different zones of the porcine knee meniscus. J Orthop Res 15: 213–220.

[95] Joshi MD, Suh JK, Marui T, Woo SL (1995) Interspecies variation of compressive biomechanical properties of the meniscus. J Biomed Mater Res 29: 823–828.

[96] Driban JB, Sitler MR, Barbe MF, Balasubramanian E (2010) Is osteoarthritis a heterogeneous disease that can be stratified into subsets? Clin Rheumatol 29: 123–131.

[97] Felson DT, Lawrence RC, Dieppe PA, Hirsch R, Helmick CG, Jordan JM, Kington RS, Lane NE, Nevitt MC, Zhang Y, Sowers M, McAlindon T, Spector TD, Poole AR, Yanovski SZ, Ateshian G, Sharma L, Buckwalter JA, Brandt KD, Fries JF (2000) Osteoarthritis: new insights. part 1: the disease and its risk factors. Ann Intern Med 133: 635-46.

[98] Wang X, Shen X, Li X, Agrawal CM (2002) Age-related changes in the collagen network and toughness of bone. Bone 31: 1–7.

[99] Verzijl N, DeGroot J, Oldehinkel E, Bank RA, Thorpe SR, Baynes JW, Bayliss MT, Bijlsma JW, Lafeber FP, Tekoppele JM (2000) Age-related accumulation of Maillard reaction products in human articular cartilage collagen. Biochem J 350 Pt 2: 381–387.

[100] Verzijl N, DeGroot J, Ben ZC, Brau-Benjamin O, Maroudas A, Bank RA, Mizrahi J, Schalkwijk CG, Thorpe SR, Baynes JW, Bijlsma JWJ, Lafeber FPJG, TeKoppele JM (2002) Crosslinking by advanced glycation end products increases the stiffness of the collagen network in human articular cartilage: a possible mechanism through which age is a risk factor for osteoarthritis. Arthritis Rheum 46: 114–123.

[101] Ingber DE (1997) Tensegrity: the architectural basis of cellular mechanotransduction. Annu Rev Physiol 59: 575–599.

[102] Ingber DE (2003) Mechanobiology and diseases of mechanotransduction. Ann Med 35: 564–577.

[103] Wang N, Butler JP, Ingber DE (1993) Mechanotransduction across the cell surface and through the cytoskeleton. Science 260: 1124–1127.

[104] Wang N, Tytell JD, Ingber DE (2009) Mechanotransduction at a distance: mechanically coupling the extracellular matrix with the nucleus. Nat Rev Mol Cell Biol 10: 75–82.

[105] Discher DE, Janmey P, Wang YL (2005) Tissue cells feel and respond to the stiffness of their substrate. Science 310: 1139–1143.

[106] Fink C, Fermor B, Weinberg JB, Pisetsky DS, Misukonis MA, Guilak F (2001) The effect of dynamic mechanical compression on nitric oxide production in the meniscus. Osteoarthritis Cartilage 9: 481–487.

[107] Fermor B, Jeffcoat D, Hennerbichler A, Pisetsky DS, Weinberg JB, Guilak F (2004) The effects of cyclic mechanical strain and tumor necrosis factor alpha on the response of cells of the meniscus. Osteoarthritis Cartilage 12: 956–962.

[108] Seedhom BB (1979) Transmission of the load in the knee joint with special reference to the role of the menisci: Part I: Anatomy, analysis and apparatus. Engineering in Medicine 8: 207–219.

[109] Englund M, Guermazi A, Lohmander LS (2009) The meniscus in knee osteoarthritis. Rheum Dis Clin North Am 35: 579-590.

[110] Englund M, Guermazi A, Lohmander SL (2009) The role of the meniscus in knee osteoarthritis: a cause or consequence? Radiol Clin North Am 47: 703-12.

[111] Englund M, Roos EM, Lohmander LS (2003) Impact of type of meniscal tear on radiographic and symptomatic knee osteoarthritis: a sixteen-year followup of meniscectomy with matched controls. Arthritis Rheum 48: 2178-87.

[112] Garrett Jr WE, Swiontkowski MF, Weinstein JN, Callaghan J, Rosier RN, Berry DJ, Harrast J, Derosa GP (2006) American Board of Orthopaedic Surgery Practice of the Orthopaedic Surgeon: part-II, certification examination case mix. J Bone Joint Surg Am 88: 660-667.

[113] Cook JL, Kuroki K, Visco D, Pelletier JP, Schulz L, Lafeber FP (2010) The oarsi histopathology initiative - recommendations for histological assessments of osteoarthritis in the dog. Osteoarthritis Cartilage 18 Suppl 3: S66-79.

[114] Gerwin N, Bendele AM, Glasson S, Carlson CS (2010) The OARSI histopathology initiative recommendations for histological assessments of osteoarthritis in the rat. Osteoarthritis Cartilage 18 Suppl 3: S24-34.

[115] Glasson S, Chambers M, Van Den Berg W, Little C (2010) The OARSI histopathology initiative–recommendations for histological assessments of osteoarthritis in the mouse. Osteoarthritis Cartilage 18: S17-S23.

[116] Kraus VB, Huebner JL, DeGroot J, Bendele A (2010) The OARSI histopathology initiative recommendations for histological assessments of osteoarthritis in the guinea pig. Osteoarthritis Cartilage 18 Suppl 3: S35-52.

[117] Laverty S, Girard CA, Williams JM, Hunziker EB, Pritzker KP (2010) The OARSI histopathology initiative - recommendations for histological assessments of osteoarthritis in the rabbit. Osteoarthritis Cartilage 18 Suppl 3: S53-65.

[118] Little CB, Smith MM, Cake MA, Read RA, Murphy MJ, Barry FP (2010) The OARSI histopathology initiative - recommendations for histological assessments of osteoarthritis in sheep and goats. Osteoarthritis Cartilage 18 Suppl 3: S80-92.

[119] McIlwraith CW, Frisbie DD, Kawcak CE, Fuller CJ, Hurtig M, Cruz A (2010) The OARSI histopathology initiative - recommendations for histological assessments of osteoarthritis in the horse. Osteoarthritis Cartilage 18 Suppl 3: S93-105.

[120] Helminen HJ, Saamanen AM, Salminen H, Hyttinen MM (2002) Transgenic mouse models for studying the role of cartilage macromolecules in osteoarthritis. Rheumatology (Oxford) 41: 848-56.

[121] Akasaki Y, Hasegawa A, Saito M, Asahara H, Iwamoto Y, Lotz M (2014) Dysregulated FoxO transcription factors in articular cartilage in aging and osteoarthritis. Osteoarthritis Cartilage 22: 162-170.

[122] Lotz MK, Otsuki S, Grogan SP, Sah R, Terkeltaub R, D'Lima D (2010) Cartilage cell clusters. Arthritis Rheum 62: 2206-18.

[123] Otsuki S, Hanson SR, Miyaki S, Grogan SP, Kinoshita M, Asahara H, Wong CH, Lotz MK (2010) Extracellular sulfatases support cartilage homeostasis by regulating BMP and FGF signaling pathways. Proc Natl Acad Sci U S A 107: 10202-7.

[124] Taniguchi N, Caramés B, Ronfani L, Ulmer U, Komiya S, Bianchi ME, Lotz M (2009) Aging-related loss of the chromatin protein HMGB2 in articular cartilage is linked to reduced cellularity and osteoarthritis. Proc Natl Acad Sci U S A 106: 1181-1186.

[125] Taniguchi N, Caramés B, Kawakami Y, Amendt BA, Komiya S, Lotz M (2009) Chromatin protein HMGB2 regulates articular cartilage surface maintenance via Îš-catenin pathway. Proc Natl Acad Sci U S A 106: 16817-16822.

[126] Sokoloff L (1956) Natural history of degenerative joint disease in small laboratory animals. I. pathological anatomy of degenerative joint disease in mice. AMA Arch Pathol 62: 118-128.

[127] Silberberg M, Silberberg R (1941) Age changes of bones and joints in various strains of mice. Am J Anat 68: 69-95.

[128] Glasson SS, Blanchet TJ, Morris EA (2007) The surgical destabilization of the medial meniscus (DMM) model of osteoarthritis in the 129/SvEv mouse. Osteoarthritis Cartilage 15: 1061-9.

[129] Mizushima N, Yamamoto A, Matsui M, Yoshimori T, Ohsumi Y (2004) In vivo analysis of autophagy in response to nutrient starvation using transgenic mice expressing a fluorescent autophagosome marker. Mol Biol Cell 15: 1101-1111.

[130] Alirezaei M, Kemball C, Flynn C, Wood M, Whitton J, Kiosses W (2010) Short-term fasting induces profound neuronal autophagy. Autophagy 6: 702-710.

[131] Shrout P, Fleiss J (1979) Intraclass correlations: uses in assessing rater reliability. Psychol Bull 86: 420-428.

[132] Lotz M, Loeser RF (2012) Effects of aging on articular cartilage homeostasis. Bone 51: 241-8.

[133] Allen P, Denham R, Swan A (1984) Late degenerative changes after meniscectomy. factors affecting the knee after operation. J Bone Joint Surg Br 66: 666-671.

[134] Englund M, Lohmander LS (2004) Risk factors for symptomatic knee osteoarthritis fifteen to twenty-two years after meniscectomy. Arthritis Rheum 50: 2811-9.

[135] Stoop R, Van Der Kraan PM, Buma P, Hollander AP, Billinghurst RC, Poole AR, Van Den Berg WB (1999) Type II collagen degradation in spontaneous osteoarthritis in C57BL/6 and BALB/c mice. Arthritis & Rheumatism 42: 2381-2389.

[136] Carames B, Hasegawa A, Taniguchi N, Miyaki S, Blanco FJ, Lotz M (2012) Autophagy activation by rapamycin reduces severity of experimental osteoarthritis. Ann Rheum Dis 71: 575-81.

[137] Grogan SP, Miyaki S, Asahara H, D'Lima DD, Lotz MK (2009) Mesenchymal progenitor cell markers in human articular cartilage: normal distribution and changes in osteoarthritis. Arthritis Res Ther 11: R85.

[138] Buckwalter JA, Brown TD (2004) Joint injury, repair, and remodeling: roles in post-traumatic osteoarthritis. Clin Orthop Relat Res 423: 7-16.

[139] Colwell Jr CW, D'Lima DD, Hoenecke HR, Fronek J, Pulido P, Morris BA, Chung C, Resnick D, Lotz M (2001) In vivo changes after mechanical injury. Clin Orthop Relat Res 391: S116-S123.

[140] D'Lima D, Hermida J, Hashimoto S, Colwell C, Lotz M (2006) Caspase inhibitors reduce severity of cartilage lesions in experimental osteoarthritis. Arthritis Rheum 54: 1814-21.

[141] D'Lima DD, Hashimoto S, Chen PC, Colwell Jr CW, Lotz MK (2001) Impact of mechanical trauma on matrix and cells. Clin Orthop Relat Res 391: S90-S99.

[142] Lotz M (2001) Cytokines in cartilage injury and repair. Clin Orthop Relat Res 391: S108-15.

[143] McKinley TO, Borrelli Jr J, D'Lima DD, Furman BD, Giannoudis PV (2010) Basic science of intraarticular fractures and posttraumatic osteoarthritis. J Orthop Trauma 24: 567.

[144] Sellam J, Berenbaum F (2010) The role of synovitis in pathophysiology and clinical symptoms of osteoarthritis. Nat Rev Rheumatol 6: 625-635.

[145] Lawrence RC, Felson DT, Helmick CG, Arnold LM, Choi H, Deyo RA, Gabriel S, Hirsch R, Hochberg MC, Hunder GG, Jordan JM, Katz JN, Kremers HM, Wolfe F, National Arthritis Data W (2008) Estimates of the prevalence of arthritis and other rheumatic conditions in the United States. part II. Arthritis Rheum 58: 26-35.

[146] Neogi T, Zhang Y (2013) Epidemiology of osteoarthritis. Rheum Dis Clin North Am 39: 1-19.

[147] Fahmy NR, Williams EA, Noble J (1983) Meniscal pathology and osteoarthritis of the knee. J Bone Joint Surg Br 65: 24-8.

[148] Englund M, Guermazi A, Roemer FW, Aliabadi P, Yang M, Lewis CE, Torner J, Nevitt MC, Sack B, Felson DT (2009) Meniscal tear in knees without surgery and the development of radiographic osteoarthritis among middle-aged and elderly persons: The multicenter osteoarthritis study. Arthritis Rheum 60: 831-839.

[149] Berthiaume MJ, Raynauld JP, Martel-Pelletier J, Labonte F, Beaudoin G, Bloch DA, Choquette D, Haraoui B, Altman RD, Hochberg M, Meyer JM, Cline GA, Pelletier JP (2005) Meniscal tear and extrusion are strongly associated with progression of symptomatic knee osteoarthritis as assessed by quantitative magnetic resonance imaging. Ann Rheum Dis 64: 556-63.

[150] Rabinowitz JD, White E (2010) Autophagy and metabolism. Science 330: 1344-1348.

[151] Kiffin R, Bandyopadhyay U, Cuervo AM (2006) Oxidative stress and autophagy. Antioxid Redox Sign 8: 152-162.

[152] Yu L, Wan F, Dutta S, Welsh S, Liu Z, Freundt E, Baehrecke EH, Lenardo M (2006) Autophagic programmed cell death by selective catalase degradation. Proc Natl Acad Sci USA 103: 4952-7.

[153] Mathew R, Karantza-Wadsworth V, White E (2007) Role of autophagy in cancer. Nat Rev Cancer 7: 961-7.

[154] Mizushima N (2009) Physiological functions of autophagy, Springer. pp. 71-84.

[155] Zhou H, Huang S (2010) The complexes of mammalian target of rapamycin. Curr Protein Pept Sc 11: 409-424.

[156] Chan EY, Kir S, Tooze SA (2007) siRNA screening of the kinome identifies ULK1 as a multidomain modulator of autophagy. J Biol Chem 282: 25464-74.

[157] Ohsumi Y, Mizushima N (2004) Two ubiquitin-like conjugation systems essential for autophagy. In: Seminars in cell & developmental biology. Academic Press, volume 15, pp. 231-236.

[158] Lopez de Figueroa P, K LM, Blanco FJ, Carames B (2015) Autophagy activation and protection from mitochondrial dysfunction in human chondrocytes. Arthritis Rheum 67: 966-76.

[159] Shigemitsu K, Tsujishita Y, Hara K, Nanahoshi M, Avruch J, Yonezawa K (1999) Regulation of translational effectors by amino acid and mammalian target of rapamycin signaling pathways. possible involvement of autophagy in cultured hepatoma cells. J Biol Chem 274: 1058-65.

[160] Sabers CJ, Martin MM, Brunn GJ, Williams JM, Dumont FJ, Wiederrecht G, Abraham RT (1995) Isolation of a protein target of the FKBP12-rapamycin complex in mammalian cells. J Biol Chem 270: 815-22.

[161] Carames B, Taniguchi N, Seino D, Blanco FJ, D'Lima D, Lotz MK (2012) Mechanical injury suppresses autophagy regulators and pharmacologic activation of autophagy results in chondroprotection. Arthritis Rheum 64: 1182-92.

[162] Baehrecke EH (2005) Autophagy: dual roles in life and death? Nat Rev Mol Cell Biol 6: 505-10.

[163] Cuervo AM, Bergamini E, Brunk UT, Dröge W, Ffrench M, Terman A (2005) Autophagy and aging: The importance of maintaining "clean" cells. Autophagy 1: 131-140.

[164] Cuervo AM, Dice JF (2000) Age-related decline in chaperone-mediated autophagy. J Biol Chem 275: 31505-13.

[165] Mizushima N, Kuma A (2008) Autophagosomes in GFP-LC3 transgenic mice. Method Mol Cell Biol 445: 119-24.

[166] Shintani T, Klionsky DJ (2004) Autophagy in health and disease: A double-edged sword. Science 306: 990-995.

[167] Hauselmann HJ, Oppliger L, Michel BA, Stefanovic-Racic M, Evans CH (1994) Nitric oxide and proteoglycan biosynthesis by human articular chondrocytes in alginate culture. FEBS Lett 352: 361-4.

[168] Murrell GA, Jang D, Williams RJ (1995) Nitric oxide activates metalloprotease enzymes in articular cartilage. Biochem Biophys Res Commun 206: 15-21.

[169] Cao M, Westerhausen-Larson A, Niyibizi C, Kavalkovich K, Georgescu HI, Rizzo CF, Hebda PA, Stefanovic-Racic M, Evans CH (1997) Nitric oxide inhibits the synthesis of type-II collagen without altering COL2A1 mRNA abundance: prolyl hydroxylase as a possible target. Biochem J 324 ( Pt 1): 305-10.

[170] Amin AR, Abramson SB (1998) The role of nitric oxide in articular cartilage breakdown in osteoarthritis. Curr Opin Rheumatol 10: 263-8.

[171] McCann SM, Licinio J, Wong ML, Yu WH, Karanth S, Rettorri V (1998) The nitric oxide hypothesis of aging. Exp Gerontol 33: 813-26.

[172] McCann SM, Mastronardi C, de Laurentiis A, Rettori V (2005) The nitric oxide theory of aging revisited. Ann N Y Acad Sci 1057: 64-84.

[173] Shen C, Yan J, Erkocak OF, Zheng XF, Chen XD (2014) Nitric oxide inhibits autophagy via suppression of JNK in meniscal cells. Rheumatology 53: 1022-1033.

[174] Hashimoto S, Takahashi K, Ochs RL, Coutts RD, Amiel D, Lotz M (1999) Nitric oxide production and apoptosis in cells of the meniscus during experimental osteoarthritis. Arthritis Rheum 42: 2123-2131.

[175] Kobayashi K, Mishima H, Hashimoto S, Goomer RS, Harwood FL, Lotz M, Moriya H, Amiel D (2001) Chondrocyte apoptosis and regional differential expression of nitric oxide in the medial meniscus following partial meniscectomy. J Orthop Res 19: 802-8.

[176] Du J, Carl M, Diaz E, Takahashi A, Han E, Szeverenyi NM, Chung CB, Bydder GM (2010) Ultrashort TE T1rho (UTE T1rho) imaging of the Achilles tendon and meniscus. Magn Reson Med 64: 834–842.

[177] Bae WC, Chen PC, Chung CB, Masuda K, D'Lima D, Du J (2012) Quantitative ultrashort echo time (UTE) MRI of human cortical bone: correlation with porosity and biomechanical properties. J Bone Miner Res 27: 848–857.

[178] Du J, Carl M, Bydder M, Takahashi A, Chung CB, Bydder GM (2010) Qualitative and quantitative ultrashort echo time (UTE) imaging of cortical bone. J Magn Reson 207: 304–311.

[179] Shao H, Chang EY, Pauli C, Zanganeh S, Bae W, Chung CB, Tang G, Du J (2015) UTE bi-component analysis of T2* relaxation in articular cartilage. Osteoarthritis Cartilage .

[180] Anastasiou A, Hall LD (2004) Optimisation of T2 and M0 measurements of bi-exponential systems. Magn Reson Imaging 22: 67–80.

[181] Sijbers J, den Dekker AJ, Van Audekerke J, Verhoye M, Van Dyck D (1998) Estimation of the noise in magnitude MR images. Magn Reson Imaging 16: 87–90.

[182] Sijbers J, den Dekker AJ (2004) Maximum likelihood estimation of signal amplitude and noise variance from MR data. Magn Reson Med 51: 586–594.

[183] Raya JG, Dietrich O, Horng A, Weber J, Reiser MF, Glaser C (2010) T2 measurement in articular cartilage: impact of the fitting method on accuracy and precision at low SNR. Magn Reson Med 63: 181–193.